THE HIGH TEMPERATURE SOLID ELECTROLYTE AMMONIA FUEL CELL

by

ROGER DEAN FARR

B.S., University of California, Los Angeles
(1978)

SUBMITTED IN PARTIAL FULFILLMENT
OF THE REQUIREMENTS FOR THE
DEGREE OF

MASTER OF SCIENCE

at the

 MASSACHUSETTS INSTITUTE OF TECHNOLOGY

(AUGUST 1979)

Signature of Author.....
Department of Chemical Engineering, August 31, 1979

Certified by.....
Thesis Supervisor

Accepted by.....
Chairman, Department Committee

THE HIGH TEMPERATURE SOLID ELECTROLYTE AMMONIA FUEL CELL

by

ROGER DEAN FARR

Submitted to the Department of Chemical Engineering
on August 31, 1979 in partial fulfillment of the
requirements for the Degree of Master of Science.

ABSTRACT

The concept of cogeneration of electric power in a solid electrolyte fuel cell while producing an industrially useful end product was demonstrated. Ammonia oxidation over a platinum catalyst being the first step during nitric acid manufacture was chosen for study. At a temperature of 1100K with an STP flow rate of 5 cm^3/min containing 1% ammonia in helium, conversions of over 97% with 47% selectivity to nitric oxide, the desired product, were obtained. At lower conversions, selectivities of 97% were obtained. Power density under these conditions was 7 $\mu watt/cm^2$ and could only be increased at the expense of ammonia selectivity. Overpotential behavior was found to be purely ohmic. The observed reaction kinetics, limited by oxygen transport through the electrolyte indicate that nitric oxide is the primary product which is subsequently reduced by ammonia to form nitrogen. A dimensionless group has been identified which governs the selectivity and power output of the fuel cell. A performance model has been created which predicts

selectivity and power output on the basis of this parameter.

Thesis Supervisor: Dr. Costas G. Vayenas, Assistant Professor of Chemical Engineering

CONTENTS

FIGURES

1. INTRODUCTION

The energy situation of today makes attractive the cogeneration of electric power during an exothermic process. In industry there are many applications of this, one being use of the excess heat of reaction to produce steam and drive a gas turbine thus producing electric energy. The aim of the present work is to utilize another method, the fuel cell, to cogenerate electric power.

The fuel cell has been customarily used as a primary energy source for projects requiring 10^{-2} - 10 Kw over a time period of 2 - 14 days (1). Typical applications for the hydrogen fuel cell are the Apollo space program and the electric car. In each case hydrogen is oxidized to water while producing the power. To use the fuel cell as a power plant is an expensive venture due to the present cost of fuel such as hydrogen and the greatly decreased value of the product.

For our study the ammonia oxidation to nitric oxide, being the first step in the production of nitric acid, is a likely candidate for cogeneration since it produces a high value end product.

Traditionally, nitric acid has been produced using the Du Pont pressure process (2). In this process, ammonia mixed with an excess of air is passed over a platinum gauze catalyst at 1050 K with very short contact times to minimize decomposition. The conversion to nitric oxide occurs with a 95% yield and a large heat production. The nitric oxide is subsequently cooled and reacts homogeneously to nitrogen peroxide (NO_2) which is then absorbed in water to form nitric acid. In our process, we propose to carry out the ammonia oxidation in a fuel cell thus obtaining electric energy from the Gibbs free energy change rather than heat as is the present practice.

Nitric acid is produced in plants with capactites upwards of 2×10^5 kg

per day at 58 wt% strength. With this production level the electric power cogenerated would be of great benefit. One problem may be that selectivity and conversion per pass in the fuel cell will be less than those of the industrial process. If this does occur then the power gained must at least compensate for the ammonia lost due to decomposition or other side reactions.

2. BACKGROUND

Fuel cells using other than solid electrolytes have been in existence since Sir William Grove in 1839 (3) observed that when hydrogen and oxygen are supplied separately to two platinum electrodes immersed in sulfuric acid, a current is produced in the external circuit connecting the two platinum electrodes through a load. Solid electrolyte fuel cells have only recently come into their own with the advent of the United States space program. Their application to industrial processes still remains to be seen.

Oxygen-ion conducting solid electrolytes are formed from either ZrO_2, ThO_2 or CeO doped with CaO, Sc_2O_3, V_2O_3 or La_2O_3 in a solid solution. Their high ionic conductivity occurs due to the O^{-2} site vacancies which occur in the fluorite type lattice structure when doped (6). For our study we have chosen an 8 mol% Y_2O_3 in ZrO_2 (yttria stabilized zirconia) solution. This composition gives high ionic conductivity and low cost, the two most important factors for industrial fuel cell applications.

During operation of a typical fuel cell, the fuel stream, here ammonia, passes through the inside of the reaction tube while air surrounds the outside. The steps involved in reaction can be visualized using figure 1. Oxygen molecules diffuse through the air to the air-electrode surface where they dissociate and are adsorbed. Surface migration then occurs over the electrode to sites at the electrode-electrolyte interface where, combining with 2 electrons from the electrodes, an oxygen atom becomes an O^{-2} ion and enters an oxygen-ion vacancy in the crystal lattice of the solid electrolyte. Oxygen-ion transport through the electrolyte then occurs. At the fuel electrode, oxygen ions leave the electrolyte, giving their electrons to the electrode, thus completing the current flow, and react with the fuel (am-

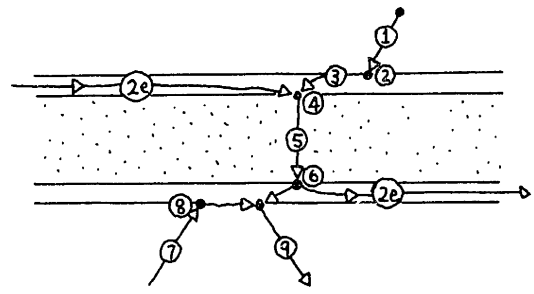

Figure 1. An electrode-reaction process chain for solid-electrolyte fuel cells. Key: 1. oxygen molecules diffuse through air to electrode surface; 2. adsorption and dissociation of O_2; 3. surface migration to reaction site; 4. oxygen combines with electrons, forming O^{-2} ions; 5. ionic transport of O^{-2} ions through electrolyte; 6. deionization and surface reaction with fuel, delivery of electrons to the fuel electrode; 7. diffusion of fuel to fuel-electrode surface; 8. adsorption of fuel on electrode, surface migration to reaction site; 9. desorption of reaction product and diffusion into fuel stream.

monia) which has diffused to the fuel electrode surface. The products of the surface reaction are desorbed from the electrode and diffused into the fuel reaction product stream. The electrodes in our case also play the role of a heterogeneous catalyst for the ammonia oxidation. At the terminals of the cell a generated voltage appears and under open-circuit conditions is expressed by the Nernst equation as,

$$E = \frac{RT}{4\mathcal{F}} \ln \frac{p_{O_2,i}}{p_{O_2,o}} \quad . \tag{1}$$

The subscripts refer to the inner, anode or fuel electrode and the outer, cathode or air electrode.

If the cell operates at a load current I, equal to the reaction of G_{O_2} moles of O_2 per second then,

$$I = 4\mathcal{F}\, G_{O_2} \quad . \tag{2}$$

The cell terminal voltage is decreased by the ohmic resistance losses caused by the transport of electrons through the electrodes and O^{-2} ions through the electrolyte and by the irreversible losses associated with the transport of reactants and reaction products to and from the electrodes. The observed terminal voltage is then,

$$E_a = E - IR - E_{irr} \tag{3}$$

where E_{irr} represents the losses due to nonohmic irreversible processes.

Etsell and Flengas (7) among others, have studied the overpotential behavior of stabilized zirconia fuel cells with platinum electrodes using hydrogen or carbon monoxide as the fuel. In each case they observed almost pure ohmic resistance overpotential, with the remainder occurring due to activation overpotential. In our cell we expect the reaction and hence power output to be somewhat limited by the electrolyte resistance to oxygen ion transport. If this restriction is severe then the kinetics will also

be governed by oxygen transport through the zirconia cell. The high temperatures used during ammonia oxidation are beneficial since cell resistance decreases with increasing temperature.

Industrially, the ammonia oxidation reaction proceeds over a pack of fine 80 mesh gauze woven from platinum or platinum-rhodium alloy wire. Reaction temperatures are in the 1100K range with a feed composition of 8-9% ammonia in air. Short contact times of approximately 0.01 sec are used and 94-98% of the ammonia is oxidized to nitric oxide (2). At temperatures below 800K or above 1250K the main product is nitrogen due to decomposition. Pignet and Schnidt (4) have studied the kinetics of ammonia oxidation on platinum wires and found that the main reactions occuring may be written as,

$$NH_3 + 5/4\ O_2 \rightarrow NO + 3/2\ H_2O \quad (4)$$

$$NH_3 + 3/2\ NO \rightarrow 5/4\ N_2 + 3/2\ H_2O \quad (5)$$

$$NH_3 \rightarrow 1/2\ N_2 + 3/2\ H_2 \quad (6)$$

$$NO \rightarrow 1/2\ N_2 + 1/2\ H_2 \quad (7)$$

$$H_2 + 1/2\ O_2 \rightarrow H_2O \quad (8)$$

Reaction (4) leads to the desired product NO while reactions (5)-(7) give the undesired product, N_2. This scheme accounts for all nitrogen containing products except N_2O.

Platinum catalysts are known to undergo extensive rearrangement under reaction conditions (5). The platinum in our fuel cell, even though applied in a thin layer, should be no exception. The question of platinum rearrangement in fuel cell electrodes will also be explored and compared to that observed in industry.

Fuel cells, as previously mentioned, offer an effective means of transforming a major portion of the Gibbs free energy change for the

desired reaction (8) into electric energy. At conditions of maximum power output it is expected that approximately 60-70% of the reaction ΔG will be transformed into useful work (1). Contrast this with the 30-40% efficiency of the traditional power conversion methods, due to Carnot cycle limitations and the value of fuel cells is evident.

With these factors in mind, the high temperature solid electrolyte ammonia fuel cell

$$NH_3,\ NO,\ H_2O,\ Pt \mid ZrO_2\ (Y_2O_3) \mid Pt,\ air$$

is a promising candidate for cogeneration research with application to industrial chemical operations.

3. EXPERIMENTAL

3.1 Apparatus

The functional parts of our experimental system can be broken down into three major sections, feed, reaction and analysis. Each of these is described below and is shown in figures 2-4. Detailed equipment specifications appear in the appendix.

3.1.1 Feed

The feed system, shown at the top of figure 2, supplied the reactor with a stream of gas at constant pressure, flowrate and compostion. The gas supplies were high pressure cylinders of NH_3, air, NO and He. The NH_3 and NO were certified Matheson standards at 4.59% and 8550 ppm in helium, respectively while the air and He were Matheson zero gas standards. Inlet pressure to the flowmeters was set by the regulators on each tank to 2.39×10^5 Pa. Pressure inside the reactor was never more than 1.36×10^5 Pa. The gas mixture from the flowmeters could then be routed to 1) the bubble meter to measure the total flowrate at STP, 2) the infrared analyzers, bypassing the cell to measure composition or check calibration or, 3) the fuel cell for reaction and then onto the analyzers to measure exit composition. The path taken was determined by closing and opening the respective on-off valves shown in figure 2. To prevent any possible reaction before the fuel cell, 316 stainless steel tubing and fittings were used throughout.

3.1.2 Reaction

The entire reaction system used is shown in the center portion of figure 2 while the specifics of the fuel cell design are detailed in figure 3. Temperature was held constant to within ± 1 K utilizing an on-off type tubular furnace with a temperature controller. Actual reactor temperature was measured by a thermocouple placed in contact with the outside reactor wall.

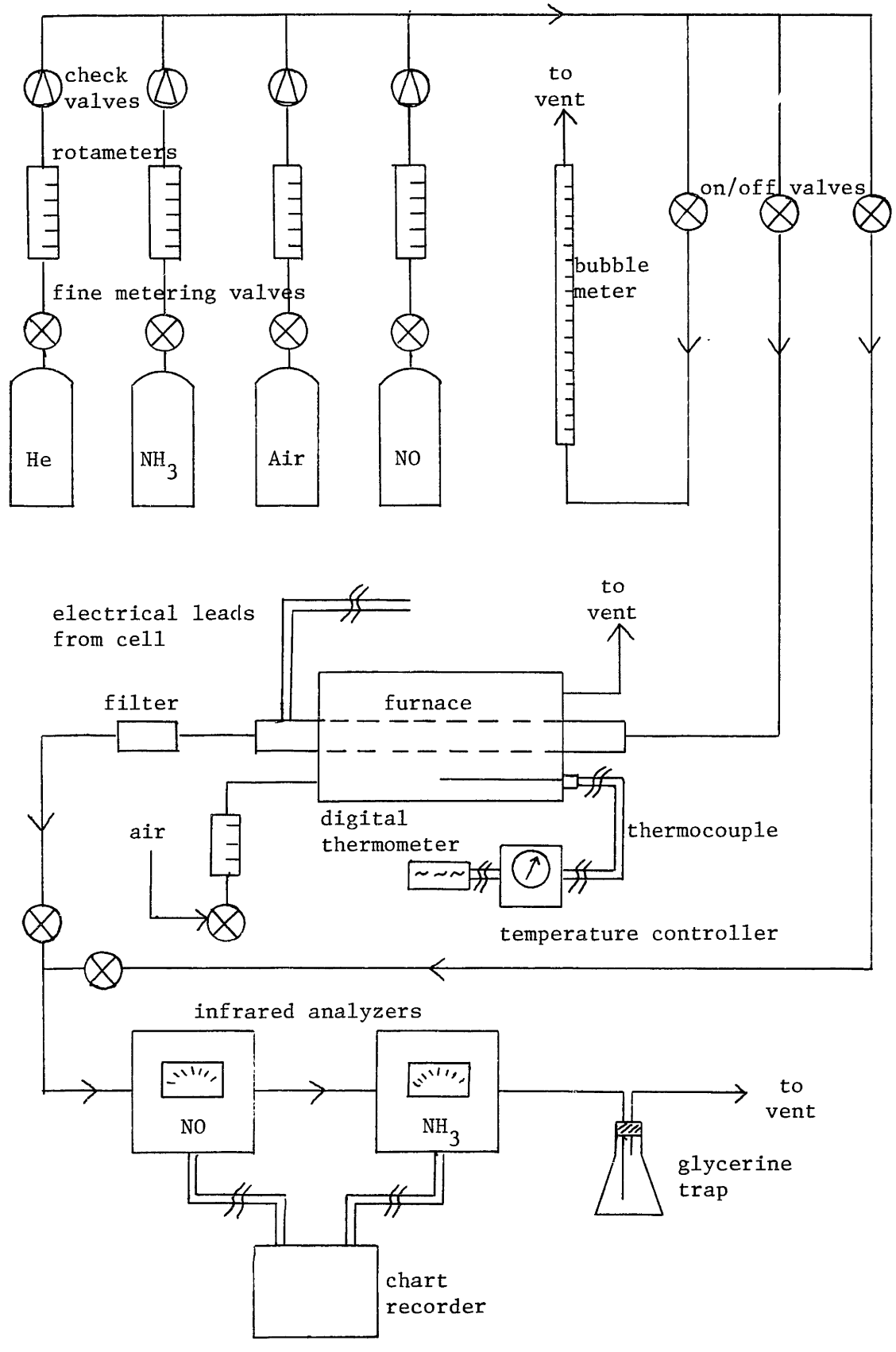

Figure 2. Experimental apparatus.

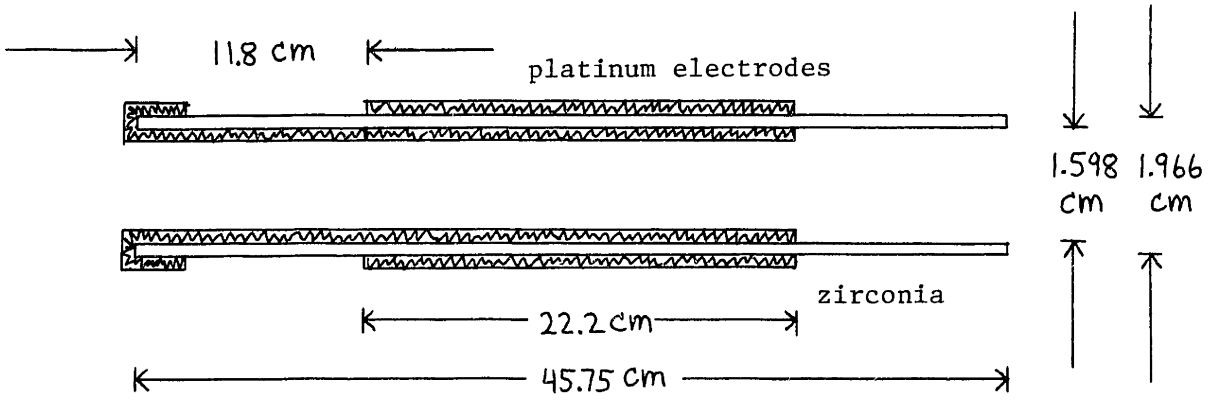

Electrode configuration

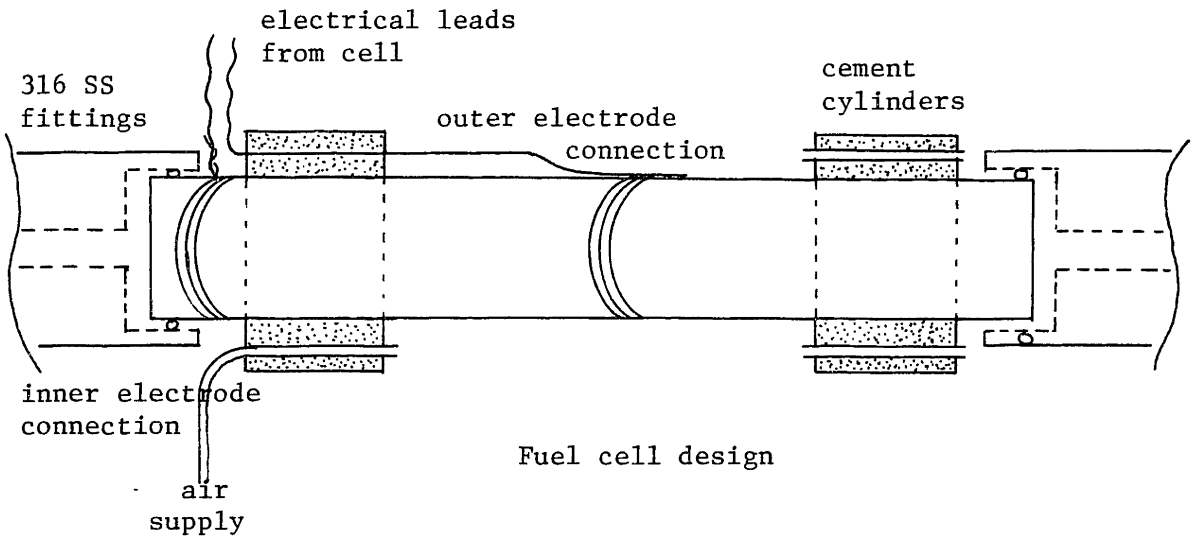

Fuel cell design

Figure 3. Fuel cell design and electrode configuration.

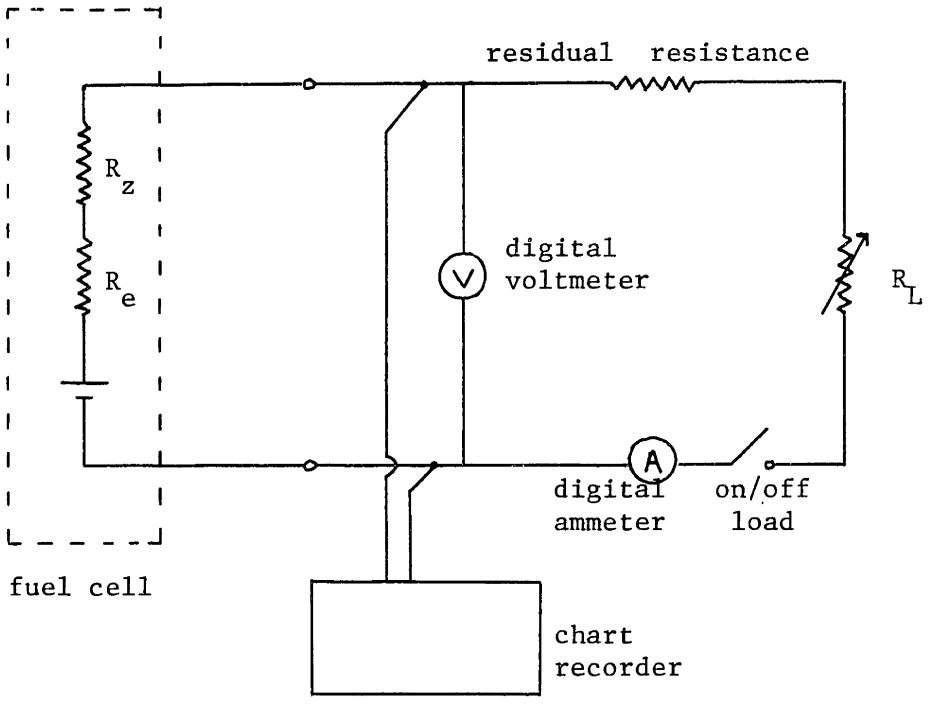

Figure 4. Electrical schematic with representation of the fuel cell voltage source and inherent electrode and electrolyte resistance.

The fuel cell design is unique and deserves special attention. The base is an 8 mol% yttria stabilized zirconia tube supplied by Corning Glass Works with the exact dimensions shown in figure 3. Upon this base a coat of platinum ink was applied inside and out with a paint brush and cotton swab according to the desired dimensions and left to air dry. When dry the platinum film was calcined at 1300K for four hours to drive off the organic suspension and leave a layer of platinum metal. The procedure was then repeated to form two coats of Englehard A3788 ink and one coat of Englehard 6926 unfluxed ink. This insured an even, highly conducting, porous electrode. Resistance measurements showed each electrode to be 0.24 ohms. Surface area was extimated to be on the order of 300 cm^2 per cm^2 of superficial catalyst area by BET. Catalyst thickness was estimated to be 3μm by gravimetric techniques. A scanning electron micrograph of the unused surface appears in figure 5. The extension of the inner electrode to the outer surface renders the actual reactor area somewhat arbitrary but allows for good electrical contact. All values reported are based on the active fuel cell length of 22.2 cm.

Zirconia is not mechanically strong under large thermal gradients and hence has a high tendency to crack. To alleviate this problem, cement cylinders made of Dylon C-3 cement were fashioned around the continuous zirconia tube at the points where it entered and exited the furnace. The outside diameter of these cylinders was such that it filled the void area between the outside diameter of the fuel cell and the inside diameter of the furnace thus providing the necessary support to prevent cracking. The thermocouple and outer electrode lead wire were imbedded in the cement. To allow air to reach the outside electrode and excess nitrogen to escape, small tubes were also cast in the cement

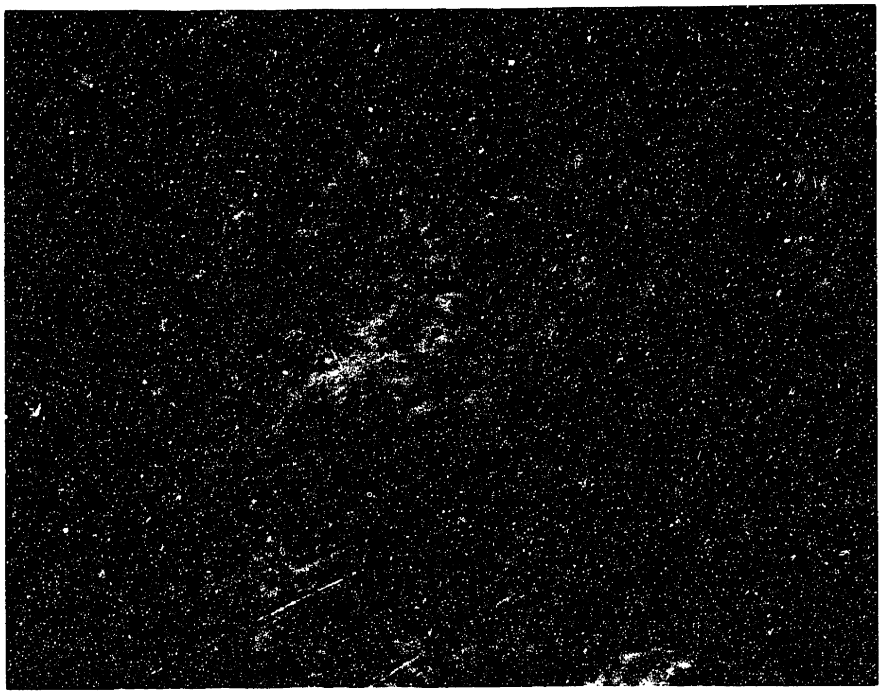

Figure 5. Scanning electron micrograph of the unused platinum electrode surface.

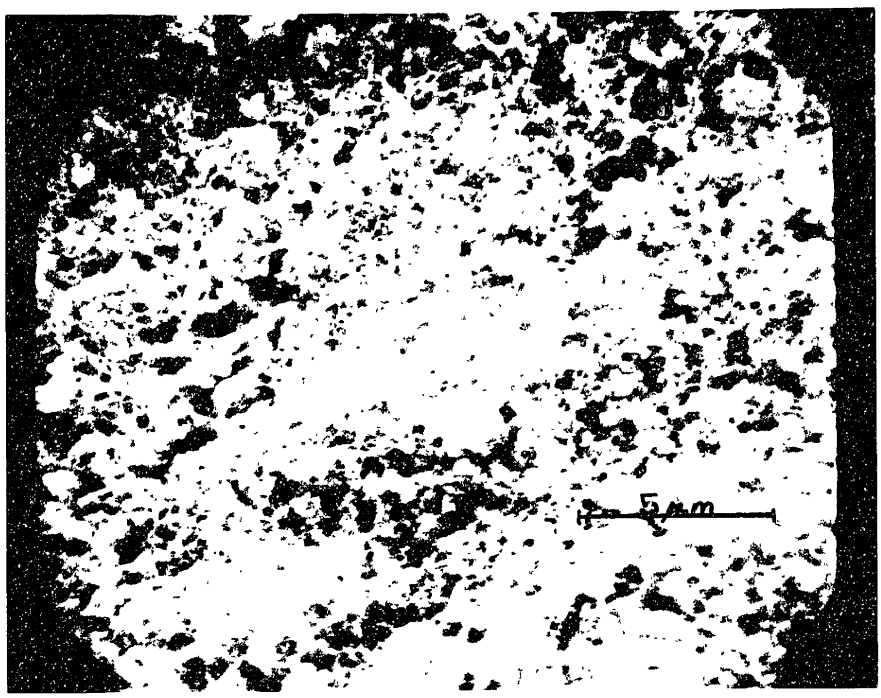

Figure 5. Scanning electron micrograph of the unused platinum electrode surface.

cylinders. Air was fed at a rate of 900 cm^3/min to the outside of the cell to prevent oxygen from limiting the reaction kinectics. Stainless steel fittings were butted onto the fuel cell ends and made leak tight with Viton O-rings placed around the zirconia. The assembly passed a helium leak test to 4.46×10^5 Pa.

3.1.3 Analysis

The analysis system for reactants and products consisted of the equipment shown in the lower third of figure 2. The reactants from the cell bypass line or the products from the fuel cell passed through the series connected NO and NH_3 analyzers, respectively. Electrical output from the analyzers was recorded on a two pen chart recorder to show the approach to steady state of each data point. The exit gas was fed through a glycerine bubbler to prevent back diffusion of air to the system when operated at very low flow rates. The analyzers were calibrated using the standard gases mentioned at least once every eight hours to insure accuracy.

To observe the power production capabilities and open circuit behavior of the cell, the electrical system of figure 4 was used. Voltage and current were measured using two separate digital multimeters with the voltage output being sent to a chart recorder. Load resistance was determined using a decade resistance box with a range of $1\text{-}10^6 \Omega$ and the circuit placed on load by a toggle switch. Lead connectors from the fuel cell to the instruments were kept short to minimize voltage losses. As figure 4 shows, a residual resistance, even with no load resistance, still was presint due to connectors and wires. The residual resistance was calculated to be $.873 \pm .017 \Omega$.

3.2 Procedure

The focus for this research was on the overpotential characteristics of the ammonia fuel cell as a function of temperature and flow rate and its selectivity to nitric oxide and power production as functions of flow rate at STP, temperature and inlet feed concentration of ammonia.

Using the 4.59% ammonia in helium mixture and diluting it with pure helium any composition below the stock was obtainable. Data were taken for 4.59, 3.0, 2.0 and 1.0 per cent NH_3 in He with STP flow rates in the 5-20 cm^3/min range. These flow rates are very low compared to those in industry but were found to yield the best selectivities after numerious trials. Temperature was varied between 900 and 1200K, the region where NO production is highest.

Cell overpotential behavior was explored by passing 4.59% NH_3 and varying the flow rate, load resistance and temperature while recording the corresponding currents and voltages. From these curves an estimate of the dominant overpotentials was obtained. Power output and selectivity, the main concern of this project were next obtained. Composition and STP flow rate were held constant while temperature was varied for each run. In addition to gathering the required data this allowed the cell to be tested under repeated thermal cycling as a prelude to industrial application. Catalyst behavior and change with time was also observed using scanning electron microscopy.

4. RESULTS

4.1 Cell Resistance

As figure 4 shows there are four resistances that must be taken into account, two of which are inaccessible individually. During all runs the load resistance R_L, was kept at zero but the residual resistance due to the lead wires remained. By applying a voltage and measuring the current, the resistance of the fuel cell can be quantified and is shown versus temperature in figure 6. The cell resistance is composed of two parts, that due to the zirconia tube R_z, and due to the two electrodes R_e. The resistance due to the two electrodes was measured at 300K and found to be 0.48Ω and is assumed not to vary with temperature. At low temperatures R_z dominates the cell resistance. A quantitative estimate of the electrolyte resistance can be made from the linear portion of figure 6 and is given by,

$$R_z = 7.649 \times 10^{-5} \exp [10623/T] \ \Omega \tag{9}$$

where T is in degrees Kelvin. The total cell resistance can then be written as,

$$R_c = R_z + R_e$$

$$R_c = 7.649 \times 10^{-5} \exp [10623/T] + 0.48 \ \Omega \tag{10}$$

with the assumption of constant R_e. At high temperatures the electrode resistance dominates R_c and becomes the limiting factor in current flow and hence oxygen flux.

4.2 Open Circuit

Figure 7 shows the observed open circuit behavior when 4.59% NH_3 at 20 cm^3/min is passed through the cell. Plotted also are the theoretical voltages for ammonia decomposition and oxidation. These

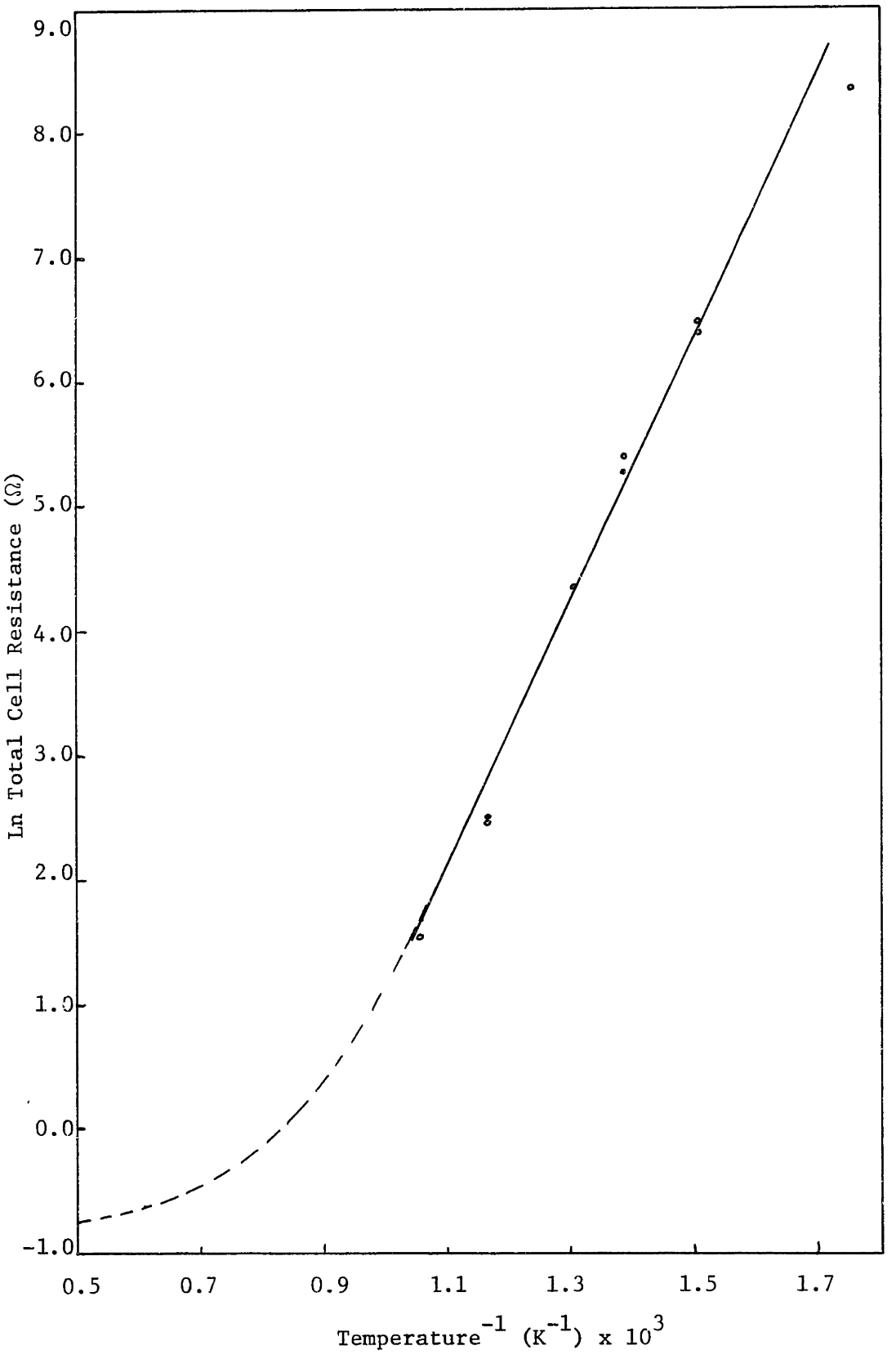

Figure 6. Total cell resistance versus temperature.

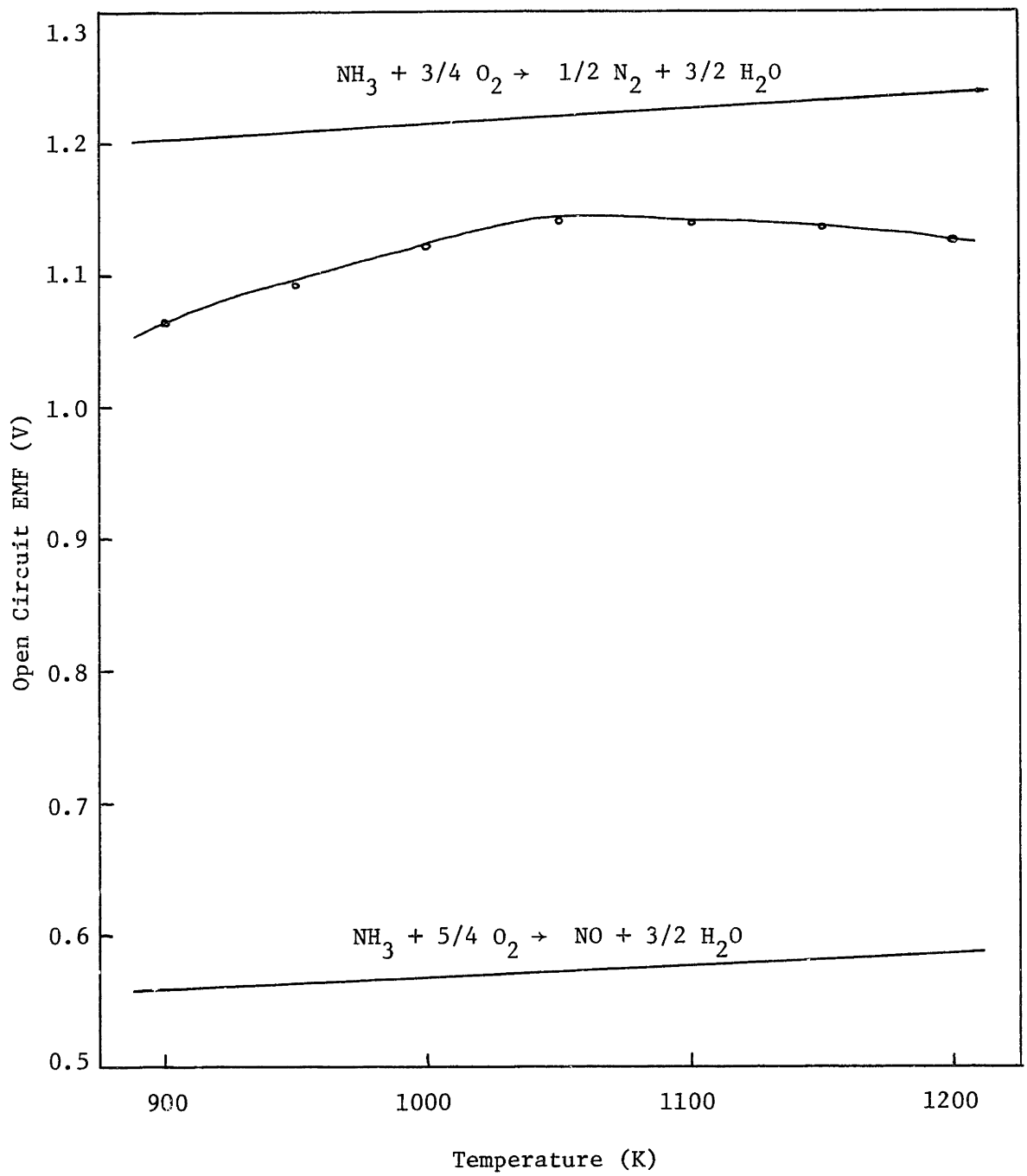

Figure 7. Open circuit voltage behavior. $y_{NH_3,f}$ = .0459, F = 20 cm^3/min STP

voltages were calculated using the Gibbs free energy change for each reaction based on the partial pressure of oxygen that would be in equilibrium with the hydrogen and nitrogen formed. The graph does not imply that these are the reactions occuring under open circuit conditions.

4.3 Overpotential

Voltage versus current curves for three different flow rates of 4.59% NH_3 appear in figures 8-10. The load resistance was varied to change the current output from the cell. Limiting currents due to fuel depleation as calculated from,

$$I_L = F\, y_{NH_3,f}\ (3/4)\ (4\mathcal{F}) \tag{11}$$

are also shown in the figures. This limiting current is never exceeded by our data.

4.4 Product Selectivity

Ammonia selectivity to the desired product, nitric oxide, as a function of temperature is shown in figures 11-14. Selectivity is traditionally defined as,

$$S = \frac{\text{reactant converted to desired product}}{\text{amount of reactant converted by all reactions}} \tag{12}$$

and is so defined here. Each graph has the flow rate held constant rather than converting it to residence time. Since we are dealing with a catalyst applied to the wall of our reactor, the proportionate increase in surface area when volume is increased is not a constant hence, two reactors of differing surface to volume ratios may have the same residence time but give wildly differing results. Residence times can easily be calculated from the data given in figure 4.

From these figures it is clear that selectivity is strongly dependent on flow rate, ammonia feed concentration and temperature.

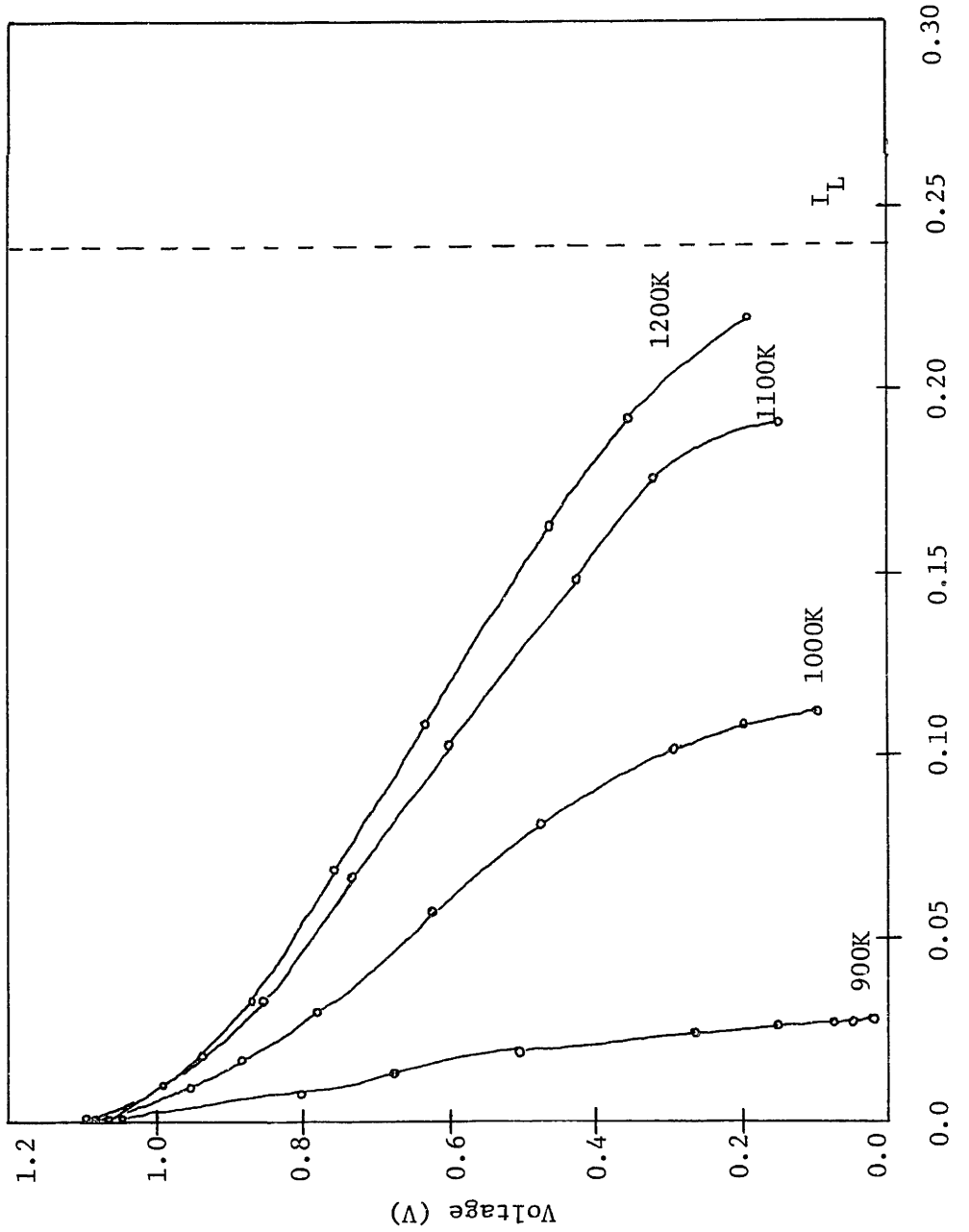

Figure 8. Overpotential behavior. $y_{NH_3,f}$ = 0.0459, F = 26.1 cm^3/min STP

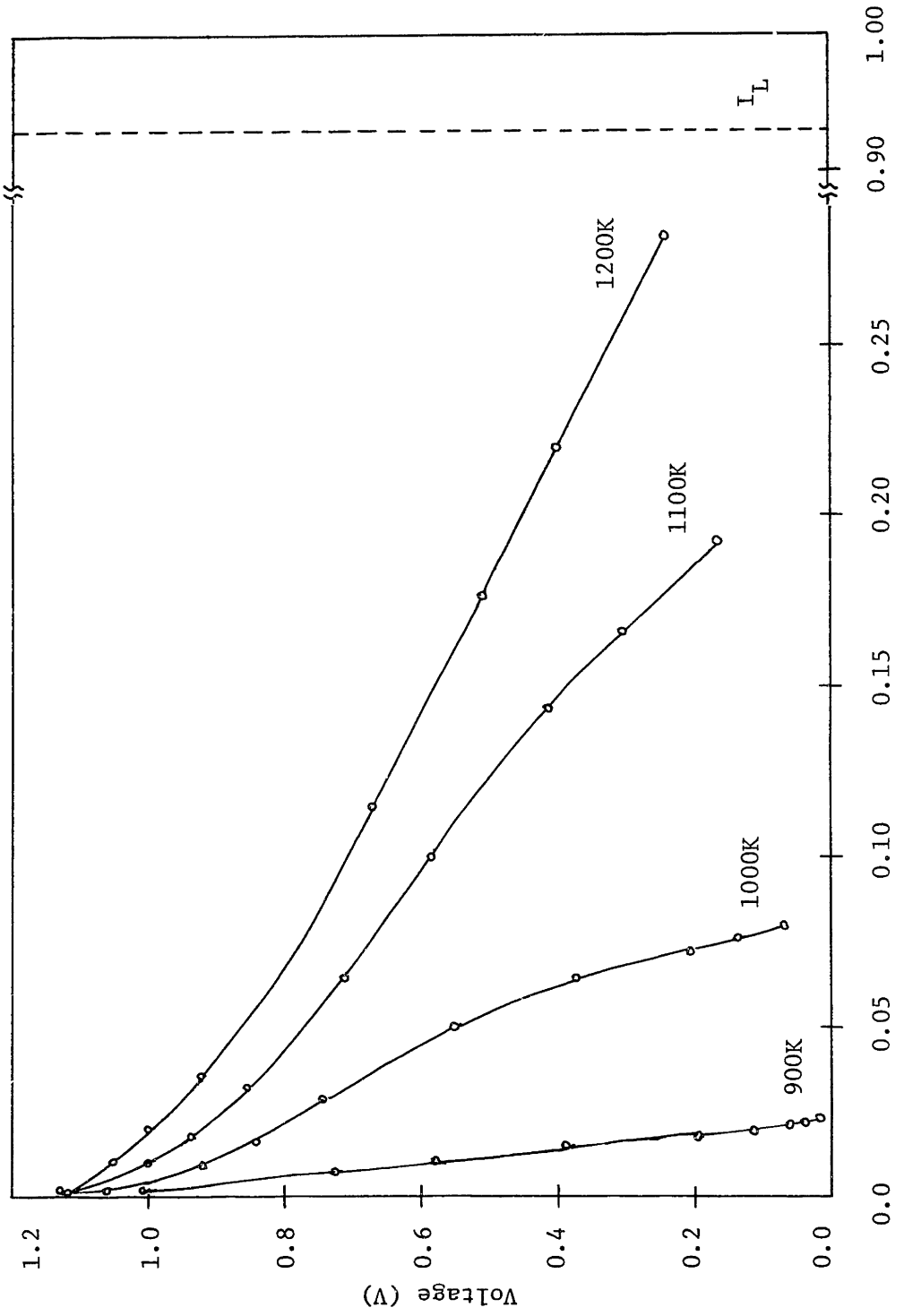

Figure 9. Overpotential behavior. $y_{NH_3,f}$ = 0.0459, F = 101.1 cm^3/min STP

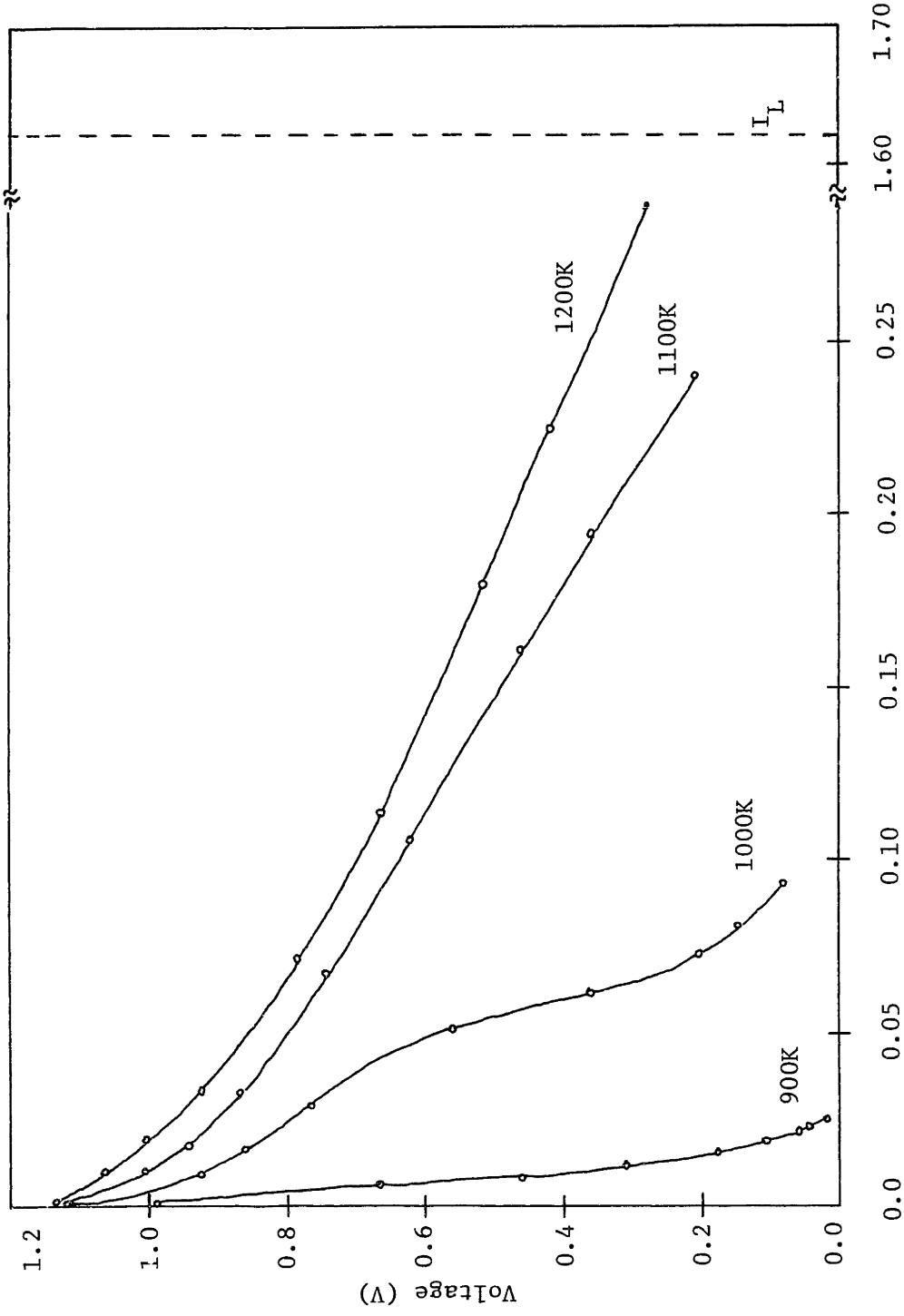

Figure 10. Overpotential behavior. $y_{NH_3,f}$ = 0.0459, F = 176.5 cm^3/min STP

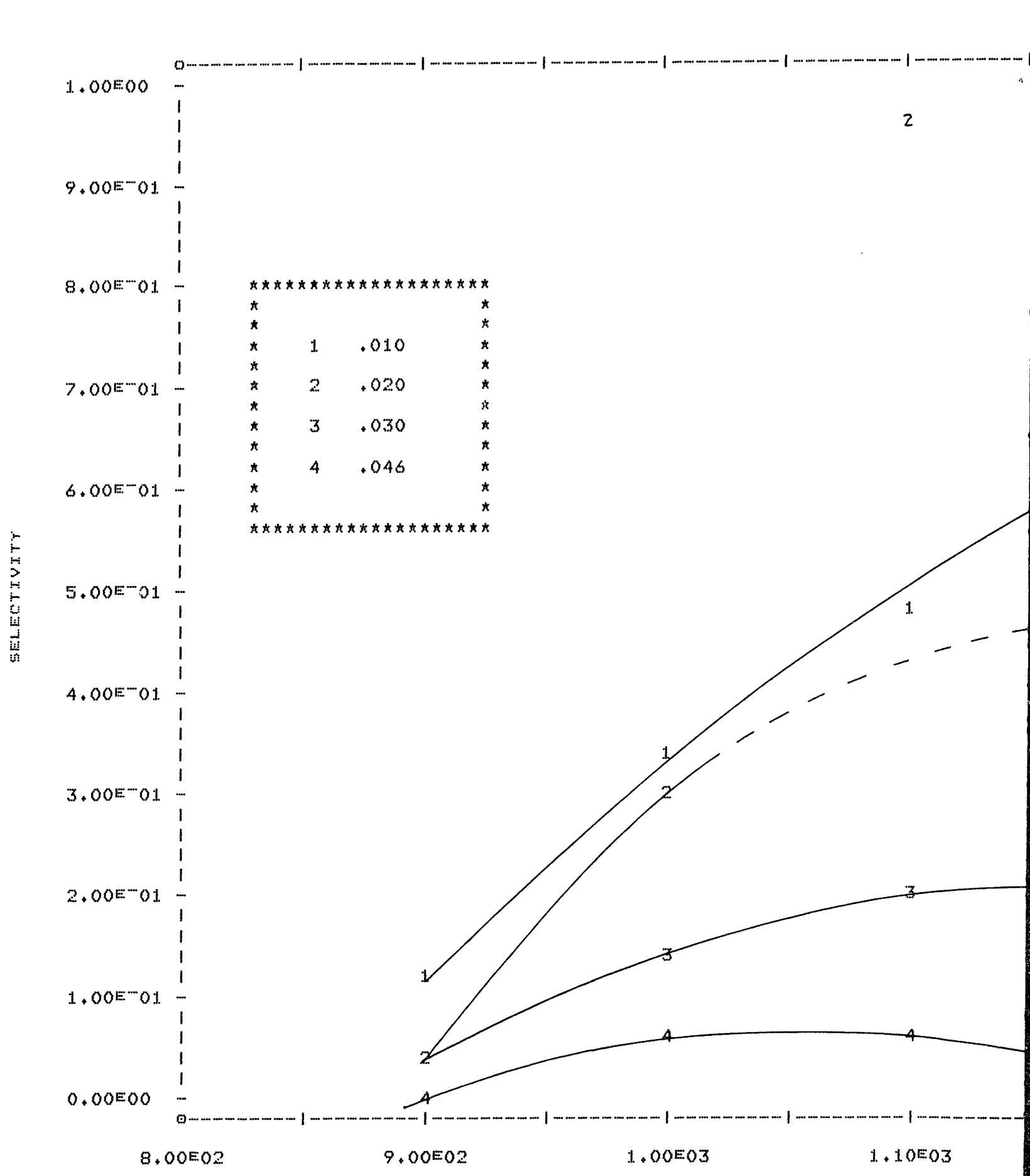

FIGURE 11. SELECTIVITY VERSUS TEMPERATURE, FLOW RATE

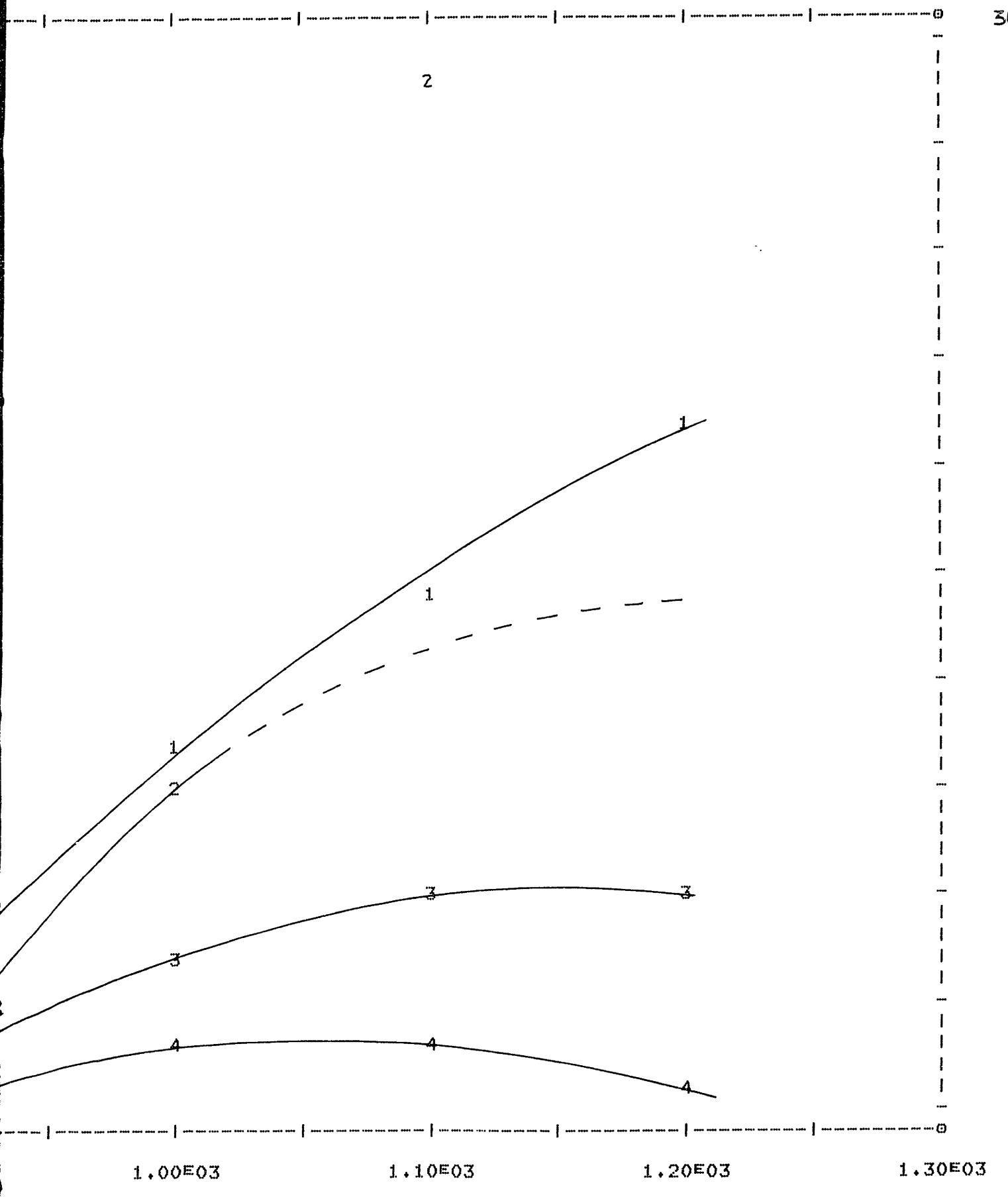

SELECTIVITY VERSUS TEMPERATURE, FLOW RATE 5 CM3/MIN STP

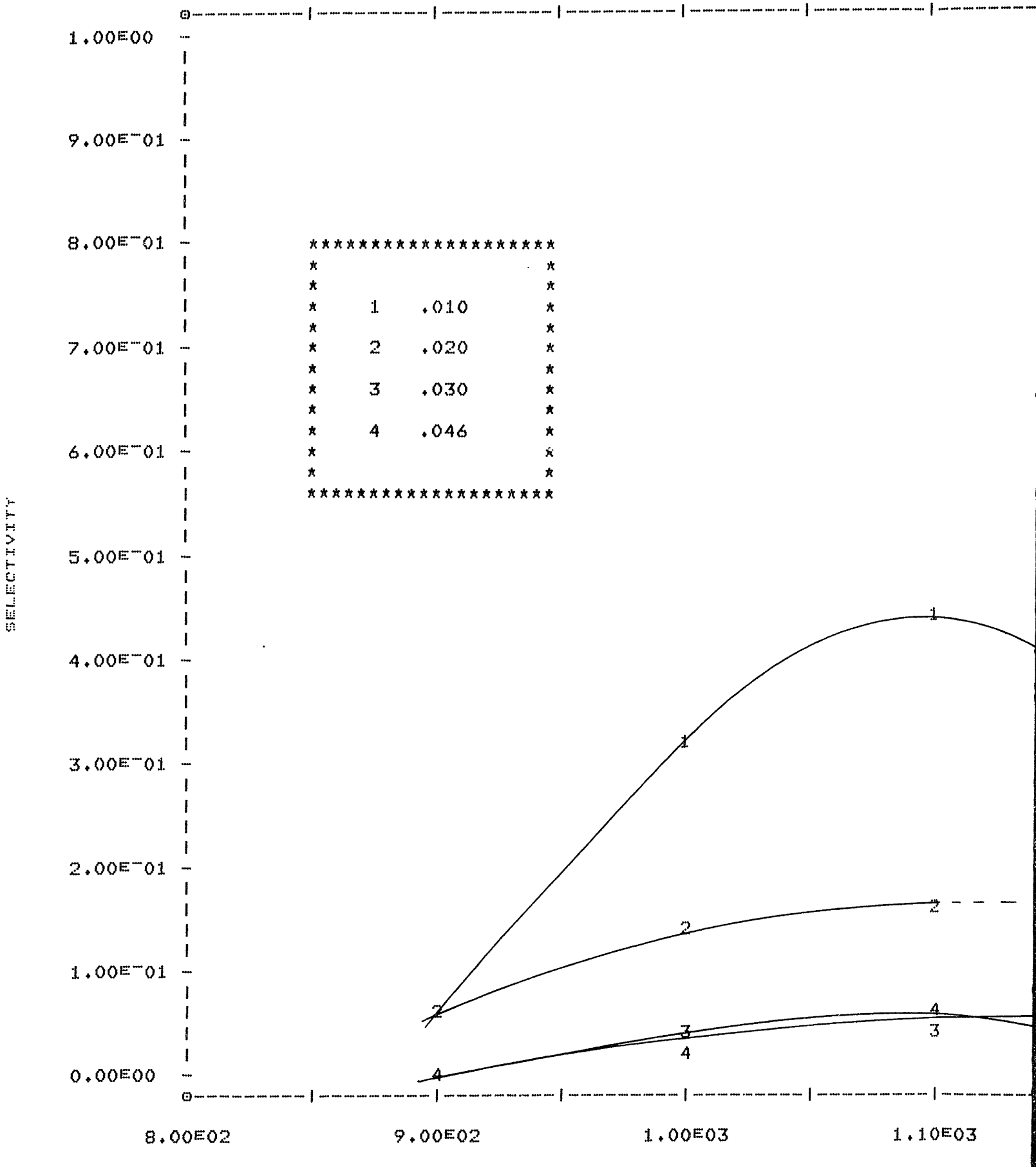

FIGURE 12. SELECTIVITY VERSUS TEMPERATURE, FLOW RATE

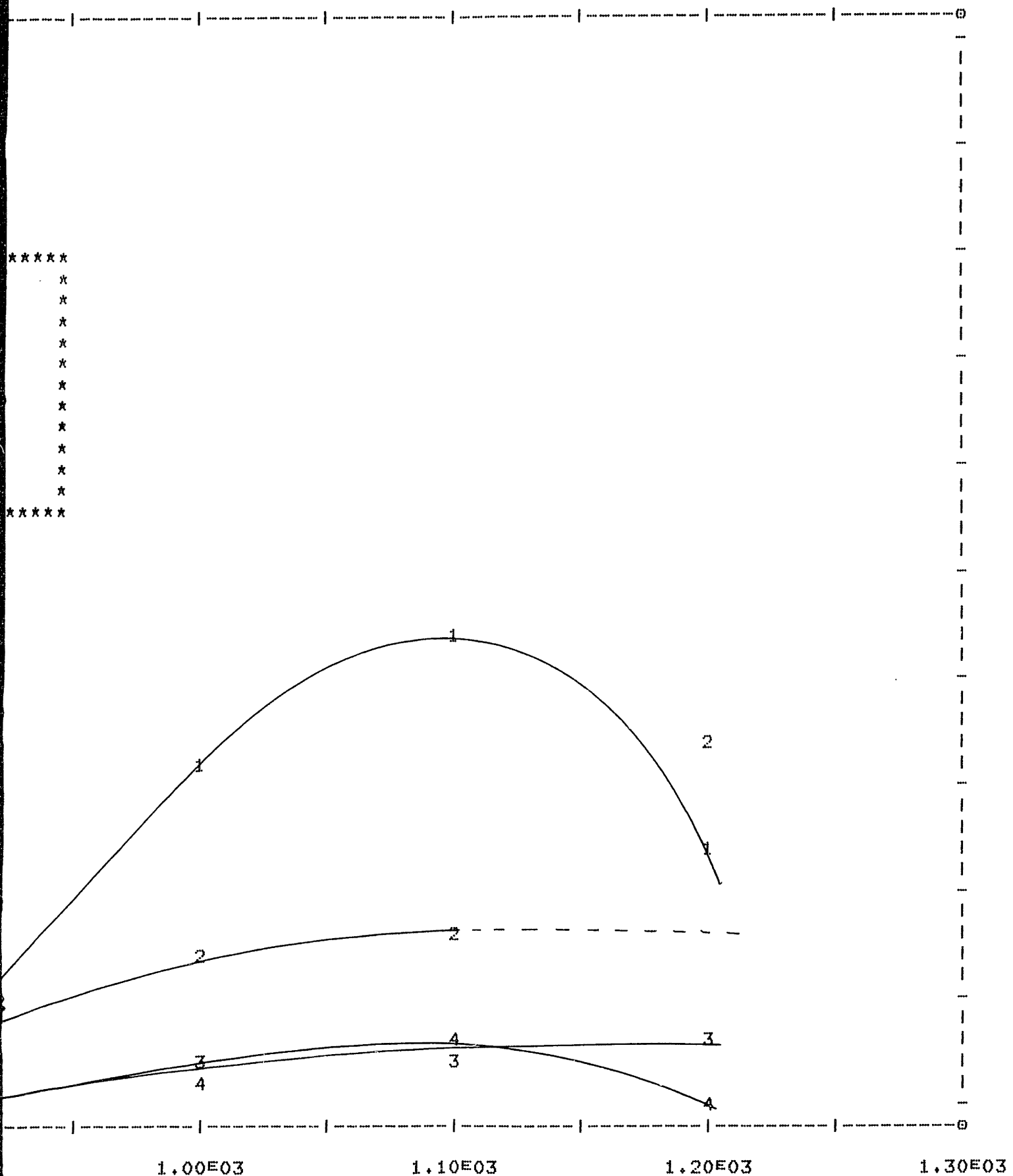

. SELECTIVITY VERSUS TEMPERATURE. FLOW RATE 10 CM3/MIN STP

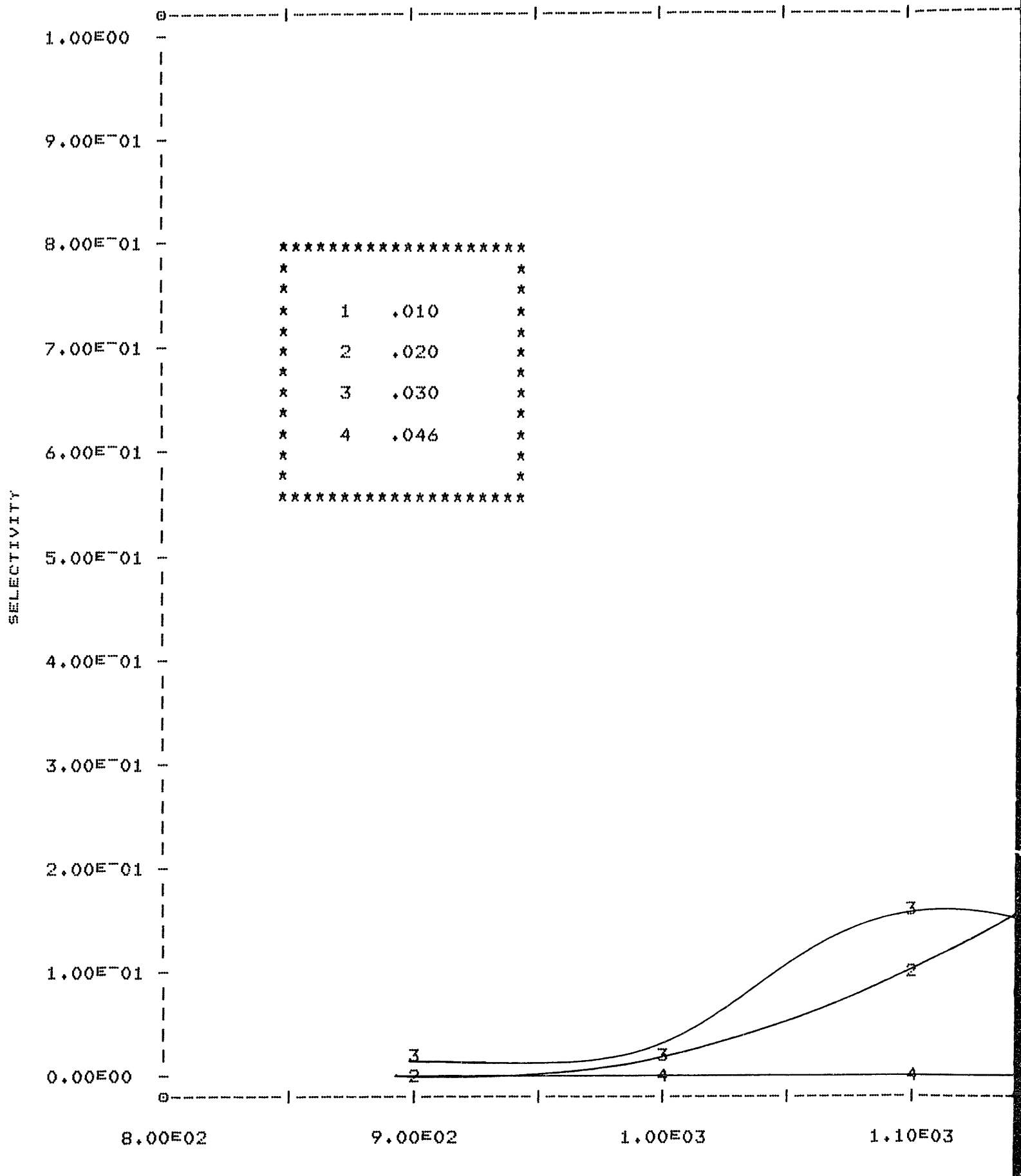

FIGURE 13. SELECTIVITY VERSUS TEMPERATURE, FLOW RA

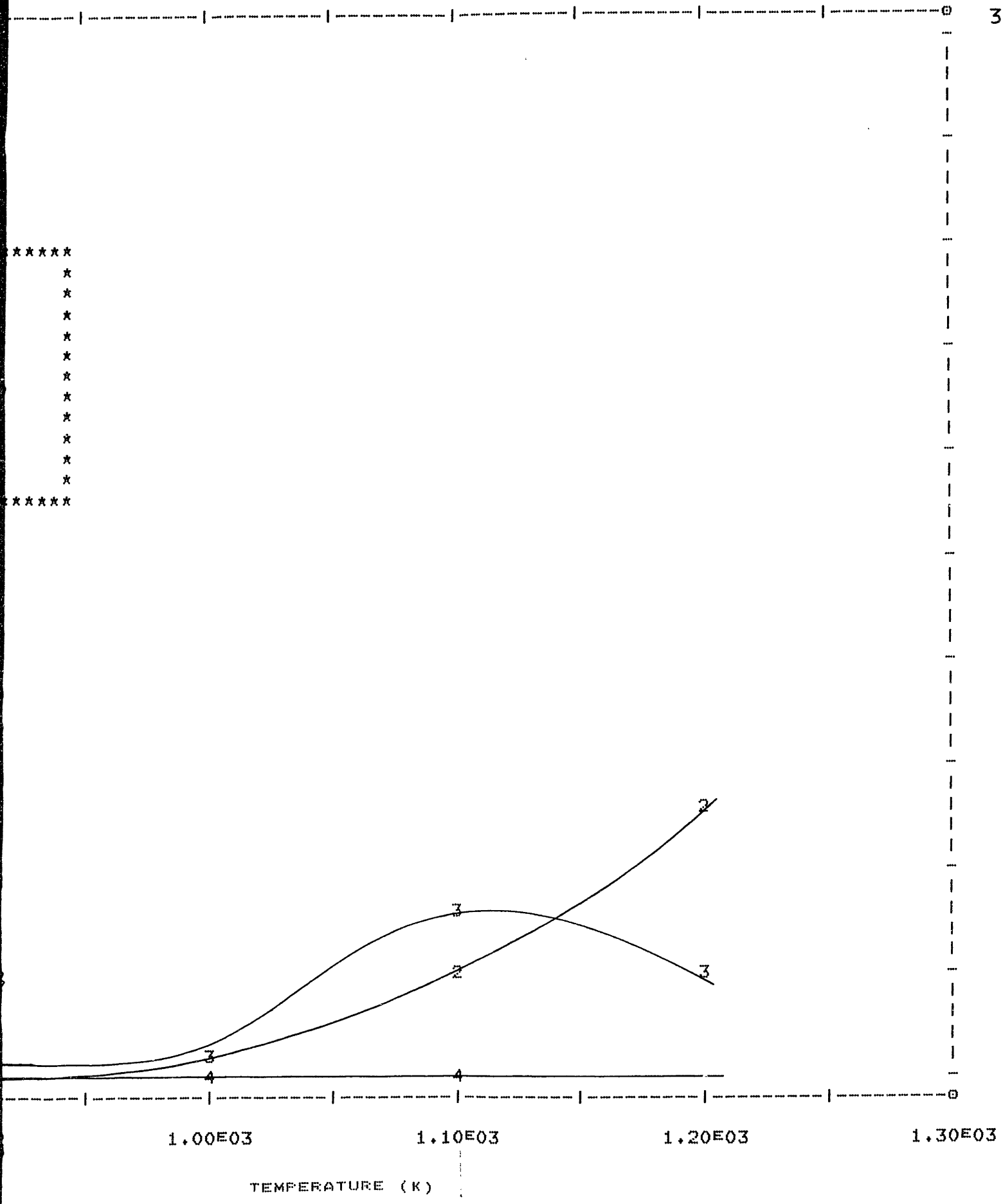

3. SELECTIVITY VERSUS TEMPERATURE, FLOW RATE 15 CM3/MIN STP

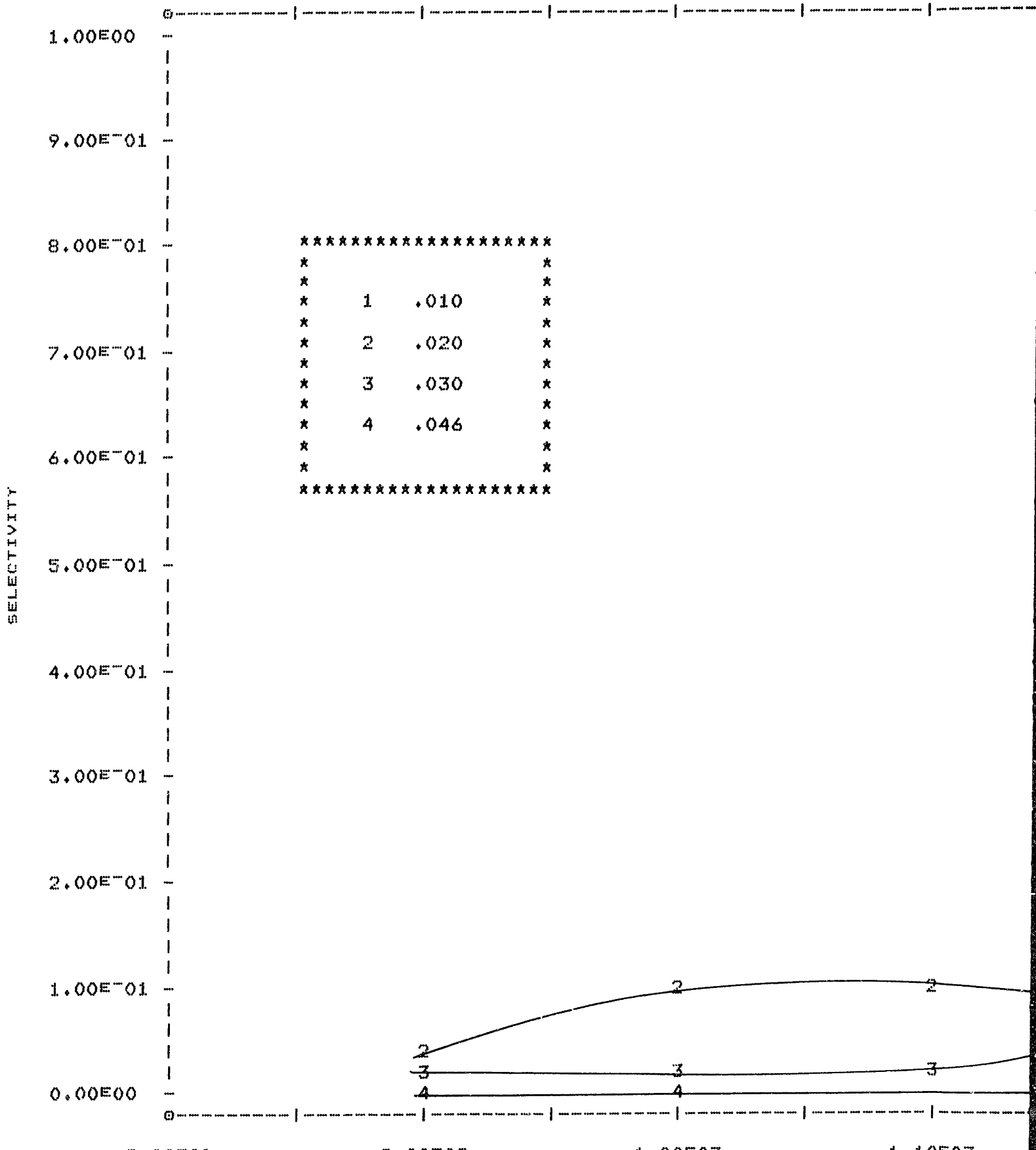

FIGURE 14. SELECTIVITY VERSUS TEMPERATURE. FLOW RAT

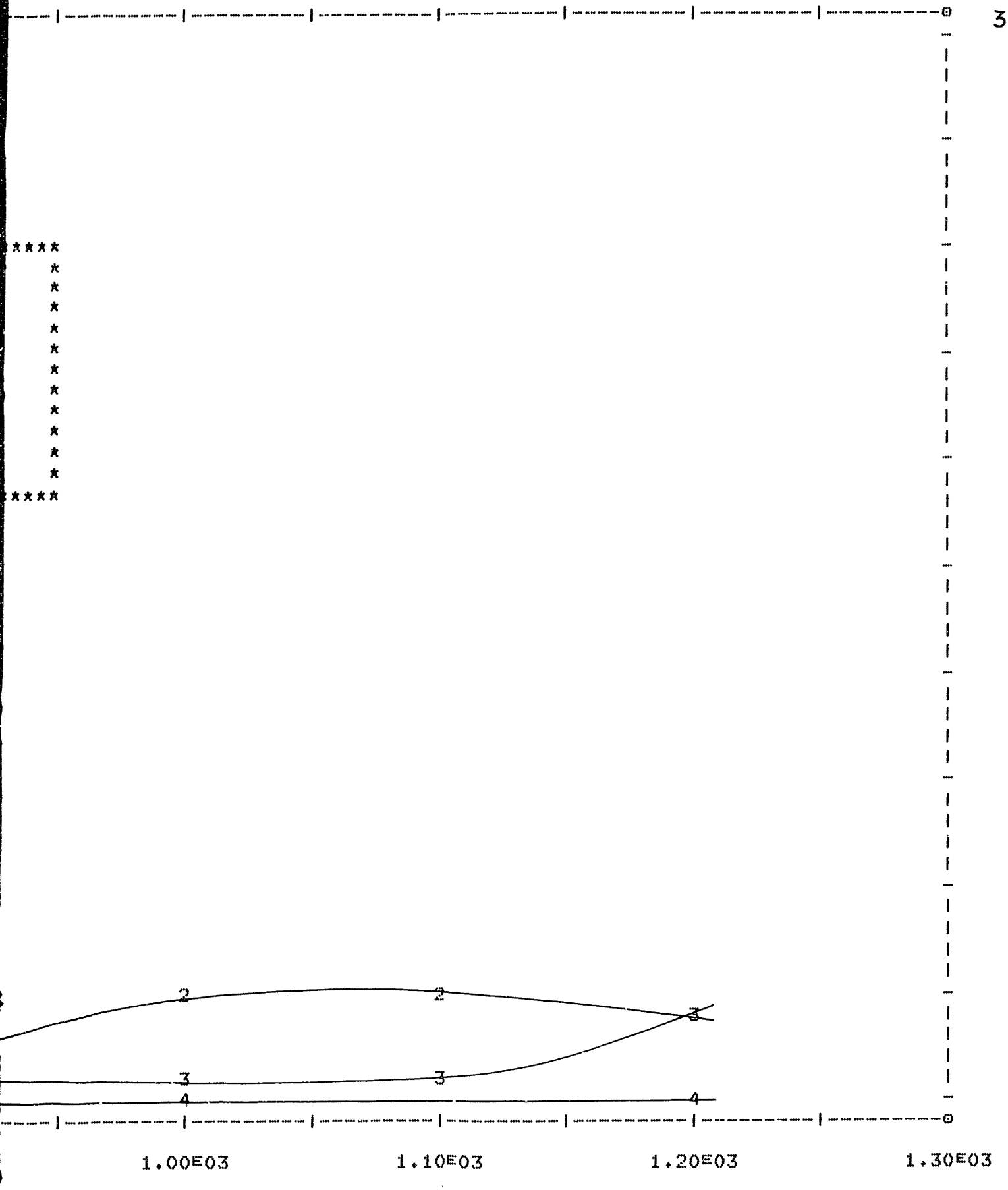

SELECTIVITY VERSUS TEMPERATURE, FLOW RATE 20 CM3/MIN STP

Over the rather limited range of values of these parameters investigated, selectivities as high as 65% were obtained.

Although the selectivity dependence on these parameters would appear to be complicated, it was found that the selectivity is almost uniquely determined by the value of the following dimensionless parameter r, defined as,

$$r = \frac{G_{O_2}}{G_{NH_3,f}} \tag{13}$$

where G_{O_2} is the molar flux of oxygen through the electrolyte, in the form of O^{-2} ions, and $G_{NH_3,f}$ is the molar flux of ammonia through the cell. This is shown in figure 15. For values of r below 0.75 the selectivity is low. However, for values of r above 0.75 the selectivity increased dramatically and values as high as 97% have been obtained for r = 1.0.

In light of this, no distinct trend exists on plotting selectivity versus conversion, figure 16. Selectivity does not tend to decrease with increasing conversion and this is an attractive feature of this cell.

4.5 Power Production

The cell power outputs obtained have been normalized to the reactor surface area, based on an average diameter of 1.782 cm and a length of 22.2 cm, and are presented as power densities in all figures. Figures 17-20 show the power densities obtained as functions of temperature. Each graph is at constant flow rate with the feed concentration of ammonia appearing as parameter.

4.6 Oxygen Introduction

Figures 21 and 22 show the effects of oxygen introduction, in the form of air, on fuel cell selectivity and power respectively. All data are at 4% nominal NH_3 concentration and a nominal STP flow rate of

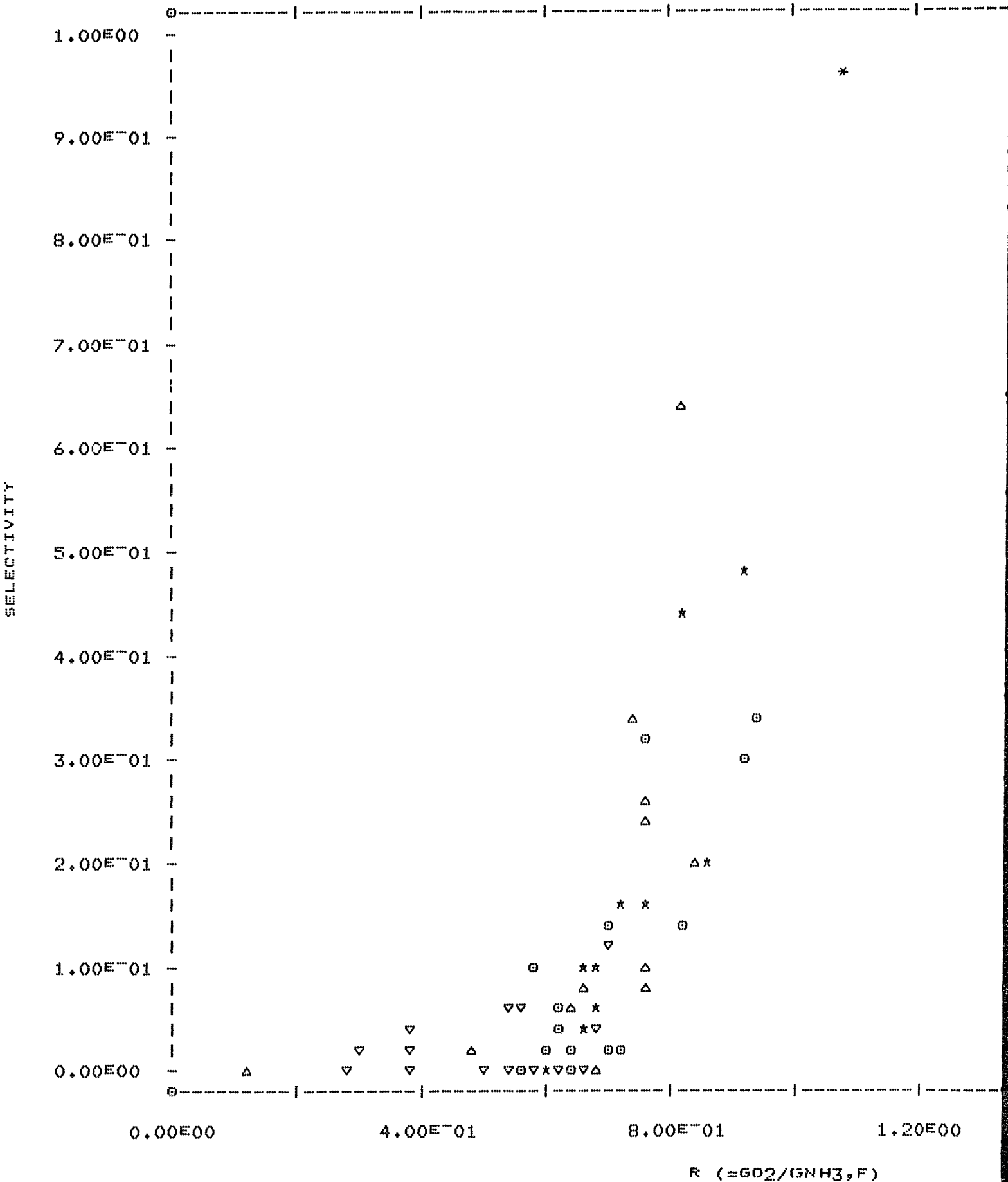

FIGURE 15. SELECTIVITY VERSUS THE MOLAR RATIO OF OXYGE

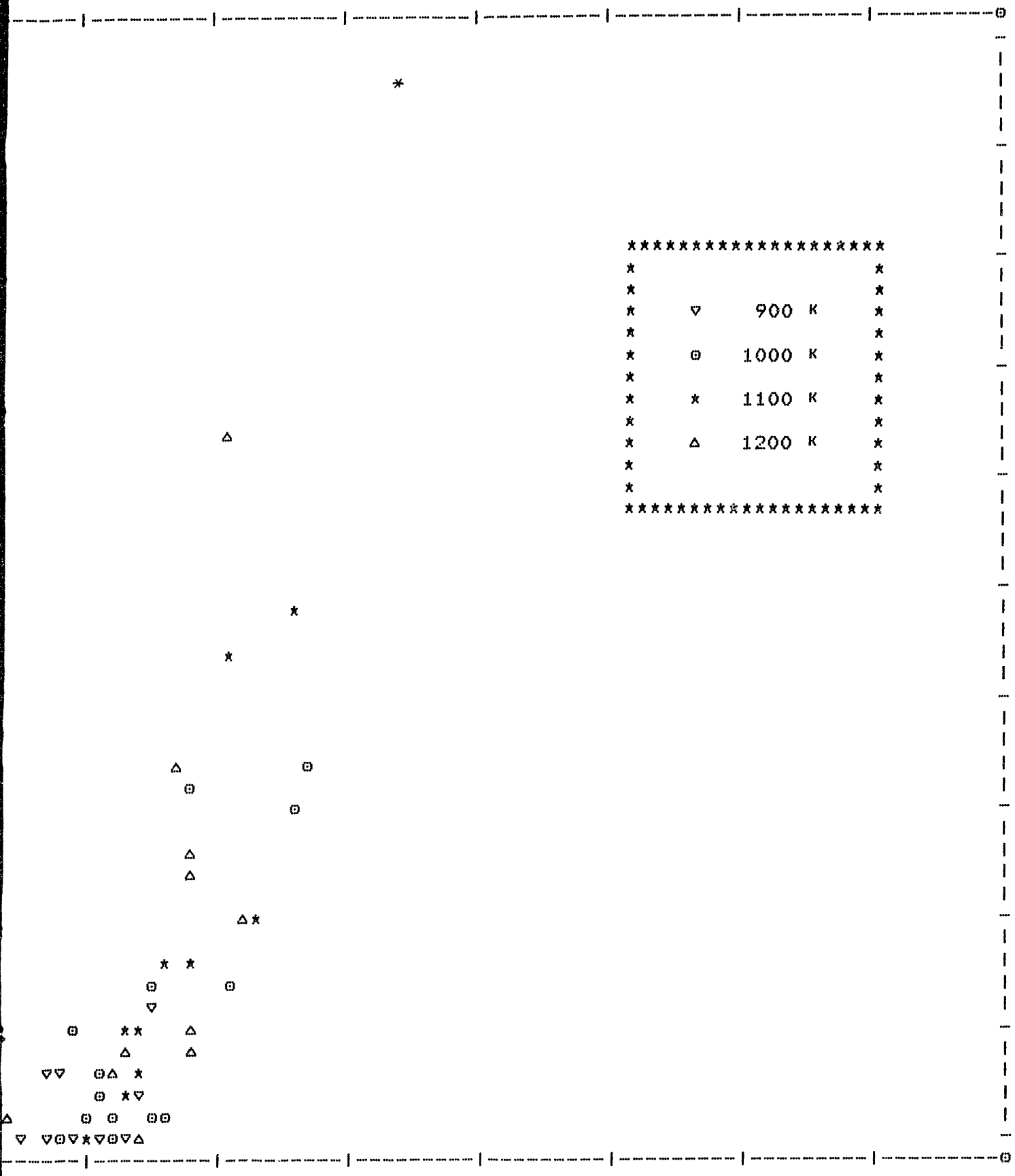

1 8.00E-01 1.20E00 1.60E00 2.00E00

R (=GO2/(GNH3,F)

SELECTIVITY VERSUS THE MOLAR RATIO OF OXYGEN FLUX TO AMMONIA FLUX.

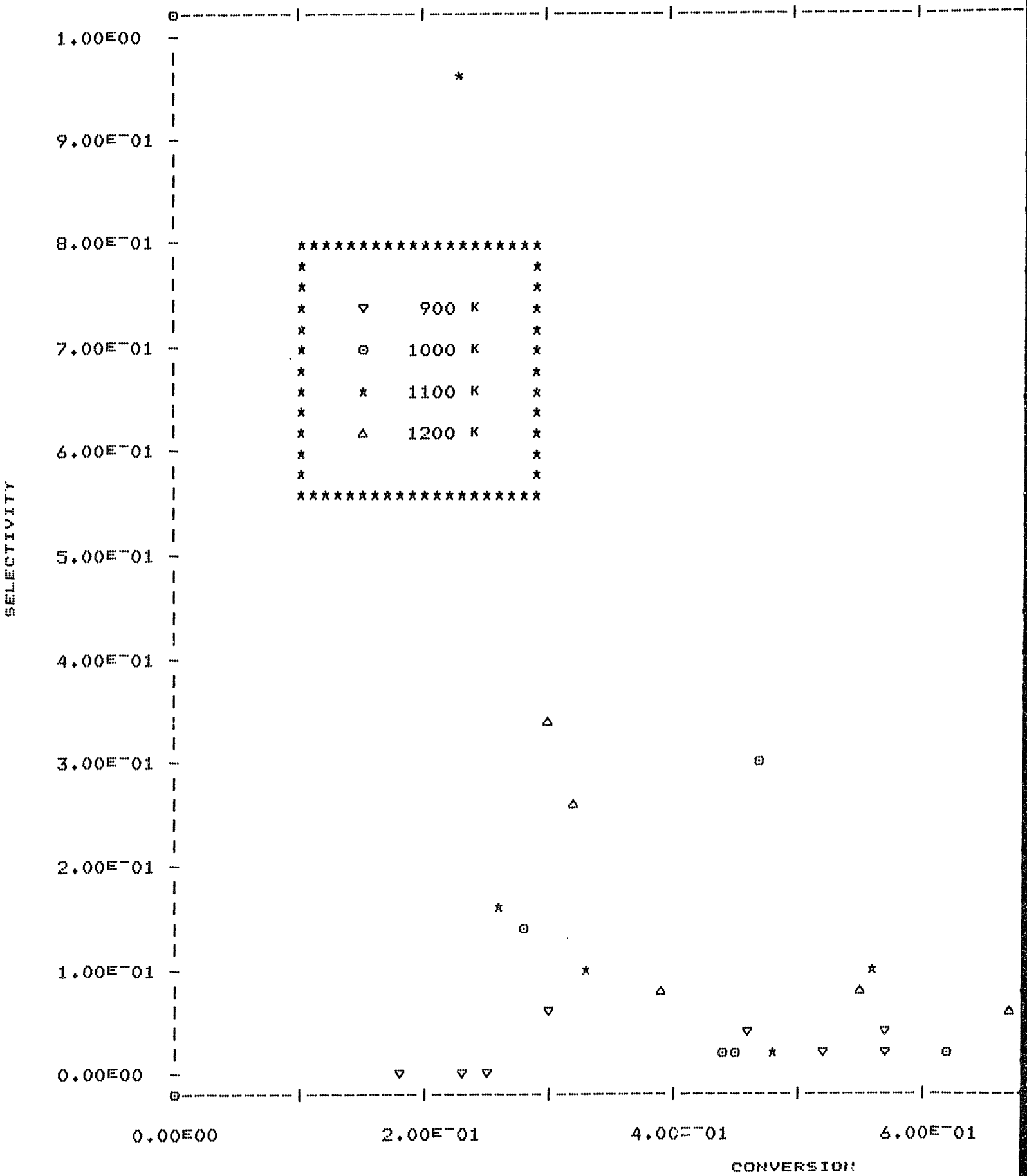

FIGURE 16. SELECTIVITY VERSUS CONVERS

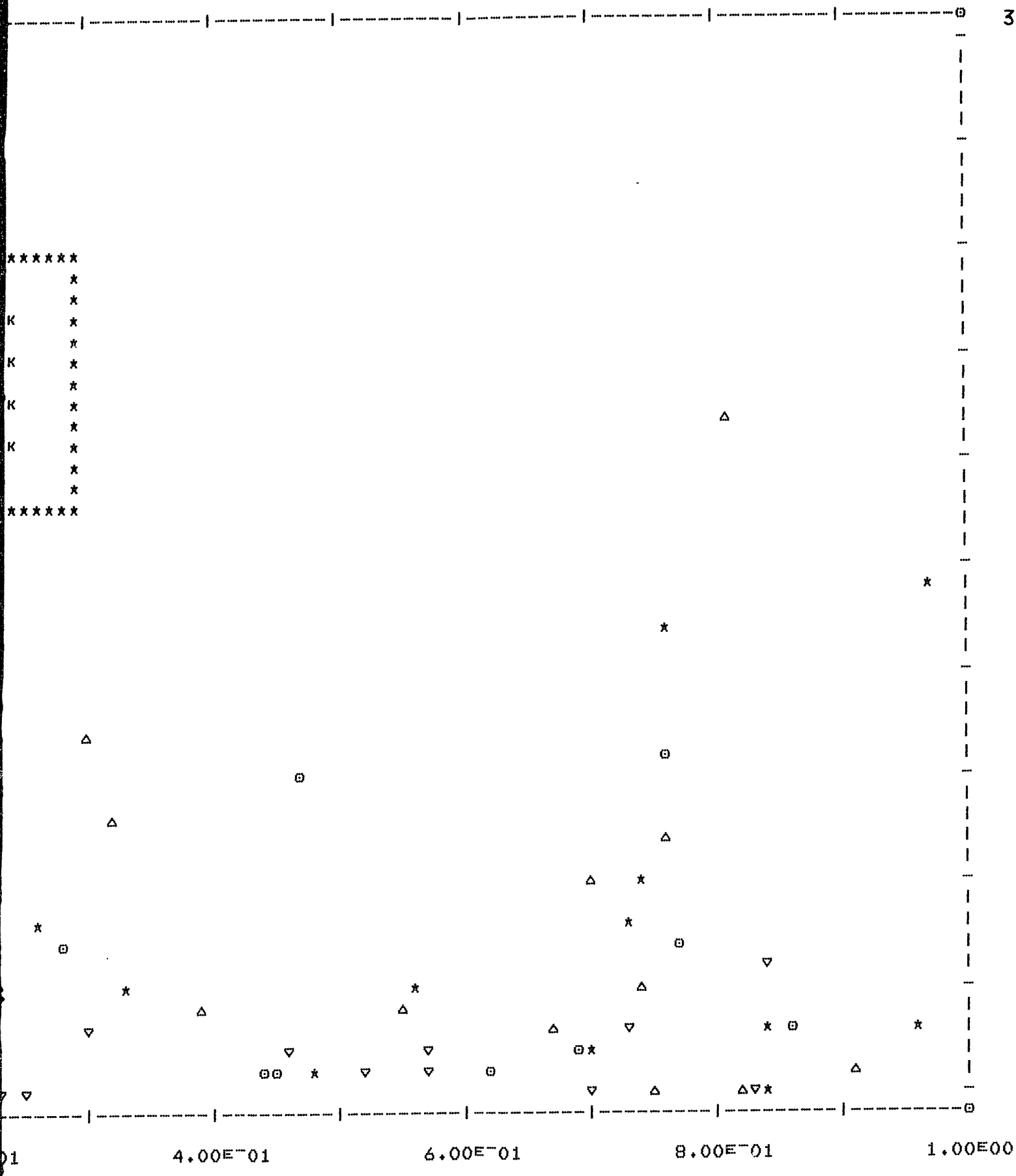

FIGURE 16. SELECTIVITY VERSUS CONVERSION

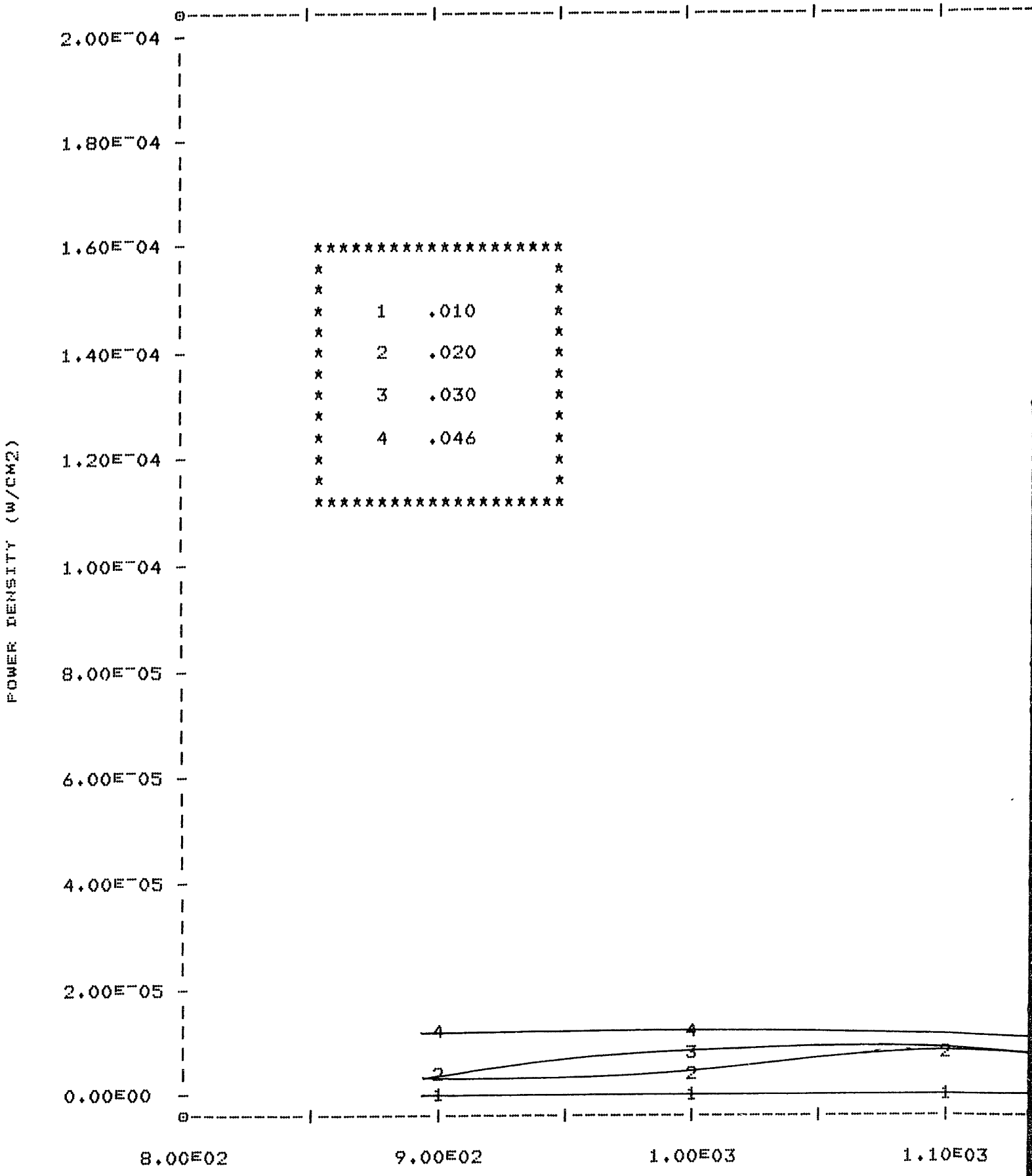

FIGURE 17. POWER DENSITY VERSUS TEMPERATURE, FLOW

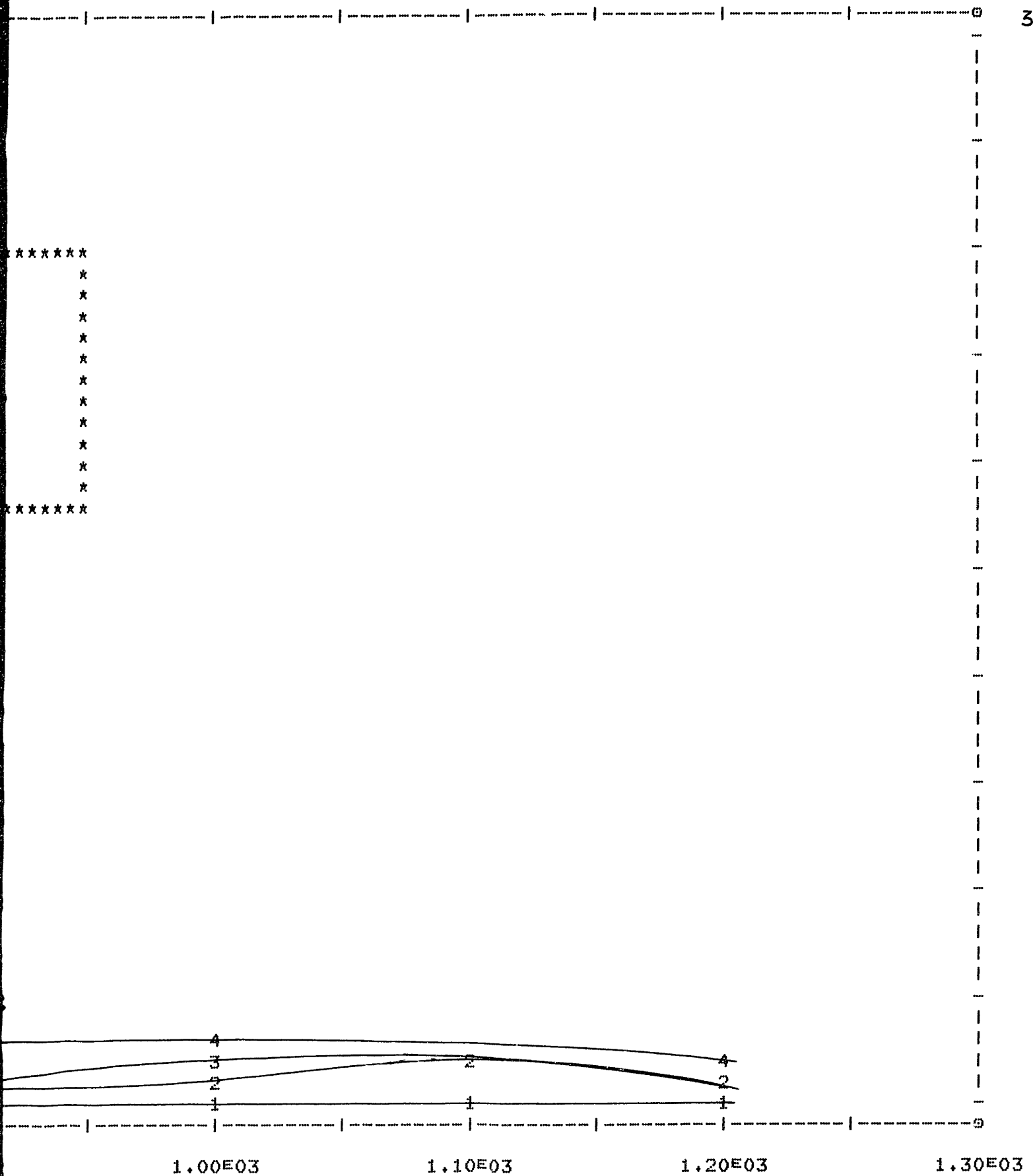

17. POWER DENSITY VERSUS TEMPERATURE, FLOW RATE 5 CM3/MIN STP

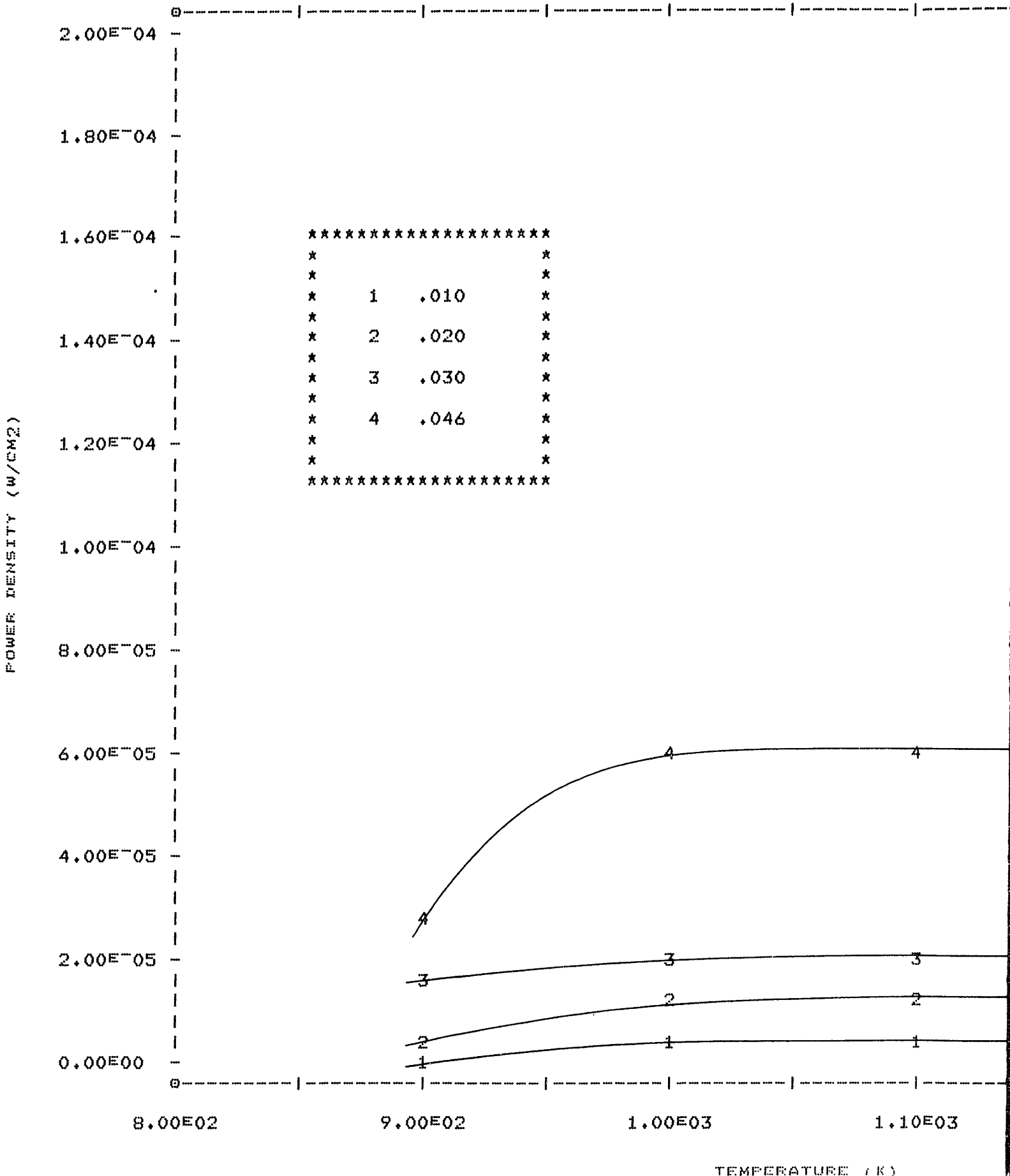

FIGURE 18. POWER DENSITY VERSUS TEMPERATURE, FLOW R

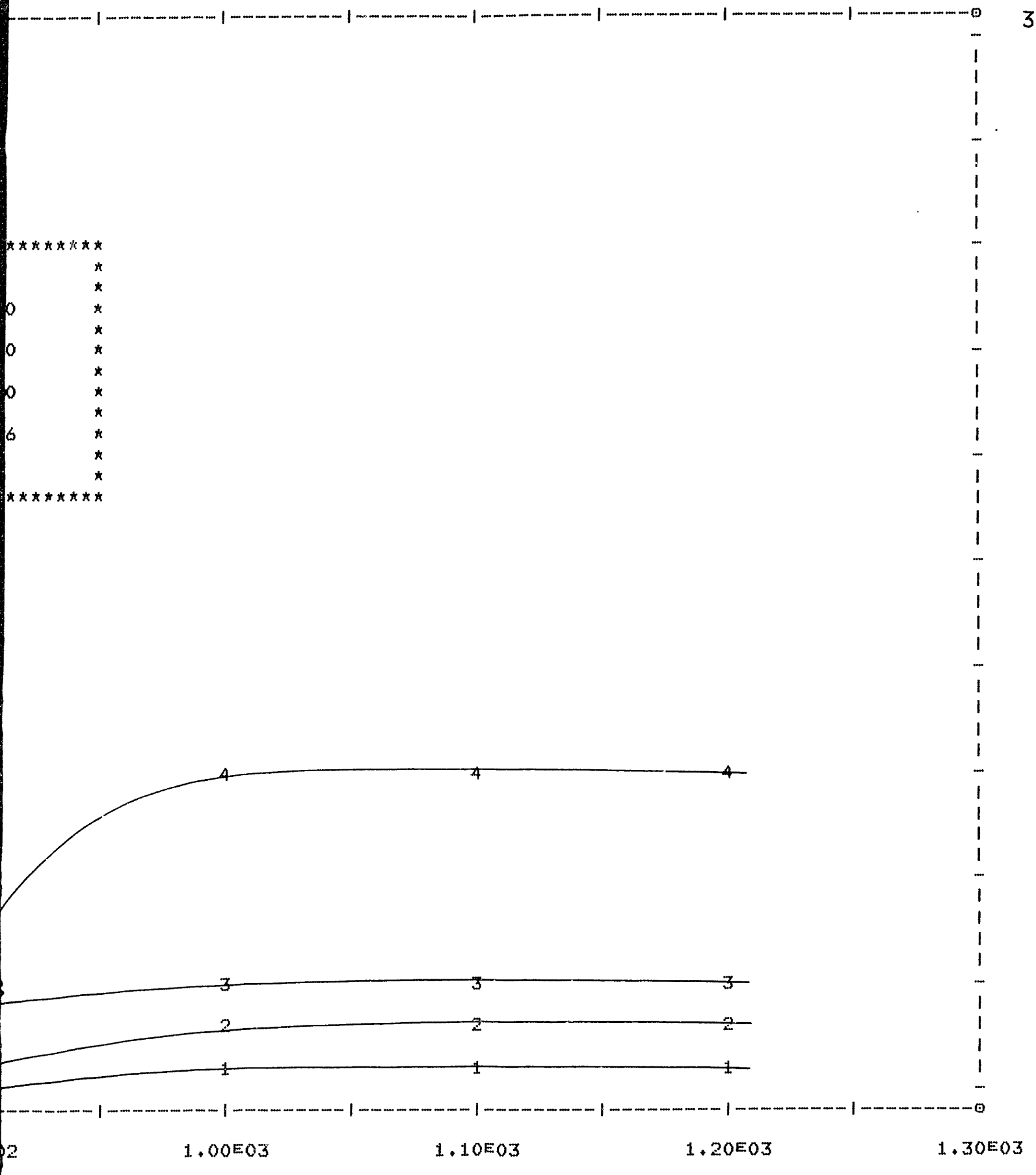

18. POWER DENSITY VERSUS TEMPERATURE. FLOW RATE 10 CM3/MIN STP

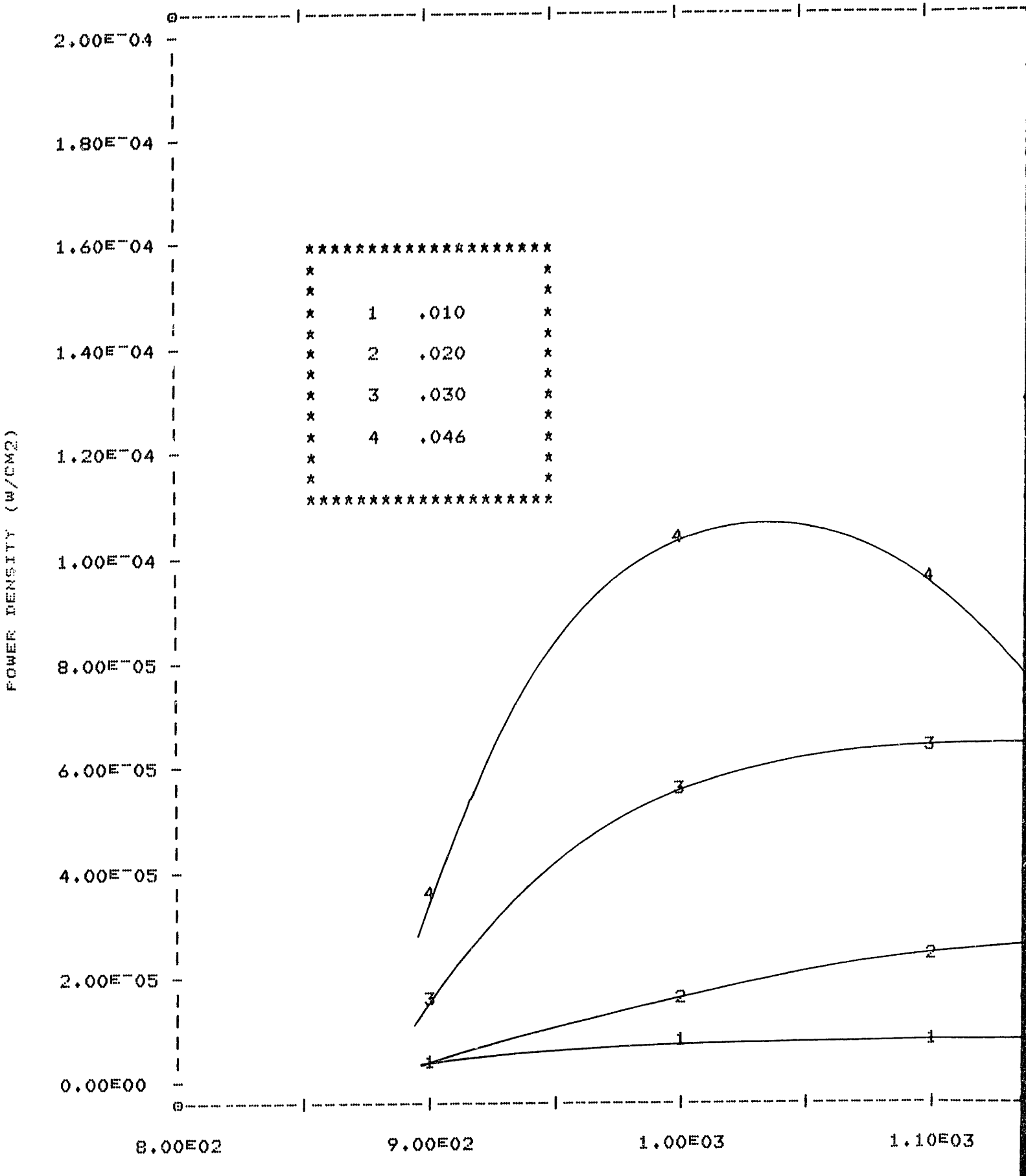

FIGURE 19. POWER DENSITY VERSUS TEMPERATURE, FLOW R

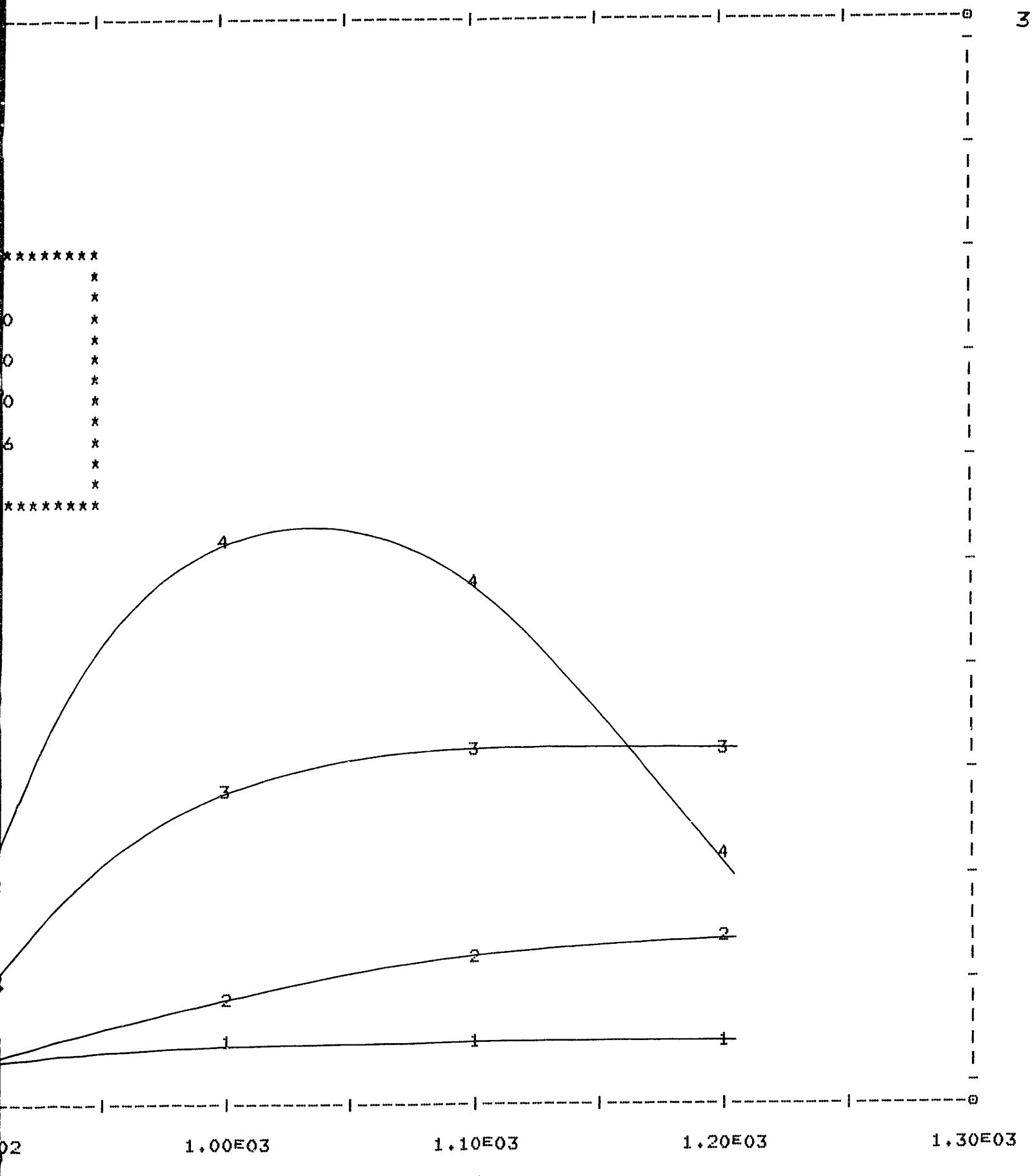

9. POWER DENSITY VERSUS TEMPERATURE, FLOW RATE 15 CM3/MIN STP

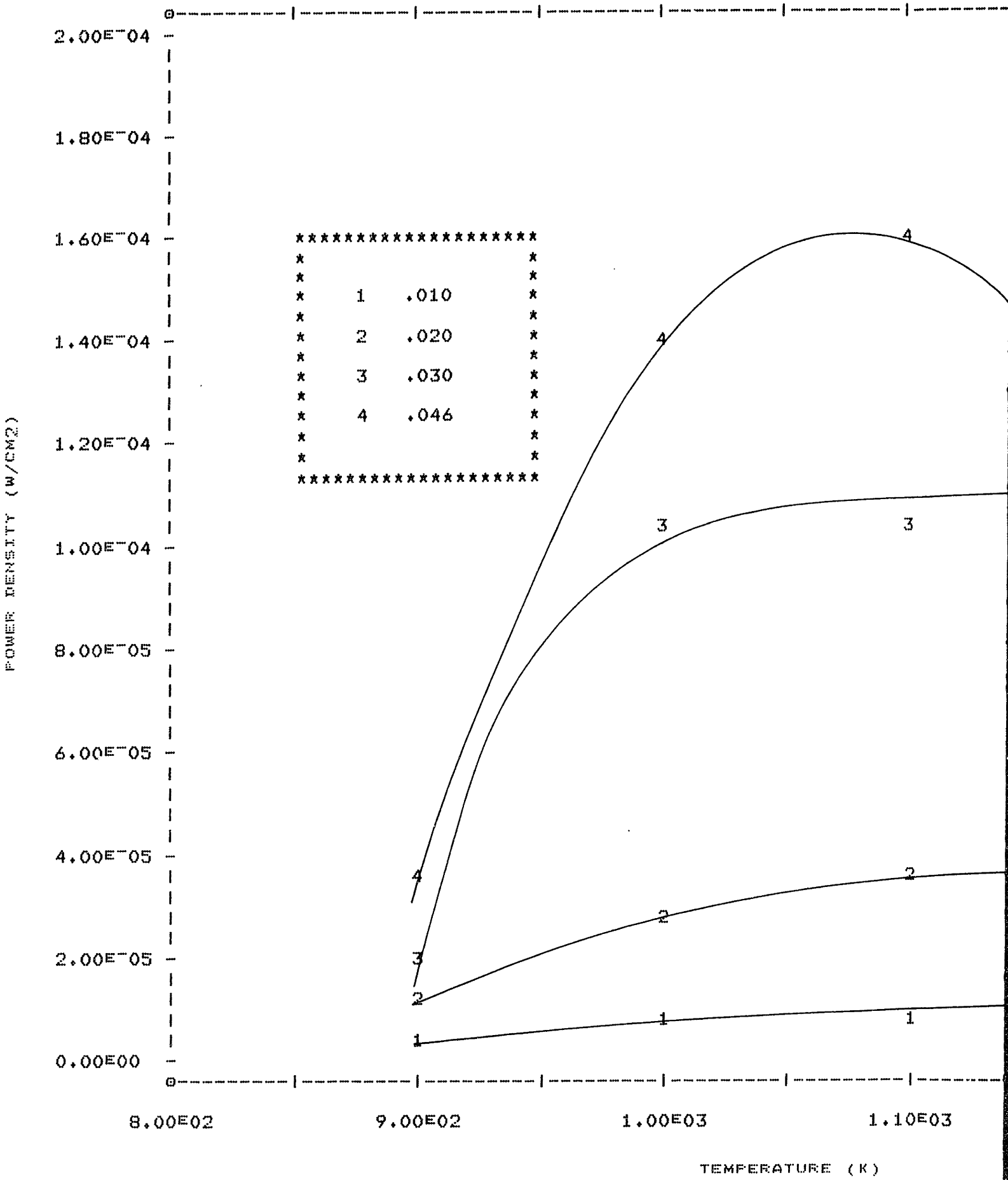

FIGURE 20. POWER DENSITY VERSUS TEMPERATURE, FLOW RA

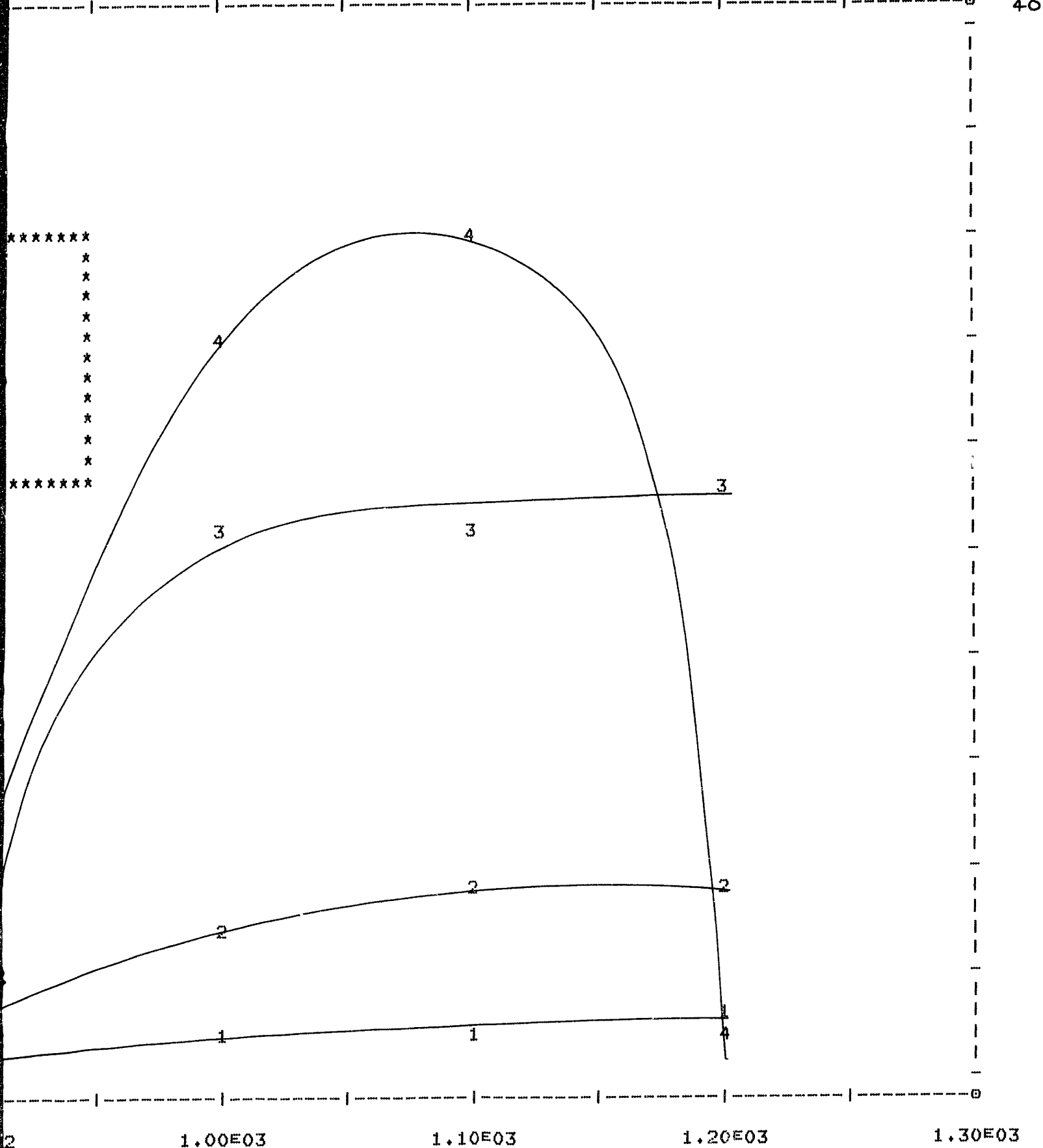

). POWER DENSITY VERSUS TEMPERATURE. FLOW RATE 20 CM3/MIN STP

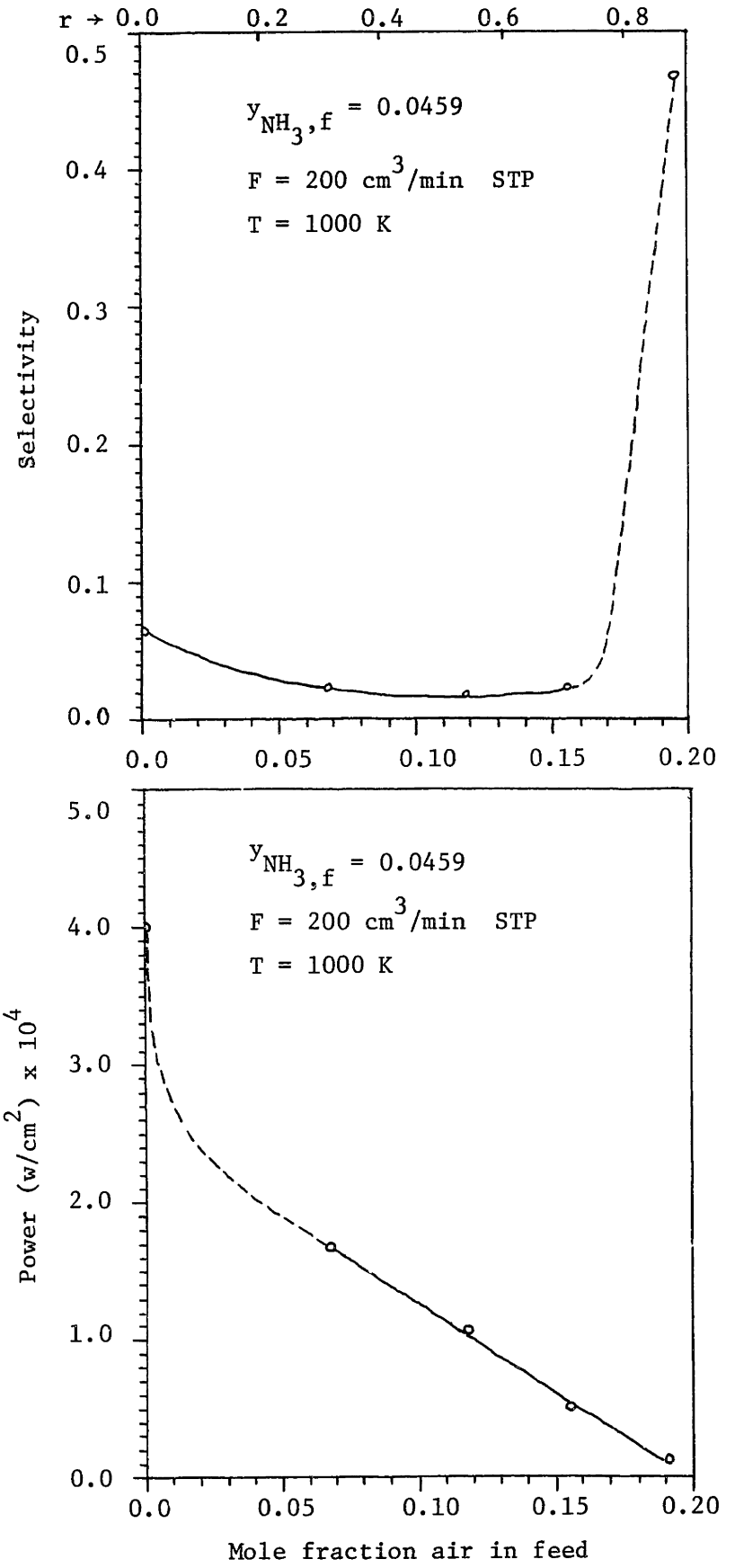

Figures 21 and 22. Selectivity and Power versus mole fraction of air.

200 cm^3/min. Notice that the sudden jump in selectivity occurs again for r = 0.78.

4.7 Catalyst

Scanning electron micrographs of the platinum catalyst-electrodes are given in figures 23 and 24. Figure 23 shows the outer, air electrode after 100 hours of continuous use while figure 24 shows the inner, ammonia electrode again after 100 hours of continuous use. These figures may be compared with the unused surface of figure 5. The merging of grain boundaries and extensive sintering should be noted.

After 500 hours of continuous use the fuel cell was disassembled. The cathode, exposed to air, remained intact and showed no signs of wear or deterioration from use. The anode, exposed to ammonia, however did show signs of considerable wear and sintering. The platinum catalyst-electrode was beginning to flake off the zirconia solid electrolyte. This flaking and sintering was accompanied by a marked increase in total cell resistance to 160 Ω at 1000K. A reapplication of platinum was necessary before further experiments could be conducted.

4.8 Oscillations

An interesting phenomenon was observed during the course of these experiments. Under particular sets of conditions, regular oscillations of the cell terminal voltage and nitric oxide exit concentration were observed. Representative samples of these appear in figures 25 and 26 along with the experimental conditions under which the oscillations occured.

Figure 23. Scanning electron micrograph of the outside, air electrode after 100 hours of continuous use.

INTENTIONAL DUPLICATE EXPOSURE

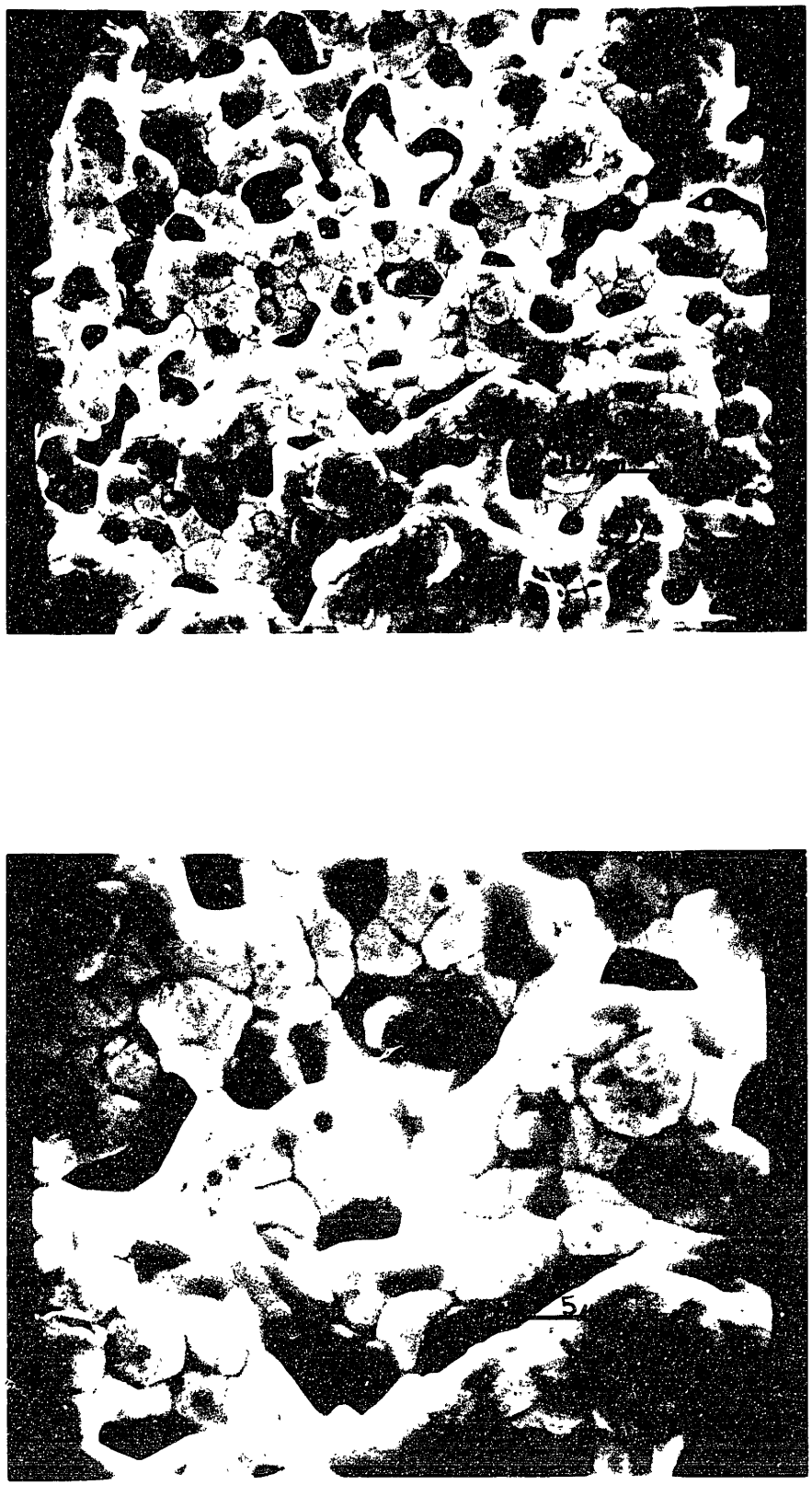

Figure 23. Scanning electron micrograph of the outside, air electrode after 100 hours of continuous use.

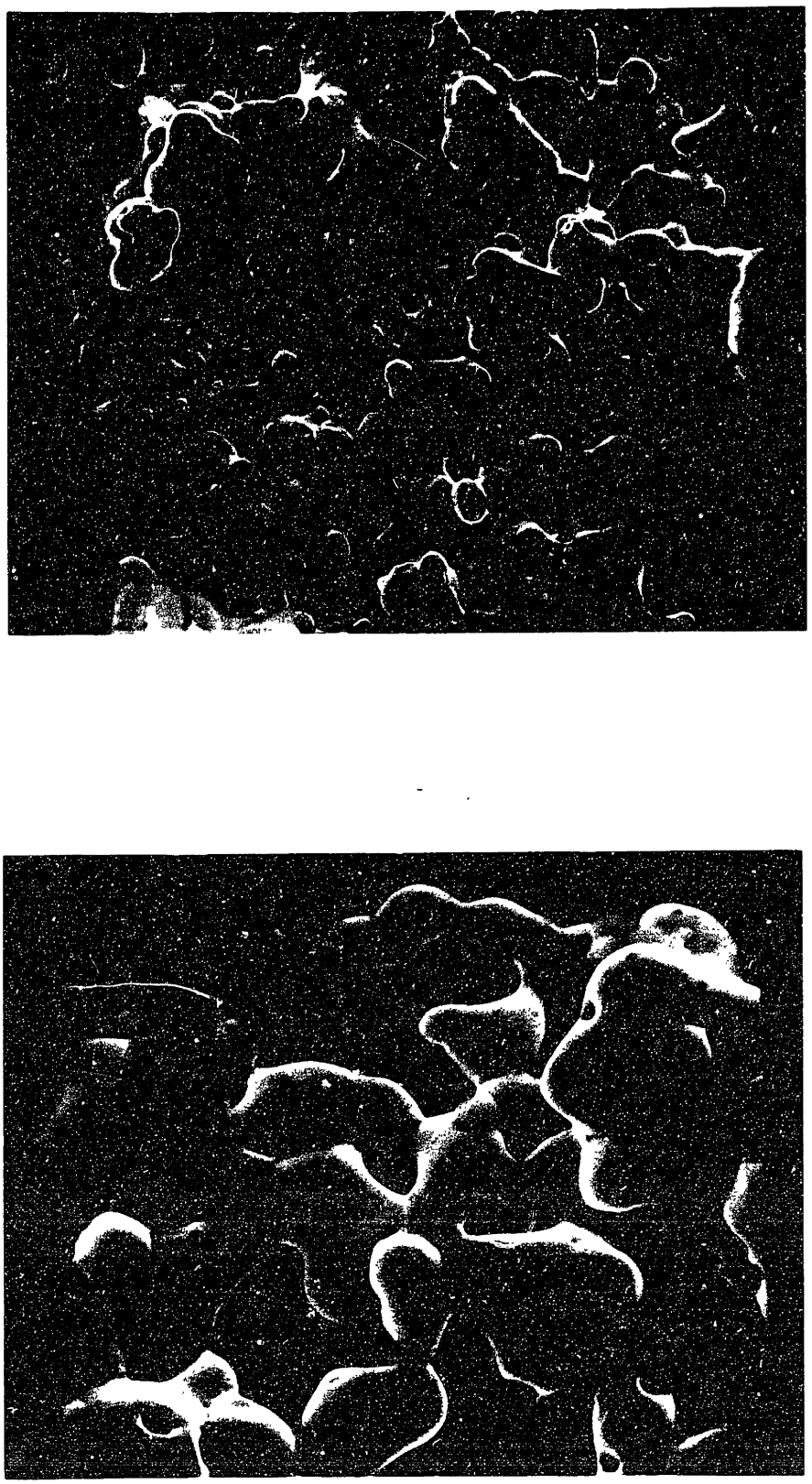

Figure 24. Scanning electron micrograph of the inside, ammonia electrode after 100 hours of continuous use.

INTENTIONAL DUPLICATE EXPOSURE

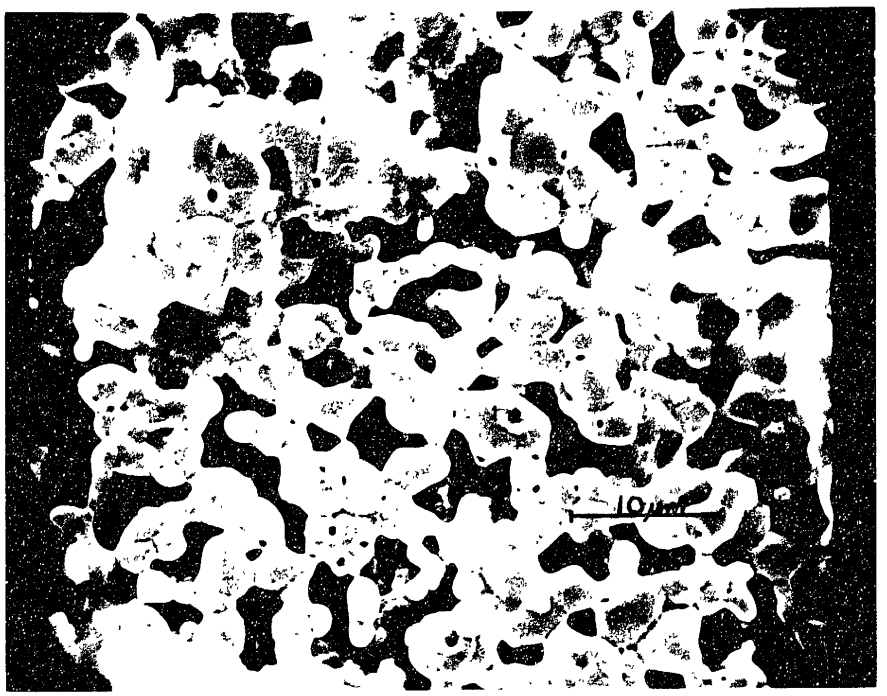

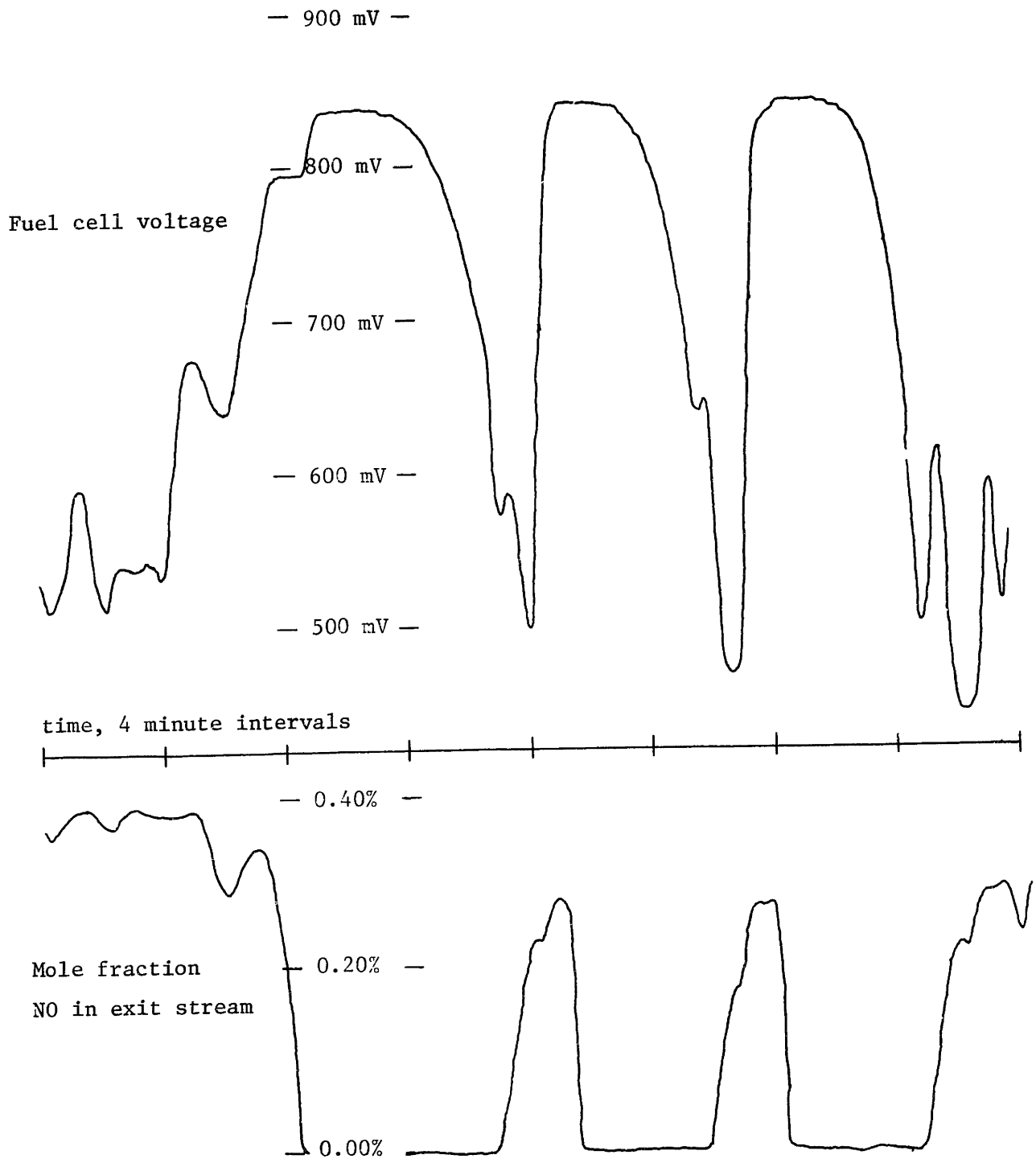

Figure 25. Cell voltage and product concentration oscillations under open circuit conditions. F = 337.5 cm^3/min STP, T = 1100K, r = 0.57, N = 5.89, $y_{NH_3,f}$ = 0.293, $y_{NH_3,e}$ = 0.0164, $y_{air,f}$ = 0.0801

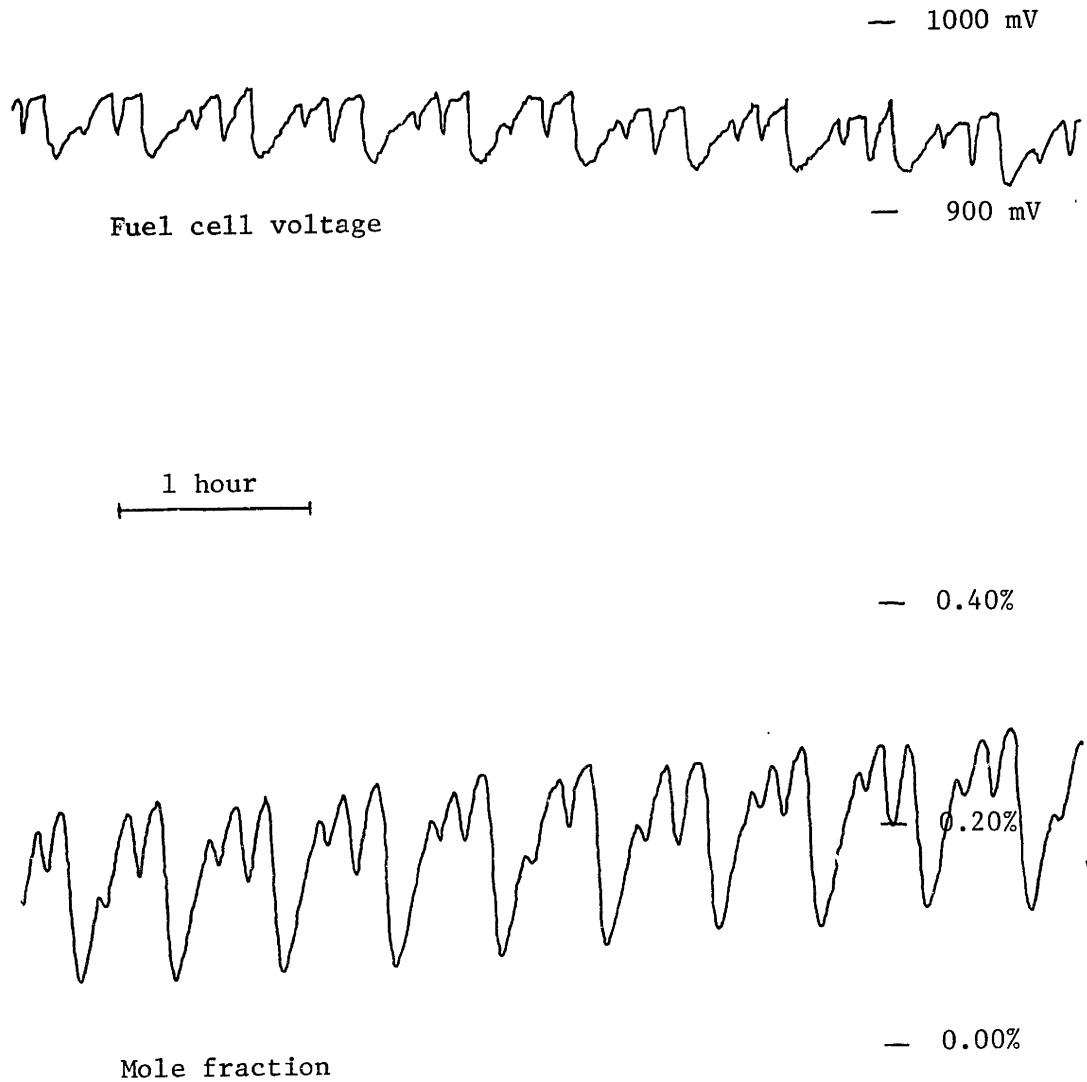

Figure 26. Cell voltage and product oscillations under closed circuit conditions. F = 12.73 cm^3/min STP, T = 1100K, r = 0.695, N = 8.63, $y_{NH_3,f}$ = 0.0459, $y_{NH_3,e}$ = 0.0135

5. DISCUSSION

5.1 Electrical Behavior

The resistance plot of figure 6 is as expected compared to those given by Archer (8). The resistivity, a better comparison between cells is defined as

$$\rho = \frac{A\ R_c}{\delta} \quad . \tag{14}$$

Our fuel cell, based on an average diameter area and a thickness of 1.84 mm, has a resistivity given by,

$$\rho = 0.0517 \exp [10623/T]\ \Omega\text{-cm} \tag{15}$$

where T is in degrees Kelvin. The resistance of the test circuit employed is the sum of resistances associated with the cell, load and lead wires, as shown in figure 4. The residual resistance in the lead wires was determined using the data points given in section 4 to be $0.873 \pm 0.017\ \Omega$.

The overpotential curves of figures 8, 9 and 10 show that ohmic overpotential is the dominant one at the temperatures and flow rates used in these experiments. This purely ohmic resistance shows that the kinetics are limited by oxygen flux through the electrolyte.

At very low currents the curves have a slight upward bend. This is characteristic of activation overpotential, which involves the speed of oxygen electronation at the cathode and the subsequent de-electronation at the anode. Activation overpotential should exhibit an increasing logarithmic behavior with increasing current which is in agreement with the data.

5.2 Selectivity

5.2.1 Reactions and Kinetics

The reactions occuring in the ammonia oxidation were given in equations 4-8 and are repeated below.

$$NH_3 + 5/4\ O_2 \rightarrow NO + 3/2\ H_2O \quad (4)$$

$$NH_3 + 3/2\ NO \rightarrow 5/4\ N_2 + 3/2\ H_2O \quad (5)$$

$$NH_3 \rightarrow 1/2\ N_2 + 3/2\ H_2 \quad (6)$$

$$NO \rightarrow 1/2\ N_2 + 1/2\ O_2 \quad (7)$$

$$H_2 + 1/2\ O_2 \rightarrow H_2O \quad (8)$$

The relative importance of reactions (6) and (7) in producing nitrogen from the fuel cell system was assesed. Decomposition of NO via reaction (7) has been reported by Chilton (2) to be negligible in the temperature range used here. This was verified by passing NO through our fuel cell at the temperatures and flow rates used in the experiments. The maximum amount of decomposition detected was 0.1% of the feed composition and hence was negligible. Ammonia decomposition via reaction (6) was also assesed. At temperatures below 1000K decomposition was negligible but as temperature increased above 1000K it became significant until at 1200K, 48% of the ammonia feed was decomposing with a residence time of 20 minutes.

The possibility of oxygen in the gas phase can be checked by defining a quanity called the oxygen selectivity,

$$S_{O_2} = \frac{\text{oxygen appearing in the desired products}}{\text{total oxygen that passed through the electrolyte}}$$

$$= \frac{G\ y_{NO}}{i/4\mathcal{F}}$$

$$= \frac{r_{NO}}{G_{O_2}} \quad (16)$$

The ammonia selectivity may then be plotted for comparison against the oxygen selectivity. This has been done in figure 27. If oxygen were present in the gas phase, the oxygen selectivity would be lower than the ammonia selectivity. Figure 27 shows that the data do indeed fall on a 45 degree line and we conclude that no gas phase oxygen is present.

The reactor configuration, although tubular in shape, is in reality a continuous flow stirred tank reactor (CFSTR). The Péclet number, a ratio of the convective flux to the diffusive flux, in a CFSTR is less than unity. For the flow rates examined, the axial Péclet number varied between 0.13 and 0.52. An F curve was obtained by introducing a step change in ammonia feed concentration to the reactor. The result is shown in figure 28 along with the theoretical curve calculated from,

$$F = 1 - \exp\ [-t/\tau] \qquad (17)$$

where τ is the residence time for the reactor and associated tubing. The data agree well hence, the reactor is considered a CFSTR for the low flow rates used in these experiments.

From the above discussion the two reactions of importance are (4) and (5) at temperatures below 1000K with (6) becoming important above 1000K. In excess oxygen Pignet and Schmidt (4) have found the rates of (4) and (5) to be first order in ammonia and first order in ammonia and nitric oxide, respectively. Since oxygen transport through the zirconia is the limiting factor, the rate of reaction (4) is exactly equal to the rate of oxygen flux. Reaction (5) is postulated to be first order in ammonia for the remainder of the discussion.

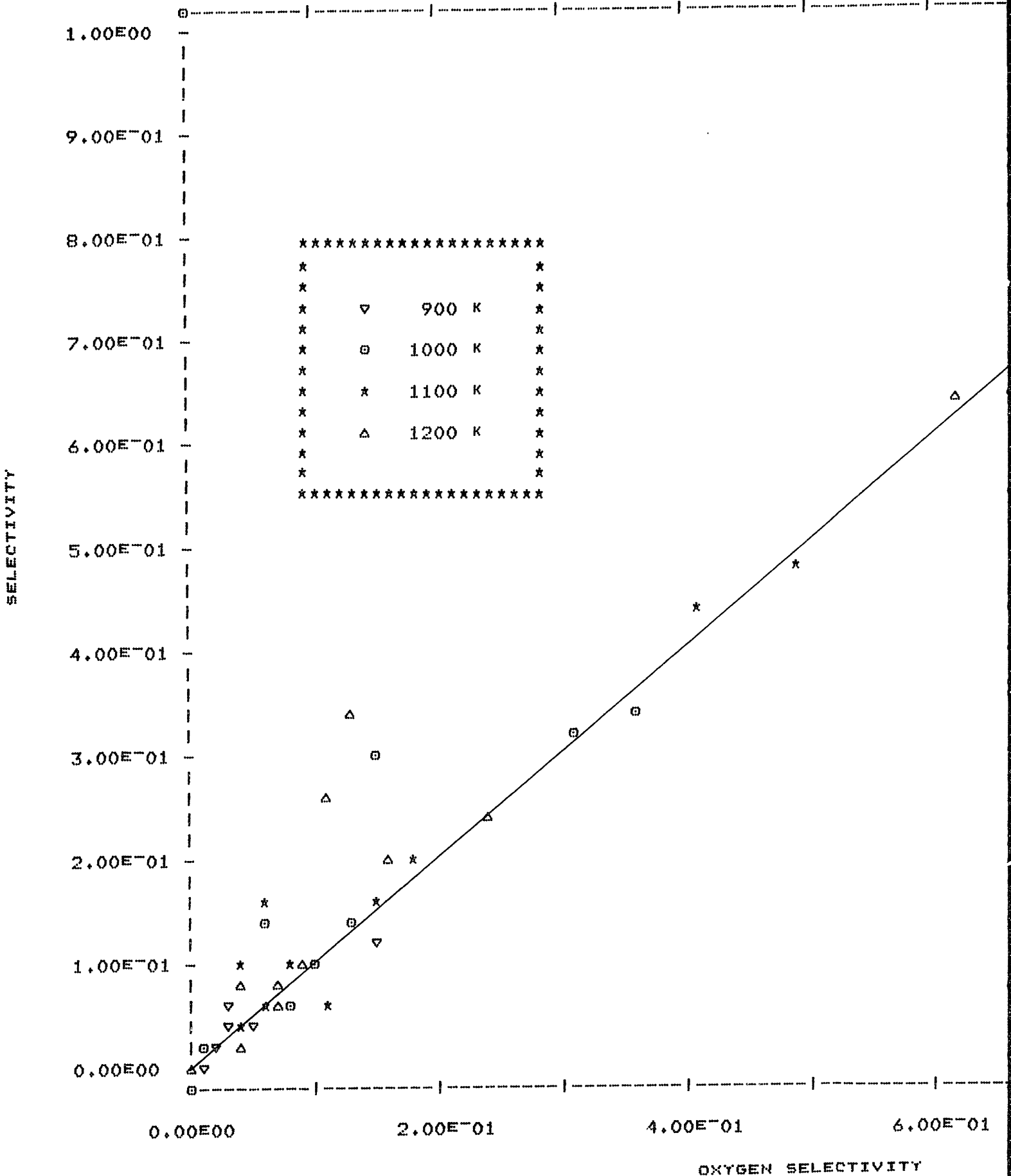

FIGURE 27. AMMONIA SELECTIVITY VERSUS OXYGEN

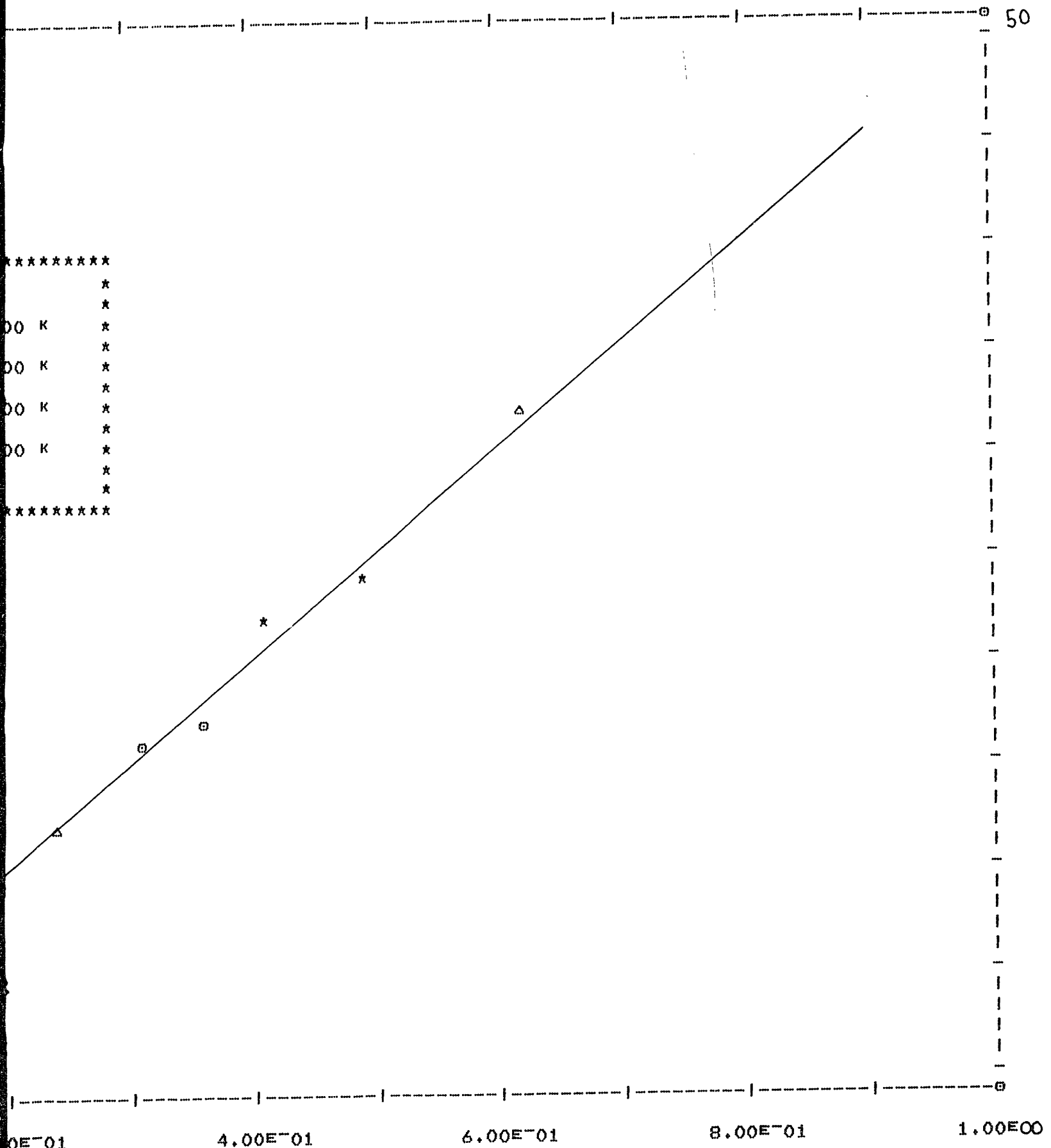

FIGURE 27. AMMONIA SELECTIVITY VERSUS OXYGEN SELECTIVITY

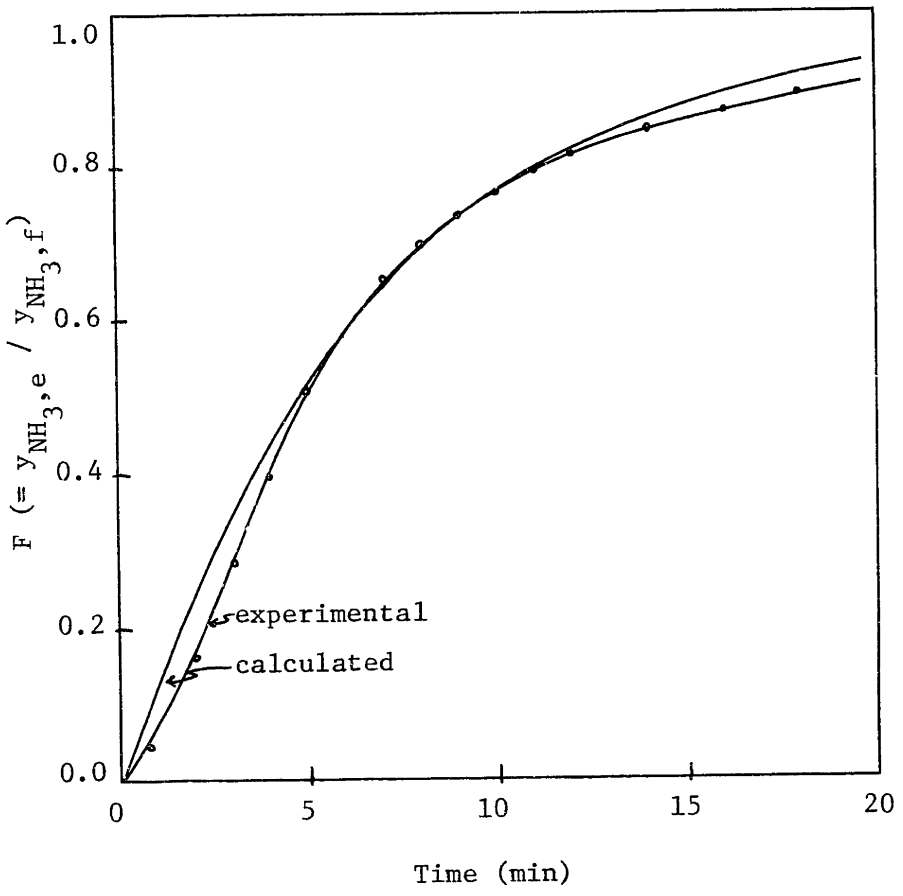

Figure 28. F curve of the fuel cell. F = 18.6 cm^3/min, volume of the reactor and associated tubing = 126 cm^3, residence time = 6.77 min

5.2.2 Discussion and Prediction

The observed trends in selectivity namely, increasing for decreasing flow rate and feed concentrations of ammonia and increasing with temperature will be explained first in a qualitative sense and secondly, with the use of a theoretical model, in a quantitative manner.

At low ammonia concentrations reaction (4) being zeroth order in ammonia is favored while reaction (5) destroys little of the ammonia present due to its first order nature in ammonia. An increase in NO production and selectivity is observed at all flow rates and temperatures below 1000K with a decrease in ammonia feed concentration.

The variation in selectivity with temperature can be explained in light of two competing effects. As temperature increases, electrolyte resistance drops thereby increasing the oxygen flux and the observed selectivity. At temperatures above 1000K ammonia decomposition via reaction (6) begins to become appreciable and the ammonia available for reaction decreases. We expect the selectivity to show a peak when plotted against temperature and indeed it does as shown by figures 11-14.

Variation of the selectivity with flow rate can be understood in light of the oxygen flux limitation. The amount of NO produced is a function of the oxygen flux but the destruction is a function of the ammonia available. At higher flowrates the production rate remains constant but the destruction rate is much faster due to the higher flux of ammonia thus causing a decrease in observed selectivity.

To formulate these results in a quantitative manner, mass balances for the three components NH_3, NO and N_2 may be written as,

$$F\, y_{NH_3,f} = (4/5)\ (i/4\mathfrak{F}) + k_2\, y_{NH_3,e}\, y_{NO,e} + F\, y_{NH_3,e} \tag{18}$$

$$0 = (-4/5)\ (i/4\mathfrak{F}) + (3/2)\ k_2\, y_{NH_3,e}\, y_{NO,e} + F\, y_{NO,e} \tag{19}$$

$$0 = (-5/4)\ k_2\, y_{NH_3,e}\, y_{NO,e} + F\, y_{N_2,e} \tag{20}$$

where reaction (4) is zeroth order in NH_3 and reaction (5) first order in NH_3 and NO with rate constant k_2. Writing these equations in dimensionless form we obtain,

$$x_A + N\, x_A\, x_D = 1 - (4/5)\ r \tag{21}$$

$$x_D + (3/2)\ N\, x_A\, x_D = (4/5)\ r \tag{22}$$

$$(5/4)\ N\, x_A\, x_D = x_F \tag{23}$$

where $x_A = y_{NH_3,e} / y_{NH_3,f}$, $x_D = y_{NO,e} / y_{NH_3,f}$, $x_F = y_{N_2,e} / y_{NH_3,f}$, $r = G_{O_2} / G_{NH_3}$, $G_{O_2} = i / 4\mathfrak{F}$, and $N = k_2\, y_{NH_3,f} / F$. Solving for x_A, x_D, and x_F gives,

$$0 = x_D^{\,2} + (1/N - 2r + 3/2)\ x_D - (4/5)\ (r/N) \tag{24}$$

$$x_A = \frac{(4/5)r - x_D}{(3/2)\ N\, x_D} \tag{25}$$

$$x_F = (5/4)\ N\, x_A\, x_D \tag{26}$$

In terms of these dimensionless parameters, the selectivity is defined as,

$$S = x_D / (1 - x_A) \tag{27}$$

For large values of N the selectivity is equal to x_D. The dependence of

x_D upon r is determined from equation 24 and two possible solutions result giving rise to three regions ,

$$r < 0.75 \qquad x_D = 0$$

$$0.75 \leq r \leq 1.25 \qquad x_D = 2r - 3/2$$

$$r > 1.25 \qquad x_D = 1$$

Figure 29 shows the selectivity data of figure 15 along with lines of constant N as a function of r. Nearly all the data taken fall within the band between N equals 1 and 200, thus substantiating the model. Values of r lower than 0.75 will still give non-zero selectivities provided the corresponding N value is low enough.

Using these equations, selectivities to nitric oxide as a function of r and N can be predicted. One such curve for r = 0.75 is shown in figure 30 by the solid line. From the data, selectivities versus r and N were calculated and appear also in figure 30. The data agree quantitatively with the model. Data at higher r values were not obtainable with the present system due to the oxygen flux limitation imposed by the zirconia resistance. The rate constant k_2, contained in the parameter N, could not be calculated due to scatter in the data indicating that reaction (5) was limited by the amount of available nitric oxide. The dimensionless parameters r and N then entirely describe the system and give quantitatively the trends in selectivity seen by varying flow rate, ammonia concentration and temperature.

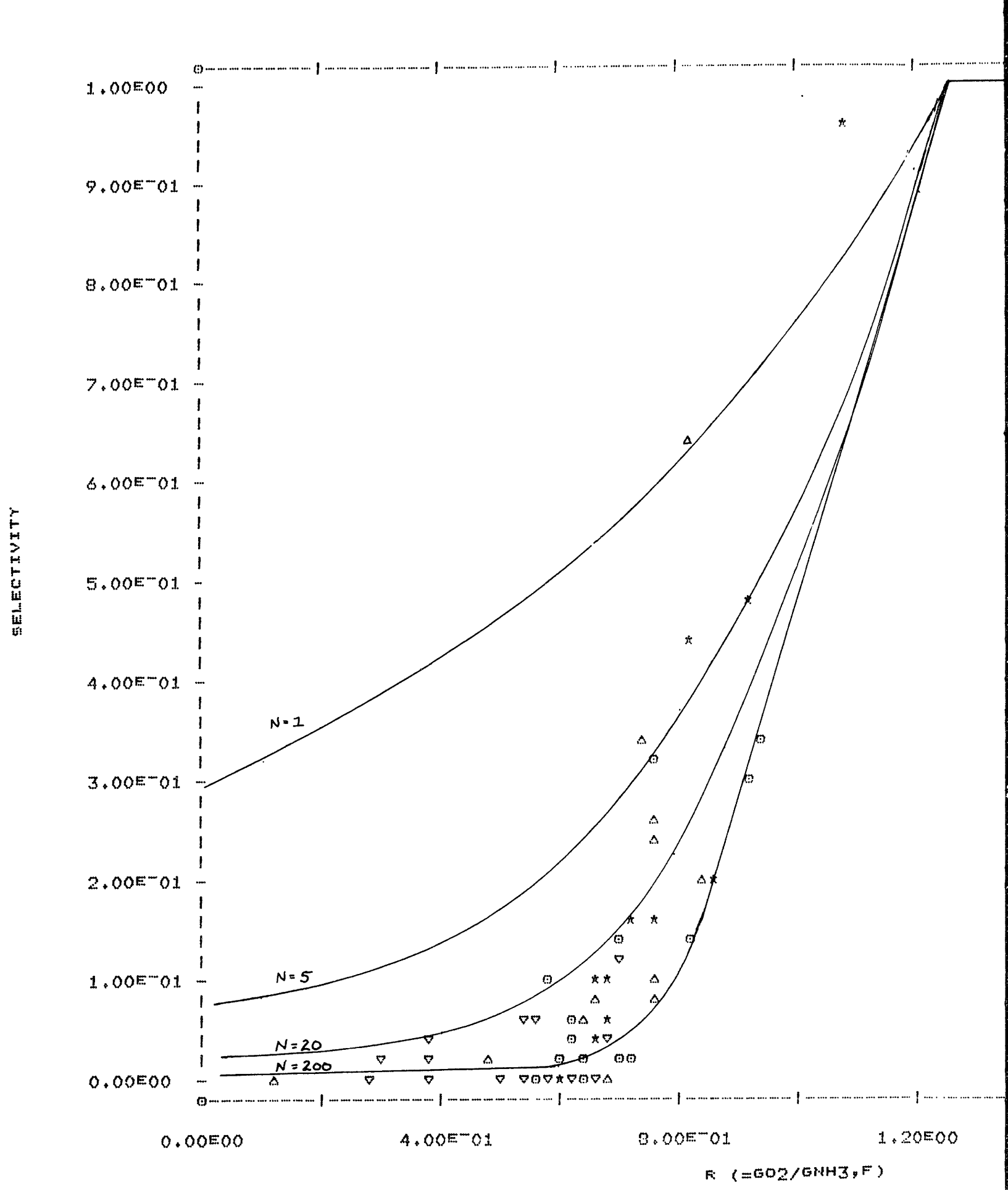

FIGURE 29. SELECTIVITY VERSUS THE RATIO OF OXYGEN FL
WITH N APPEARING AS PARAMETER.

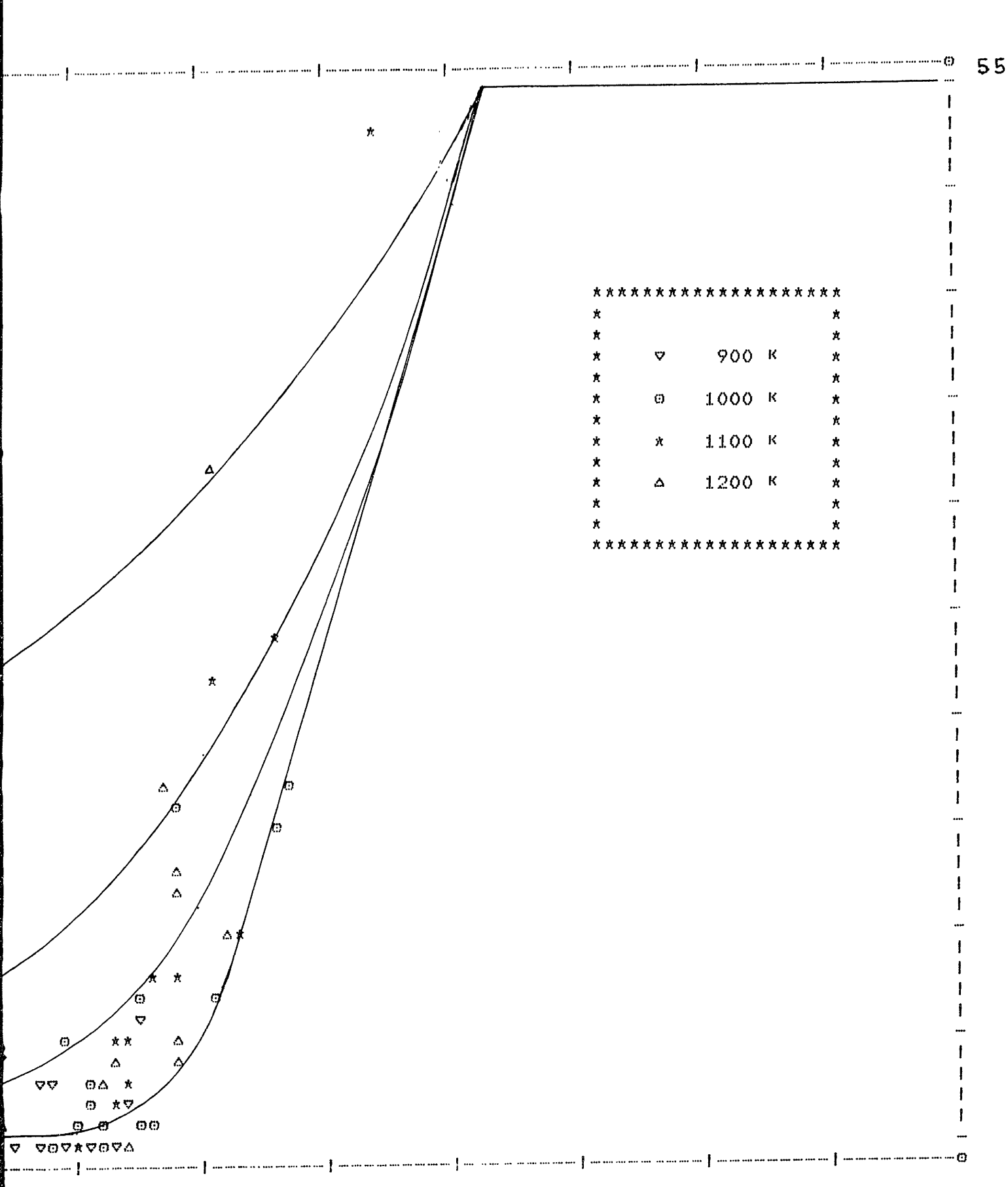

SELECTIVITY VERSUS THE RATIO OF OXYGEN FLUX TO AMMONIA FLUX
BEARING AS PARAMETER.

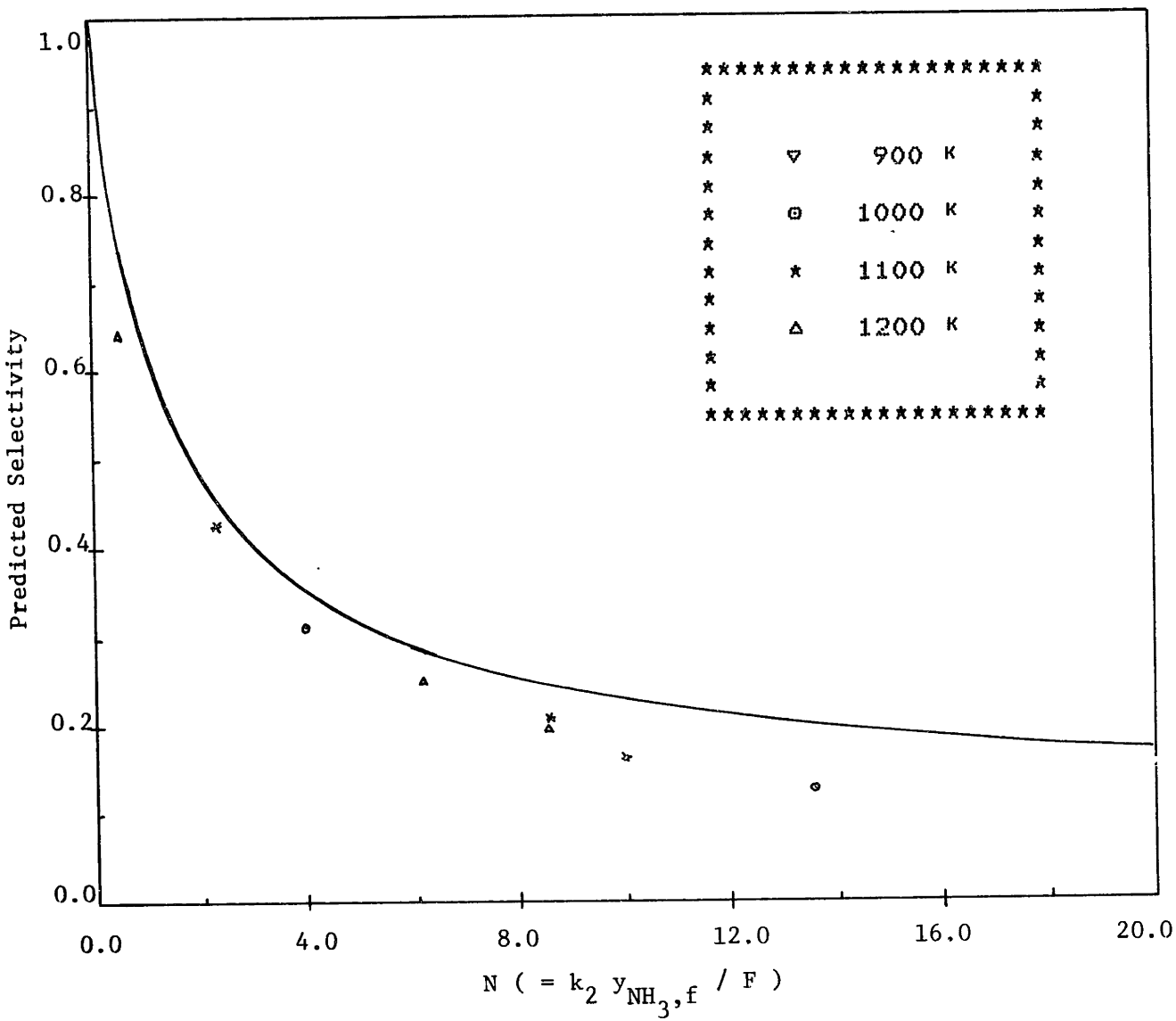

Figure 30. Predicted selectivity versus N from the model at r = 0.75. Experimental data are also shown.

5.3 Power Production

The main incentive for adapting industrial processes to fuel cell use was the added benefit of electric power while generating a useful end product. Figures 17-20 show the power densities obtained with the present cell. Power outputs as high as 1.6×10^{-4} watts/cm^2 were obtained. From these graphs the trend is clear, high concentrations and high flow rates of ammonia produce the largest amount of power. These conditions give rise to low partial pressures of oxygen and consequently only nitrogen and water as products with the present cell.

The power produced from this cell is limited by the flux of oxygen ions through the zirconia which is purely a function of the cell resistance. At the temperatures of interest between 900 and 1200K the resistance of the solid electrolyte is substantial for this cell. To improve the power outputs and selectivity, a thinner electrolyte is suggested to increase the oxygen flux.

Power density as a function of current is shown in figure 31 for a flow rate of 20 cm^3/min. It is normally expected that such a graph will have a maximum in it due to reactant depletion at some value of the current. Such behavior is not seen here since oxygen transport is limiting total reaction rate rather, a parabloic increase is observed. This is easily explained by considering that most of the overpotential occurs due to ohmic resistance. We then write,

$$E = R_T I$$
$$P = E I$$
$$P = R_T I^2 \qquad (28)$$

and a parabola is expected. It is noted that power and current are low

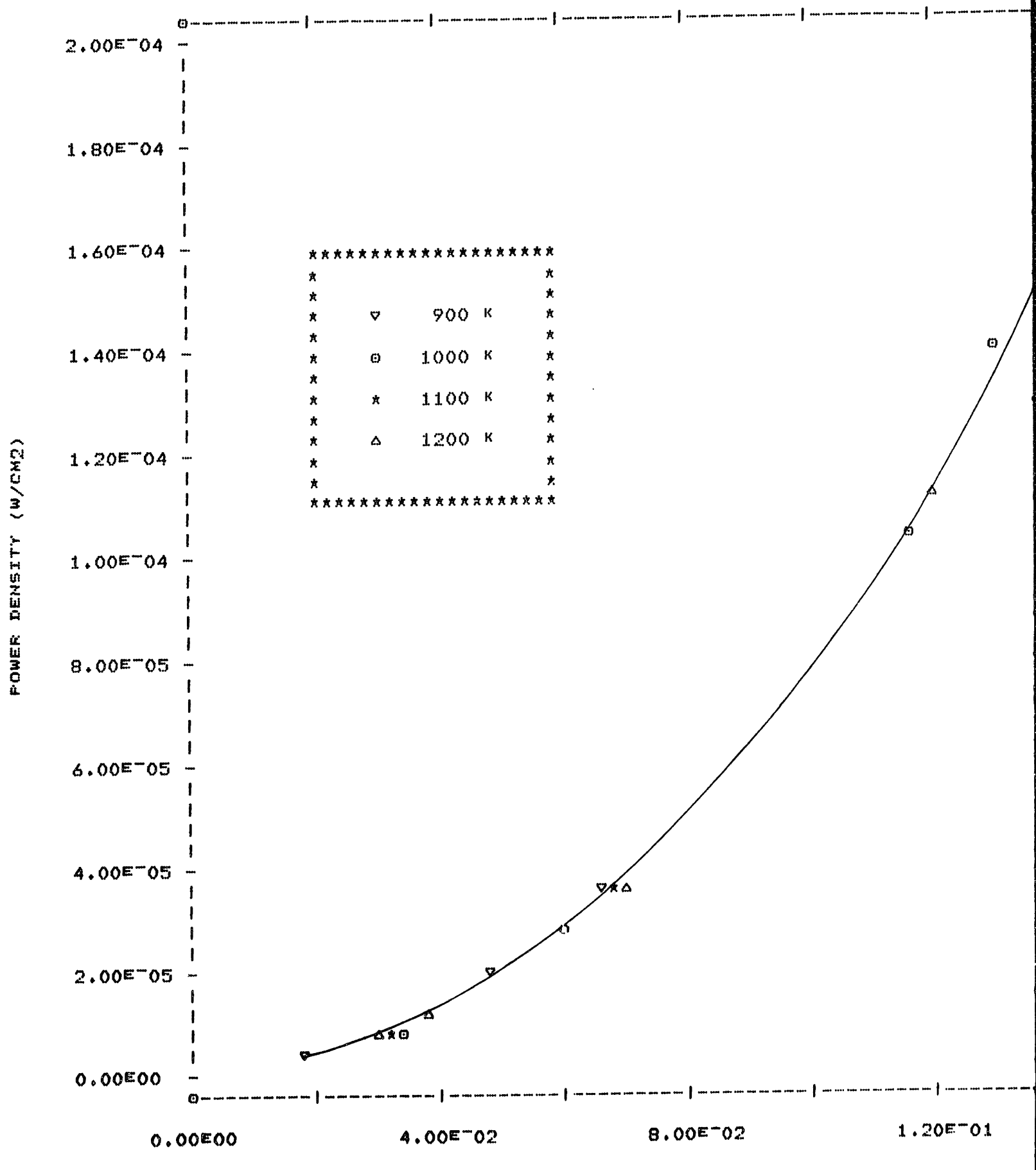

FIGURE 31. POWER DENSITY VERSUS CURRENT, P=20

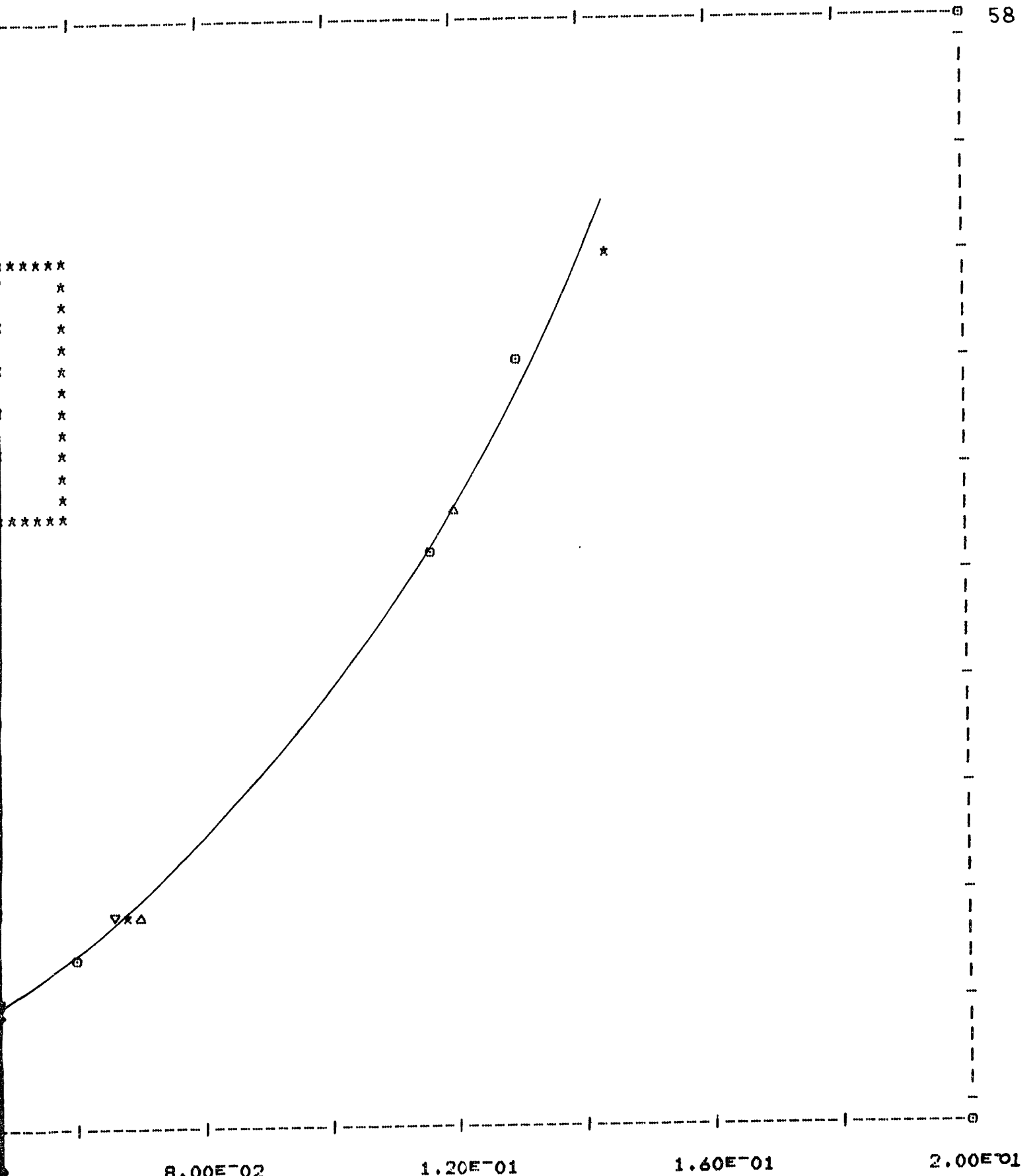

E 31. POWER DENSITY VERSUS CURRENT, F=20 CM3/MIN STP

at the lowest feed concentration and increase in an orderly fashion with increasing ammonia concentration.

5.4 Oscillations

The oscillations shown in figures 25 and 26 occur between two plateaus that may correspond to different steady states. In some cases over long periods of time one of the two plateaus eventually becomes the time independent behavior.

A qualitative explanation is offered for this oscillatory behavior. At high voltages the oxygen partial pressure is low and hence the NO production rate is small. The surface concentration of oxygen then begins to rise because of the low NO production rate. This causes the cell voltage to drop and the ammonia oxidation reaction to be favored thus causing an increase in NO production. As this proceeds a point comes when the oxidation rate begins to exceed the rate at which oxygen is transported through the zirconia. Nitric oxide production falls off rapidly, the voltage again rises due to a low partial pressure of oxygen and the cycle is ready to begin again. During this entire process the ammonia conversion level remains constant.

5.5 Industrial Application

Application of the high temperature ammonia fuel cell to industry depends mainly upon two important factors namely, the ability to produce levels of conversion and selectivity to NO comparable with that of the present day process and if short of these levels, power more than able to balance the decrease in selectivity. Figures 32-35 show selectivity as a function of power density at each of the four flow rates examined.

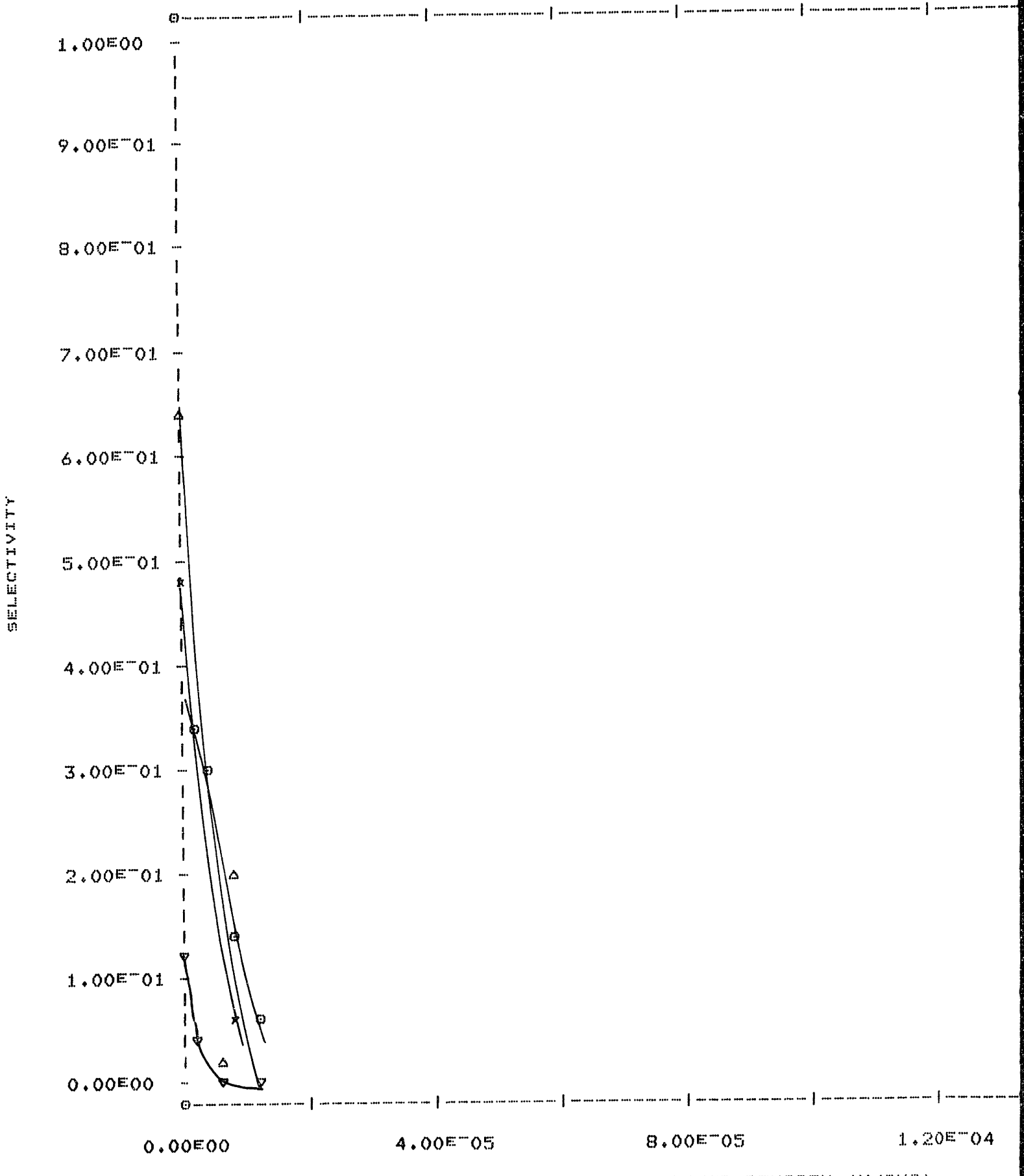

FIGURE 32. SELECTIVITY VERSUS POWER DENSITY, FLOW

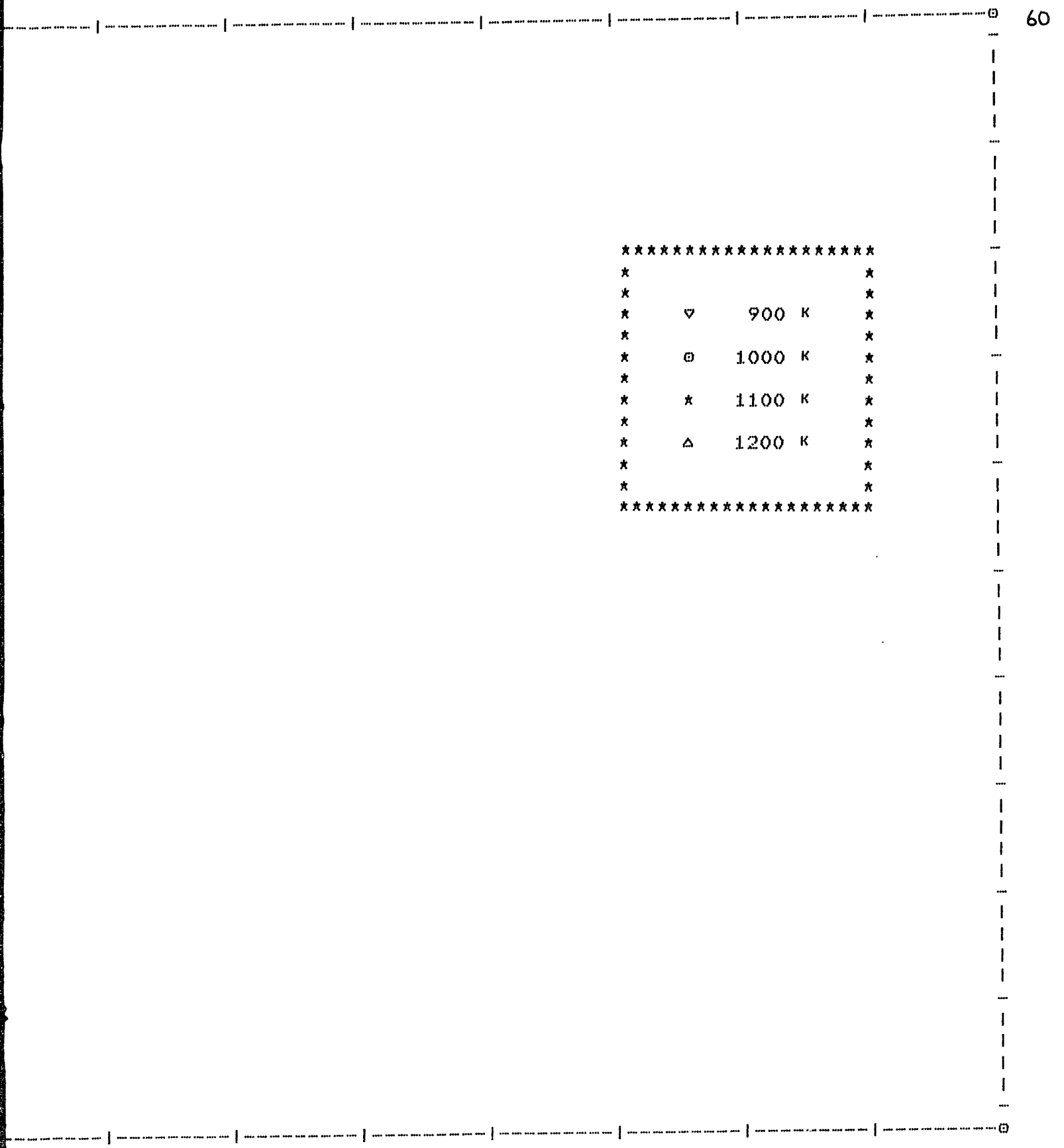

32. SELECTIVITY VERSUS POWER DENSITY, FLOW RATE 5 CM3/MIN STP

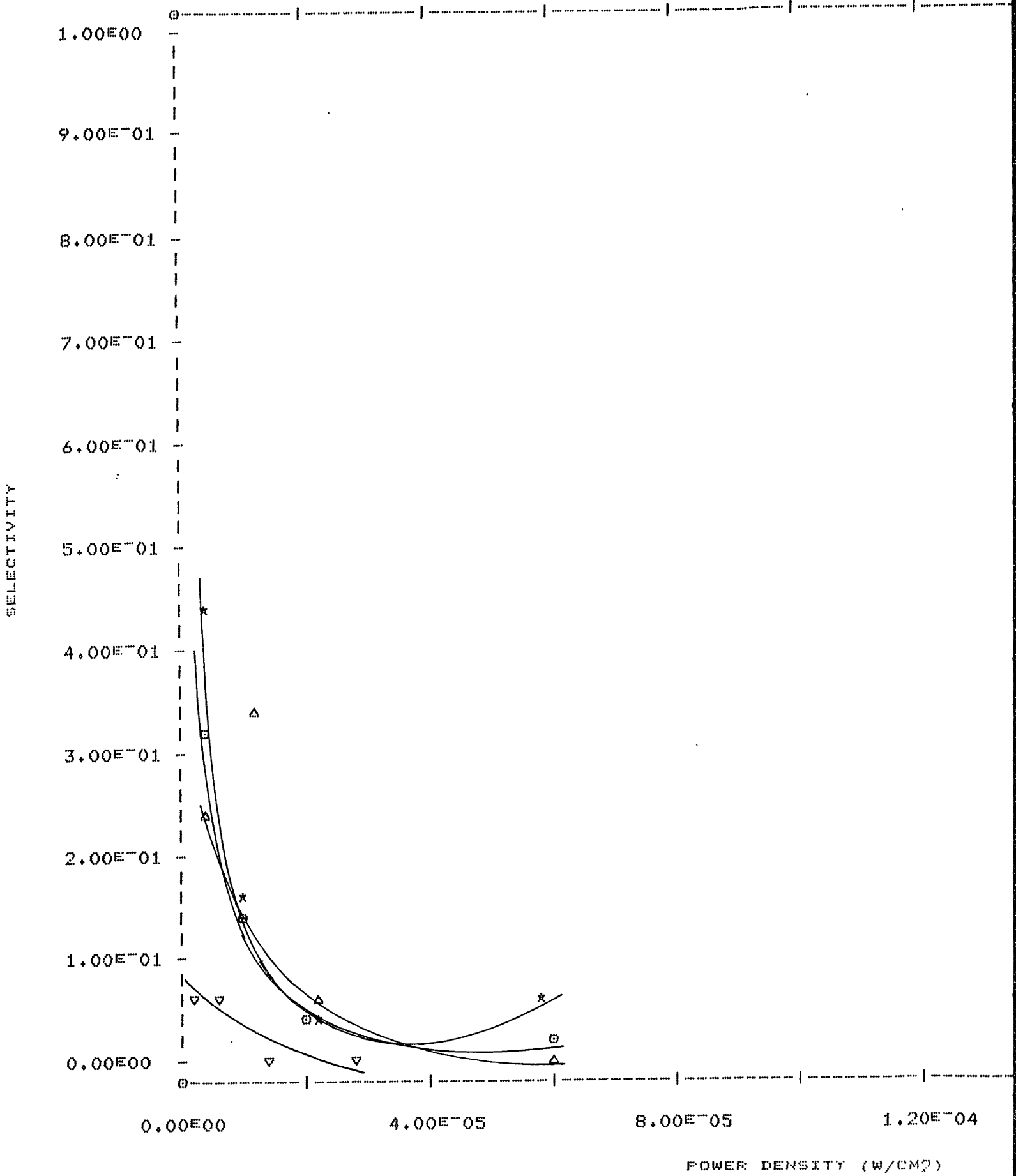

FIGURE 33. SELECTIVITY VERSUS POWER DENSITY, FLOW R

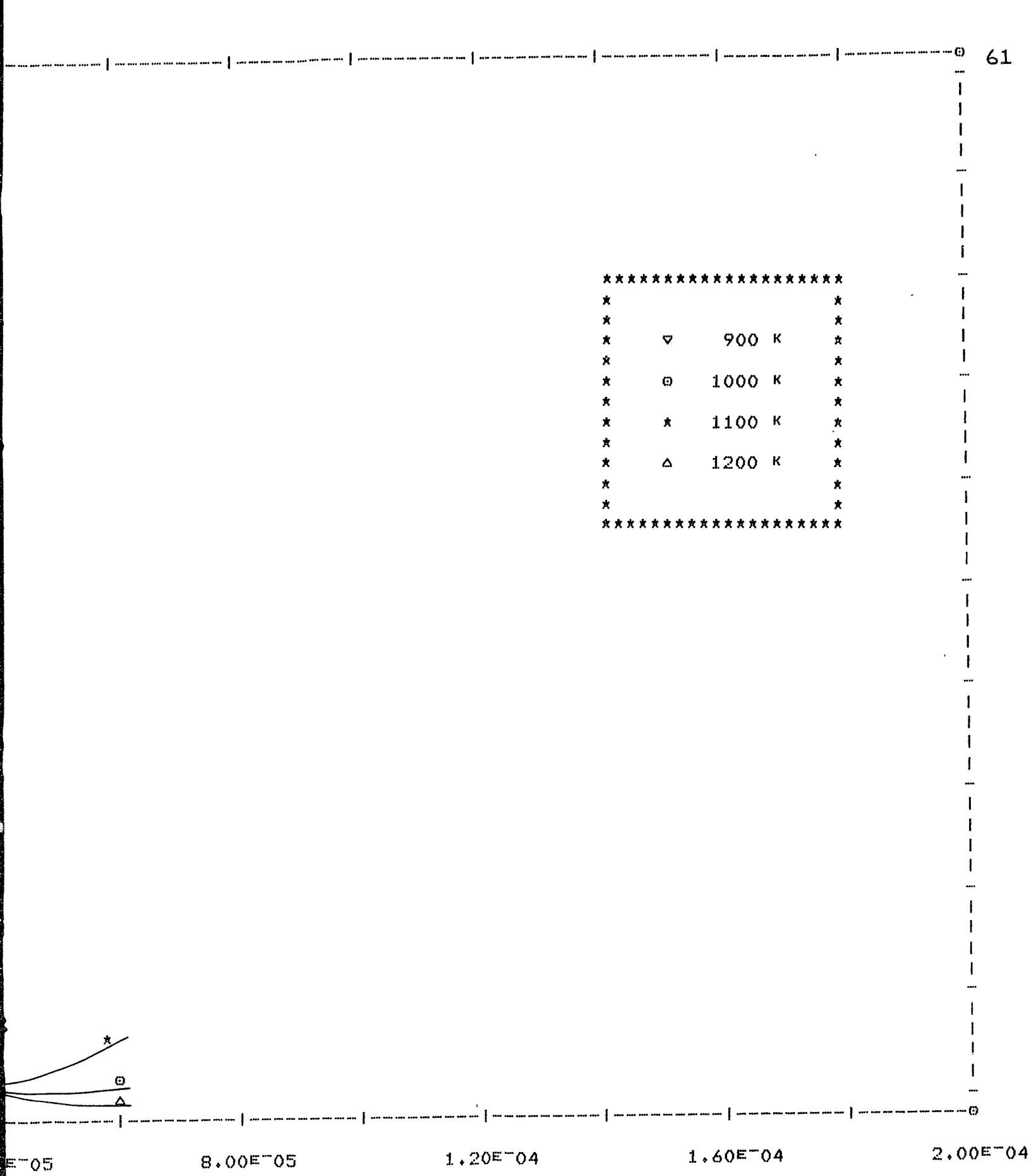

33. SELECTIVITY VERSUS POWER DENSITY, FLOW RATE 10 CM3/MIN STP

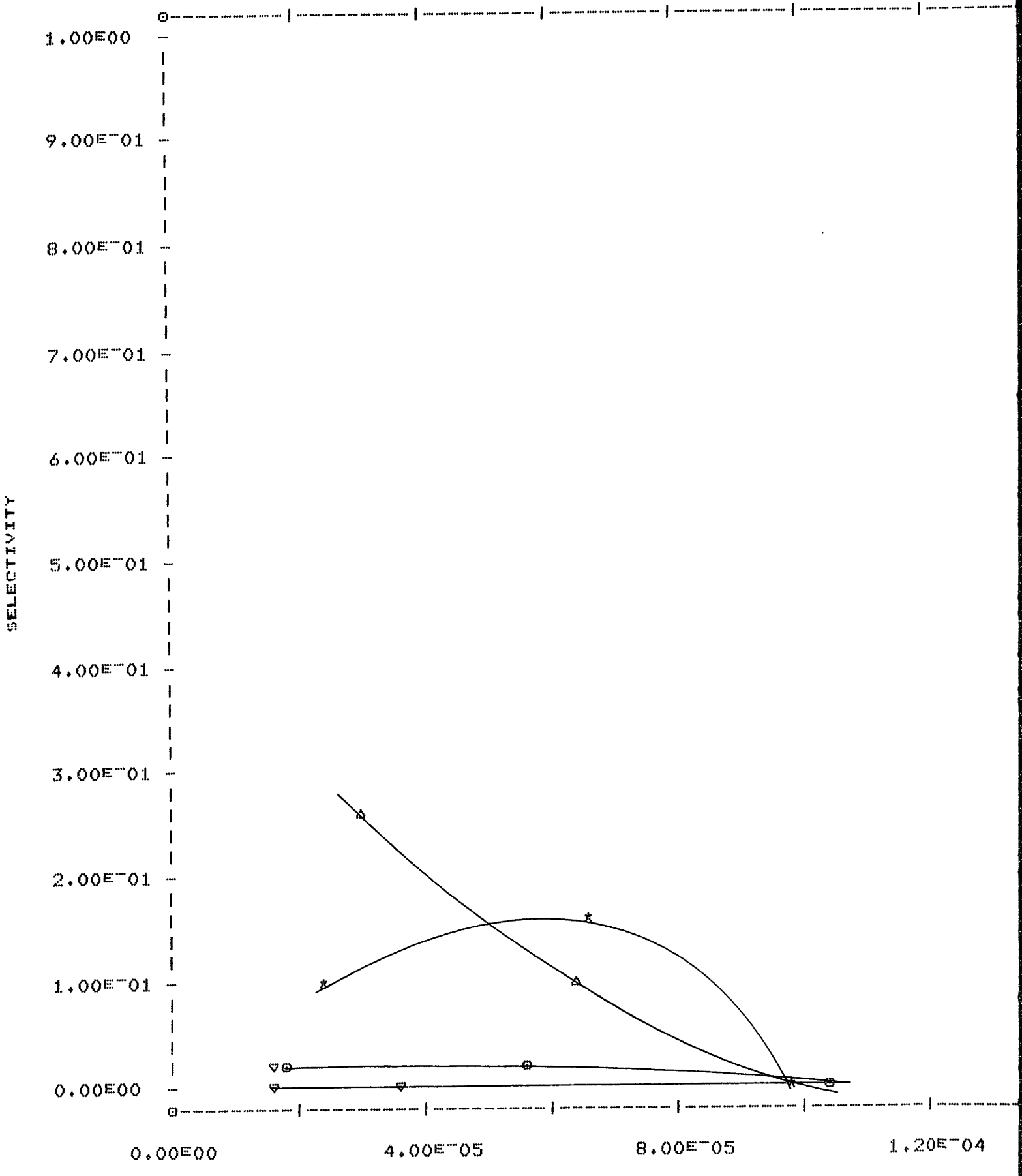

FIGURE 34. SELECTIVITY VERSUS POWER DENSITY, FLOW R

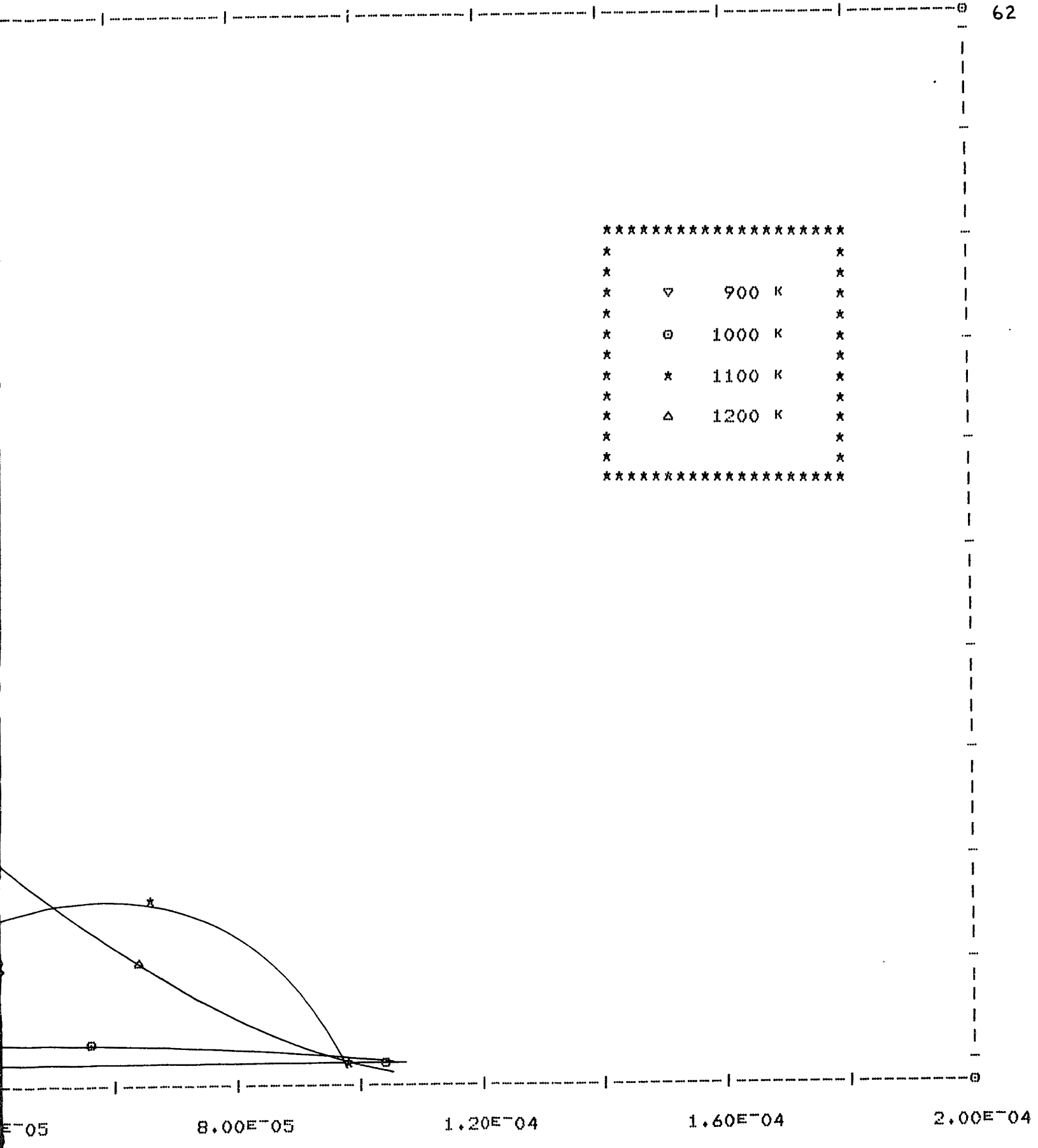

34. SELECTIVITY VERSUS POWER DENSITY, FLOW RATE 15 CM3/MIN STP

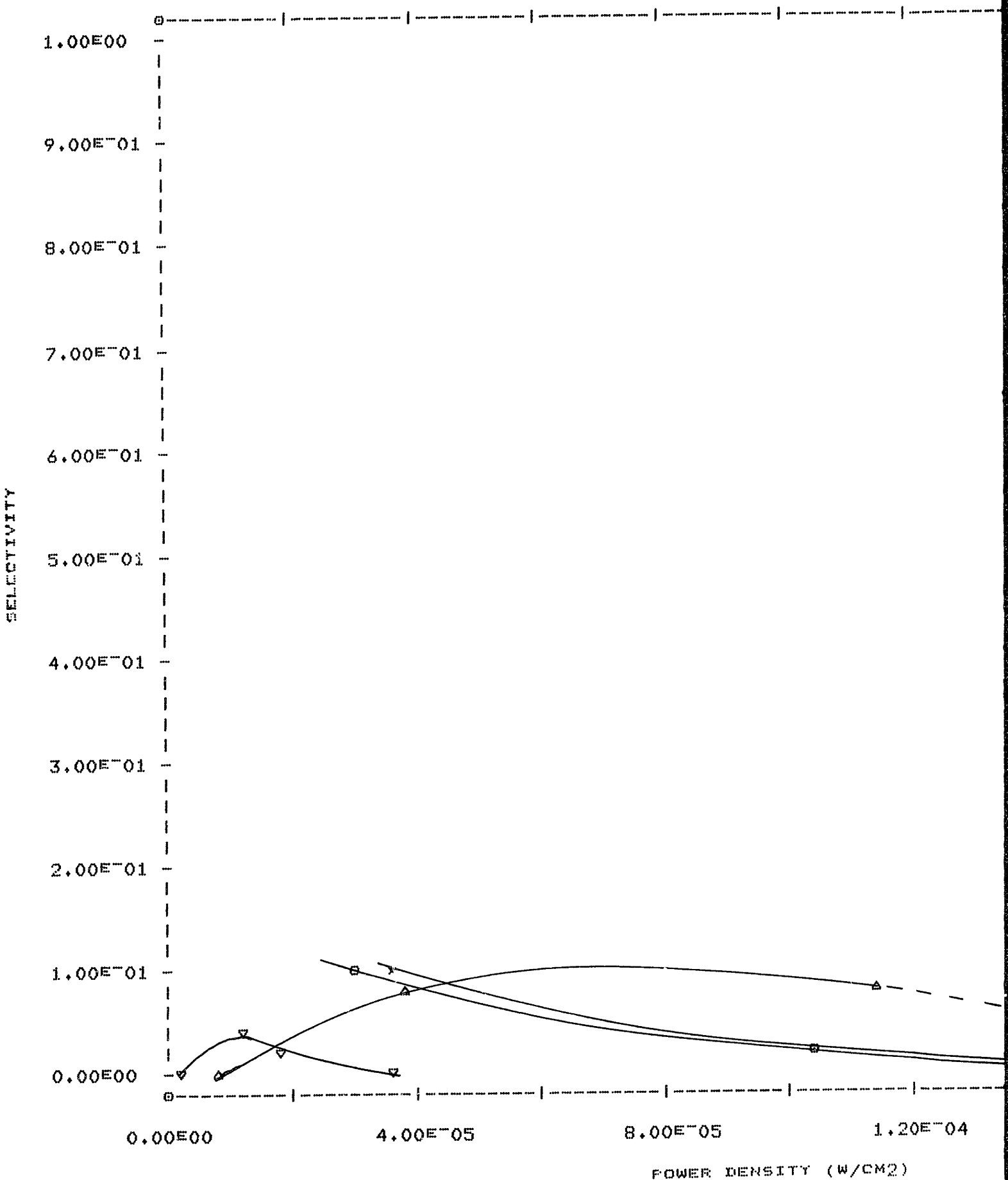

FIGURE 35. SELECTIVITY VERSUS POWER DENSITY, FLOW R

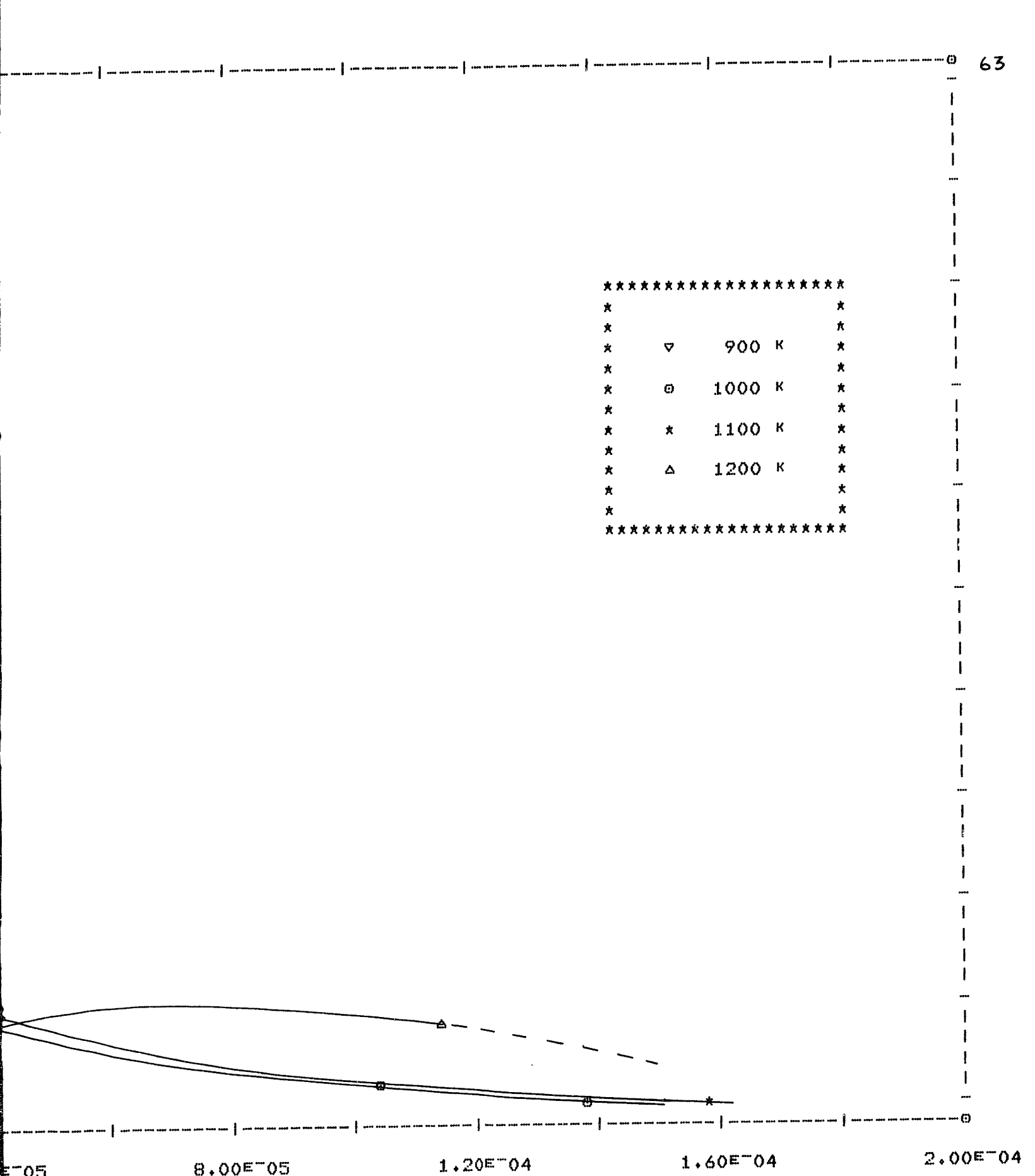

35. SELECTIVITY VERSUS POWER DENSITY, FLOW RATE 20 CM3/MIN STP

The power output generally decreases with increasing selectivity. This is due to the change in the dimensionless parameter r which has been found to govern the selectivity. In order to increase r either the oxygen flux must be increased or the ammonia flux decreased. The high resistance of our cell prevents great increases in oxygen flux thus a decrease in ammonia flux, either by increasing the dilution or lowering the flow rate is the only route to increased selectivity with the present cell. In either case the power drops considerably. If however, the zirconia walls were made considerably thinner the cell resistance would decrease to the limiting value of the electrodes and allow an increase in oxygen flux allowing higher ammonia flow rates to be used thus increasing power while retaining the same or higher selectivity.

The fuel cell design and catalyst-electrode system tested performed well. As shown by the scanning electron micrographs of figures 5, 23 and 24, catalyst rearrangement similar to that observed in industry does occur. After 500 hours of continuous use as a fuel cell the inner platinum electrode showed signs of blistering. This will cause problems in industry and a more suitable method of electrode application is necessary.

The high selectivities obtained in industry can be explained by comparing their r value against our model. For r values greater than 1.25 our model predicts 100% selectivity. Typically 8 mol% NH_3 is fed with 92 mol% air giving an r value of 2.4 thus, the 98% selectivities observed.

The economics of this process cannot be fully evaluated due to resistance restrictions to low r values. The present fuel cell

design is not economically feasable but may prove so by using a thinner electrolyte.

6. CONCLUSIONS

A high temperature solid electrolyte ammonia fuel cell operating at 1100K which exhibits 80-100% conversion of ammonia with greater than 60% selectivity to nitric oxide has been constructed. Under these conditions a maximum power output of 7 $\mu w/cm^2$ was generated with a ratio of oxygen flux to ammonia flux equal to 0.75. Ohmic overpotential is the dominant effect at all temperatures. The electrolyte resistance causes the oxygen flux through the zirconia to be the limiting kinetic factor as well as the limiting factor for selectivity. The selectivity depends critically on the ratio of oxygen flux through the electrolyte to the flux of ammonia through the cell. This dimensionless number r is the important parameter for scale up and operation of the ammonia fuel cell. Both power output and selectivity can be significantly increased by using a thinner solid electrolyte and thereby reducing the resistance to oxygen flux.

Cogeneration of electric power and useful industrial products employing a fuel cell is a sound idea. Application to the nitric acid industry may be economically feasable but more work is needed. Other industries with similar oxidation reactions should also be considered as likely candidates for future cogeneration projects.

7. RECOMMENDATIONS

Data obtained during these experiments bore out areas which require future work. Selectivity and power output data in a region where the r value is close to 1.25 need to be gathered. These data would substantiate the proposed model and allow an economic analysis of the process to be completed. To obtain high values of oxygen flux and allow more ammonia to be processed, lower cell resistances must be obtained. This can be accomplished by using a thinner electrolyte to reduce the resistance down to the limiting value of the electrodes.

Before industrial application is practicable two improvements to the present design must be accomplished. A suitable method for repairing the fragile zirconia tubes and for applying the platinum electrodes. The thin layer of zirconia desired may be applied to a porous substrate, while the electrodes may then be applied as usual. For long periods of operation either a new method of application or composition of platinum and rhodium must be found to eliminate electrode deterioration.

8. ACKNOWLEDGMENTS

This research was funded in part through a National Science Foundation Grant. Full use was made of the Massachusetts Institute of Technology, Department of Chemical Engineering facilities.

Sincerest appreciation is extended to Professor Costas Vayenas for his encouragement and enthusiasm throughout the trials and tribulations this project faced on the road to its successful conclusion.

Gratitude is also extended to Mr. David Ortman for his helpful consultations and constant companionship during the course of this work.

9. APPENDIX

9.1 Equipment List

Below are the detailed specifics of each component used in this research. Where applicable specific model numbers or compositions are given to insure reproducible results.

Ammeter	Fluke model 8600A digital multimeter
Analyzers	Ammonia: Beckman model 864 infrared analyzer
	Nitric Oxide: Beckman model 865 infrared analyzer
Bubble Meter	50ml precision glassware
Catalyst	Englehard composition A3788 platinum ink
	Englehard composition 6926 unfluxed platinum ink
Chart Recorder	Houston Instruments model B5111-5 one pen
	Houston Instruments model B5216-2 two pen
Filter	Nupro model 4F, 15 micron
Flow Meters	Matheson model R7640 series 601 and 602
Furnace	Hoskins model 303A
Gas	Air: Matheson air zero gas
	Ammonia: Matheson certified standard 4.59% ammonia in helium
	Helium: Matheson helium zero
	Nitric Oxide: Matheson certified standard 8550ppm nitric oxide in helium
Load	Clarostat model 250 power resistance decade
Temperature Controller	Love Controls model 48 on-off
Thermometer	Omega Emgineering model 175, chromel-alumel

Voltmeter	Fluke model 8040A digital multimeter
Zirconia	Corning Glass Works composition 1372, 8.0 mol% Y_2O_3 in ZrO_2, 0.75 x 0.62 x 24.0 in cylindrical tube

9.2 Data Table

The following table gives the data obtained during the course of this work. Missing values indicate, very low concentrations of nitric oxide or low conversions of ammonia, where the instruments were inaccurate.

T= 900

NO.	YNH3,F	F	YNH3,E	YNO	E	I	C
1	.0459	20.09	.0372	.00000	.0586	.0667	.184
2	.0459	14.58	.0343	.00000	.0590	.0682	.245
3	.0459	10.07	.0350	.00000	.0524	.0604	.231
4	.0459	5.14	.0000	.00000	.0335	.0386	1.000
5	.0297	20.51	.0140	.00017	.0418	.0481	.521
6	.0293	15.54	.0123	.00020	.0388	.0446	.572
7	.0311	9.84	.0090	.00010	.0374	.0431	.703
8	.0306	4.88	.0052	.00005	.0227	.0260	.825
9	.0204	19.48	.0086	.00039	.0339	.0388	.574
10	.0200	15.31	.0000	.00000	.0403	.0463	1.000
11	.0198	9.90	.0138	.00030	.0242	.0276	.299
12	.0206	4.84	.0111	.00035	.0155	.0177	.456
13	.0100	19.48	.0197	.00005	.0152	.0173	
14	.0103	14.81	.0126	.00003	.0173	.0197	
15	.0099	9.93	.0027	.00045	.0127	.0145	.726
16	.0091	5.08	.0015	.00095	.0076	.0085	.838

T= 1000

NO.	YNH3,F	F	YNH3,E	YNO	E	I	C
17	.0459	19.11	.0000	.00007	.1190	.1300	1.000
18	.0459	14.89	.0000	.00000	.0992	.1159	1.000
19	.0459	11.45	.0000	.00067	.0760	.0882	1.000
20	.0459	5.42	.0061	.00235	.0348	.0403	.861
21	.0297	20.51	.0161	.00022	.1007	.1160	.450
22	.0293	15.54	.0109	.00030	.0734	.0845	.622
23	.0311	9.84	.0093	.00093	.0440	.0505	.693
24	.0306	4.88	.0069	.00326	.0279	.0320	.769
25	.0204	19.48	.0089	.00115	.0531	.0609	.559
26	.0200	15.31	.0111	.00020	.0417	.0476	.440
27	.0198	9.90	.0143	.00081	.0316	.0360	.276
28	.0206	4.84	.0107	.00284	.0213	.0243	.474
29	.0100	19.48	.0200	.00013	.0289	.0330	
30	.0103	14.81	.0143	.00175	.0281	.0321	
31	.0099	9.93	.0023	.00233	.0175	.0199	.763
32	.0091	5.08	.0000	.00309	.0100	.0114	1.000

T= 900

YNO	E	I	C	S	I/A
.00000	.0586	.0667	.184	.000	3.51E-05
.00000	.0590	.0682	.245	.000	3.61E-05
.00000	.0524	.0604	.231	.000	2.84E-05
.00000	.0335	.0386	1.000	.000	1.16E-05
.00017	.0418	.0481	.521	.011	1.80E-05
.00020	.0388	.0446	.572	.012	1.55E-05
.00010	.0374	.0431	.703	.005	1.45E-05
.00005	.0227	.0260	.825	.002	5.30E-06
.00039	.0339	.0388	.574	.034	1.18E-05
.00000	.0403	.0463	1.000	.000	1.67E-05
.00030	.0242	.0276	.299	.051	5.99E-06
.00035	.0155	.0177	.456	.038	2.46E-06
.00005	.0152	.0173			2.36E-06
.00003	.0173	.0197			3.06E-06
.00045	.0127	.0145	.726	.063	1.65E-06
.00095	.0076	.0085	.838	.126	5.80E-07

T= 1000

YNO	E	I	C	S	I/A
.00007	.1190	.1300	1.000	.002	1.39E-04
.00000	.0992	.1159	1.000	.000	1.03E-04
.00067	.0760	.0882	1.000	.015	6.01E-05
.00235	.0348	.0403	.861	.062	1.26E-05
.00022	.1007	.1160	.450	.017	1.05E-04
.00030	.0734	.0845	.622	.017	5.57E-05
.00093	.0440	.0505	.693	.044	1.99E-05
.00326	.0279	.0320	.769	.142	8.01E-06
.00115	.0531	.0609	.559	.102	2.90E-05
.00020	.0417	.0476	.440	.023	1.78E-05
.00081	.0316	.0360	.276	.149	1.02E-05
.00284	.0213	.0243	.474	.294	4.64E-06
.00013	.0289	.0330			8.56E-06
.00175	.0281	.0321			8.09E-06
.00233	.0175	.0199	.763	.311	3.12E-06
.00309	.0100	.0114	1.000	.343	1.02E-06

T= 1100

NO.	YNH3,F	F	YNH3,E	YNO	E	I	C	S
33	.0459	19.93	.0073	.00000	.1233	.1432		
34	.0459	15.58	.0070	.00013	.0966	.1120	.840	.00
35	.0459	10.61	.0070	.00201	.0748	.0867	.840	.05
36	.0459	4.92	.0015	.00291	.0285	.0331	.965	.06
37	.0297	20.91	.0152	.00034	.1007	.1161	.481	.02
38	.0293	15.54	.0078	.00326	.0799	.0918	.727	.15
39	.0311	9.84	.0092	.00076	.0458	.0525	.698	.03
40	.0306	4.88	.0077	.00460	.0292	.0335	.743	.20
41	.0204	19.48	.0089	.00108	.0595	.0683	.559	.09
42	.0200	15.31	.0133	.00059	.0483	.0552	.329	.09
43	.0198	9.90	.0146	.00083	.0327	.0374	.261	.16
44	.0206	4.84	.0156	.00465	.0249	.0285	.235	.96
45	.0100	19.48	.0195	.00017	.0271	.0310		
46	.0103	14.81	.0140	.00189	.0277	.0315		
47	.0099	9.93	.0023	.00328	.0184	.0210	.765	.43
48	.0091	5.08	.0002	.00413	.0099	.0112	.974	.47

T= 1200

NO.	YNH3,F	F	YNH3,E	YNO	E	I	C	S
49	.0459	19.74	.0110	.00000	.0268	.0307	.751	.00
50	.0459	15.00	.0084	.00000	.0653	.0755		
51	.0459	10.58	.0080	.00020	.0764	.0880	.820	.00
52	.0459	4.92	.0038	.00081	.0247	.0287	.913	.02
53	.0297	20.51	.0178	.00084	.1047	.1205	.392	.07
54	.0293	15.54	.0075	.00195	.0782	.0902	.738	.09
55	.0311	9.84	.0099	.00135	.0454	.0522	.673	.06
56	.0306	4.88	.0089	.00415	.0291	.0333	.703	.19
57	.0204	19.48	.0090	.00088	.0601	.0690	.552	.07
58	.0200	15.31	.0135	.00170	.0531	.0609	.322	.26
59	.0198	9.90	.0138	.00195	.0335	.0383	.299	.33
60	.0206	4.84	.0205	.00586	.0236	.0270		
61	.0100	19.84	.0202	.00083	.0331	.0379		
62	.0103	14.81	.0138	.00134	.0265	.0301		
63	.0099	9.93	.0023	.00180	.0174	.0198	.765	.24
64	.0091	5.08	.0017	.00465	.0089	.0100	.812	.63

T= 1100

YNO	E	I	C	S	I/A
.00000	.1233	.1432			1.58E-04
.00013	.0966	.1120	.840	.004	9.71E-05
.00201	.0748	.0867	.840	.054	5.82E-05
.00291	.0285	.0331	.965	.069	8.46E-06
.00034	.1007	.1161	.481	.024	1.05E-04
.00326	.0799	.0918	.727	.156	6.58E-05
.00076	.0458	.0525	.698	.036	2.16E-05
.00460	.0292	.0335	.743	.207	8.78E-06
.00108	.0595	.0683	.559	.096	3.65E-05
.00059	.0483	.0552	.329	.090	2.39E-05
.00083	.0327	.0374	.261	.162	1.10E-05
.00465	.0249	.0285	.235	.968	6.37E-06
.00017	.0271	.0310			7.54E-06
.00189	.0277	.0315			7.83E-06
.00328	.0184	.0210	.765	.437	3.47E-06
.00413	.0099	.0112	.974	.471	9.95E-07

T= 1200

YNO	E	I	C	S	I/A
.00000	.0268	.0307	.751	.000	7.38E-06
.00000	.0653	.0755			4.42E-05
.00020	.0764	.0880	.820	.006	6.03E-05
.00081	.0247	.0287	.913	.020	6.36E-06
.00084	.1047	.1205	.392	.073	1.13E-04
.00195	.0782	.0902	.738	.092	6.33E-05
.00135	.0454	.0522	.673	.066	2.13E-05
.00415	.0291	.0333	.703	.197	8.69E-06
.00088	.0601	.0690	.552	.079	3.72E-05
.00170	.0531	.0609	.322	.266	2.90E-05
.00195	.0335	.0383	.299	.332	1.15E-05
.00586	.0236	.0270			5.72E-06
.00083	.0331	.0379			1.13E-05
.00134	.0265	.0301			7.16E-06
.00180	.0174	.0198	.765	.240	3.09E-06
.00465	.0089	.0100	.812	.635	7.99E-07

REFERENCES

(1) Bockris, J. O'M. and Srinivasan, S. , "Fuel Cells: Their Electrochemistry", p.30, McGraw-Hill (1969)

(2) Chilton, T.H., Chemical Engineering Progress Monograph Series, No. 3, Vol.56 (1960)

(3) Grove, W.R., Phil. Mag., 14, 127 (1839)

(4) Pignet, T. and Schmidt, L.D., J. Catal., 40, 212 (1975)

(5) Bond, G.C., "Catalysis By Metals" p.456-460, Academic Press (1962)

(6) Kiukkola, K. and Wagner, C.T., J. Electrochem. Soc. 104, 379 (1957)

(7) Etsell, T.H. and Flengas, S.N., Trans. Electrochem. Soc., 118, 1890 (1971)

(8) Archer, D.H. et al, "Westinghouse Solid Electrolyte Fuel Cells" in "Fuel Cell Systems", Adv. in Chem. Ser. 47, p.332 (1965)

SYMBOLS

English

A	area (cm^2)
E	electromotive force (V)
F	STP flow rate (cm^3/min); reactor response to a step input
$\mathcal{F}$	Faraday constant, 96485 (coul/eq)
G	molar flow rate (mol/sec), Gibbs free energy (kcal/mol)
i,I	current (A)
k	rate constant (mol/sec)
N	dimensionless group equal to $k_2\ y_{NH_3,f}\ /\ F$
p	partial pressure (Pa)
P	power (J)
r	rate of reaction ((mol/sec); the dimensionless ratio of oxygen flux to ammonia flux
R	universal gas constant, 8.314 (J/mol K); resistance
S	selectivity
T	temperature (K)
x	dimensionless concentration
y	mole fraction

Greek

δ	electrolyte thickness (cm)
Δ	change in a quantity
ρ	resistivity (ohm-cm)
τ	residence time (min)

Subscripts

a	available amount
c	referring to the total fuel cell
e	exit value; referring to the electrode
f	feed stream value
i	inside the fuel cell
L	limiting value
o	outside the fuel cell
T	total quantity
z	referring to the solid electrolyte
irr	irreversible processes
max	maximum
NH_3	ammonia
NO	nitric oxide
N_2	nitrogen
O_2	oxygen